NATIONAL AERONAUTICS AND SPACE ADMINISTRATION
GRANT # NsG 280-63

TECHNICAL REPORT NO. 3

JUNE 1, 1968

THE STABILITY OF MOTION IN A PERIODIC CUBIC FORCE FIELD

by

CURTIS A. WAGNER

N68-30120
(ACCESSION NUMBER)
156
(PAGES)
CR-95836
(NASA CR OR TMX OR AD NUMBER)
(THRU)
1
(CODE)
19
(CATEGORY)
FACILITY FORM 602

DEPARTMENT OF PHYSICS
UNIVERSITY OF ILLINOIS
Urbana, Illinois

JUN 1968
RECEIVED
NASA STI FACILITY
INPUT BRANCH

THE STABILITY OF MOTION IN A PERIODIC CUBIC FORCE FIELD

Curtis Arthur Wagner, Ph.D.
Department of Physics
University of Illinois, 1968

The object of this research has been to investigate numerically the possible existence of closed, invariant regions of stability for solutions of a particular nonlinear differential equation. The Illiac II computer at the University of Illinois has been utilized for an accurate study of the stability properties of solutions of the "Cubic Equation". This nonautonomous equation has the form $d^2X/dt^2 + p(t)\, X^3 = 0$, where $p(t)$ is a periodic square-wave function of time with magnitude p_o and period τ. This equation can be integrated piecewise in terms of Jacobian elliptic functions, and hence is suitable for a high-speed digital computer. Not relying on numerical integration techniques allows us to perform many highly accurate computations over thousands of periods of τ.

For fixed values of p_o and τ we have studied the motions in a global neighborhood of a particular solution with period 11τ which has an elliptic fixed point on the X-axis. Initial exploratory calculations using numerical integration revealed a region associated with fixed points of period 55τ which apparently did not allow any of its interior points to escape to infinity. This

discovery suggested that we make a more careful study of solutions associated with the clusters of multiple points (fixed under multiples of 11τ periods) which surround the original elliptic fixed point. The solutions with 22τ and 44τ periods quickly carried points to infinity. The solutions with 11τ and 33τ periods possessed characteristic oscillating hyperbolic invariant curves, whereas the solutions with a 55τ period did not. It was found that the outer 33τ oscillating invariant curves intersected the outgoing 11τ oscillating invariant curves. However the inner 33τ oscillating invariant curves formed a tangled mesh of self-intersections. This "entanglement" effectively prevented them from intersecting the 55τ hyperbolic invariant curves. Consequently points in the domain of the 55τ solutions were "stable".

The final results clearly show (to the 10^{-12} accuracy of the Illiac II computer) the existence of a closed invariant region, associated with fixed points of period 55τ, around the original 11τ elliptic fixed point. This region is bounded by the doubly-periodic union of the non-oscillating hyperbolic invariant curves associated with the 55τ solutions. It is surrounded by a jumbled global structure of oscillating and intersecting hyperbolic invariant curves belonging to mappings with lesser multiplicities. This intersection property provides the escape mechanism for points just outside the invariant region. Points initially inside the invariant region always map inside that region, even after an infinite number of repeated mappings of the phase-space. The points belonging to this region are said to be stroboscopically stable.

If we scale our flat nearly-elliptical twist mappings up to nearly-circular ones (by scaling p_o), then the conditions of Moser's theorem on invariant curves for certain twist mappings apply. However they are not sufficient to locate the observed invariant region accurately. (Testing Moser's conditions involves as much work as actually searching for the non-oscillating invariant curves.) Thus the best method at present for obtaining practical knowledge about the precise location of invariant regions of stability is to use a digital computer. The most important features of our work should be reproducible on less accurate computers, even utilizing standard numerical integration techniques for the equations of motion. Our empirical methods would then afford some practical guidelines for a quantitative global understanding of the absolute stability of solutions of any particular nonautonomous differential equation.

ACKNOWLEDGEMENT

The author wishes to take this opportunity to thank Dr. James H. Bartlett, now at the University of Alabama, for his constant encouragement and interest as well as his original suggestion of this research. For, without his understanding and patient guidance this work would not have been completed. In addition the author extends his thanks to the many students who assisted in the work: Mr. Gary Carney; Mr. George Edes; Mr. Len Olson; Mr. Tom Schroeder; and especially to Mr. Kenneth L. Caldwell for Illiac programing; Mr. Anil K. Raheja for plotting and calculating; and Mr. James A. Turek for his excellent draftmanship. Much of this research was supported in part by a grant from the National Aeronautics and Space Administration (Grant NsG 280-62), essential for the use of the Illiac II and IBM-7094 computers at the University of Illinois. Finally the author wishes to dedicate this research to his wife, Gretchen, whose love, understanding, and sacrifices catalyzed the writing of this work.

TABLE OF CONTENTS

LIST OF FIGURES

I. INTRODUCTION

The stability of motion is a concept which is defined analogously to the stability of equilibrium, with which we are all familiar. Just as small displacements from an equilibrium position may result in a particle moving permanently away from that position (which is then said to be one of unstable equilibrium), so small initial displacements from a periodic orbit can result in steady motion away from that orbit, and the initial motion is termed unstable.

The planetary orbits appear to be "stable" since they have changed very little over several thousands of years. However, astronomical evolution occurs over billions of years, and it would be nice to know how stable the solar system is during such a time span. Evidence may be gained for this problem by observing the stability properties of charged particle trajectories in accelerators and magnetic bottles. These trajectories may involve millions of orbit repetitions in relatively short times, so that any instabilities will show up vividly. In fact the elimination of plasma instabilities may help in controlling nuclear fusion, so that precise knowledge of "long-period" stability is vital. To attain this, we need an adequate mathematical theory of stability of motion for dynamical systems in general, and for stellar systems, accelerators, and stellerators in particular.

In general, the dynamical equations are nonlinear, either explicitly time-dependent (i.e. non-autonomous) or else time-independent. The solutions of the equations may be found numerically, but then we have to examine their totality in order to make conclusions about stability. General treatises on the "stability of motion" (e.g. the survey by Sansone and

Conti[1] or Bellman[2], with references) list many different definitions of "stability", depending partly on the approximations which are to be made. We shall begin by briefly discussing <u>first-order stability</u>. Let us consider a set of n coupled first-order equations of the motion

$$dX_i/dt = F_i(X_j) \qquad \text{for } i,j = 1,2,\ldots,n \tag{1}$$

which possess periodic (closed) solutions of the form

$$X_i(t) = f_i(t) = f_i(t+T) \tag{2}$$

where T is the period of the motion. If we now look at some "nearby" solution whose n coordinates $X_i'(t)$ at time t differ from $X_i(t)$ by infinitesimal perturbations $\delta X_i(t)$, we can write

$$X_i'(t) = X_i(t) + \delta X_i(t) \quad . \tag{3}$$

Since this is also a solution of equation (1) by definition, we can obtain n <u>variational equations</u> for the $\delta X_i(t)$ infinitesimals, namely

$$\frac{d}{dt}\,\delta X_i = \sum_{j=1}^{n} \frac{\partial F_i}{\partial X_j}\,\delta X_j \qquad i = 1,2,\ldots,n \; . \tag{4}$$

These linear differential equations (with coefficients periodic in t) will possess solutions for the δX_i of the form

$$\delta X_i(t) = \sum_{k=1}^{n} e^{\alpha_k t} M_{ik} \tag{5}$$

where M_{ik} is an array of functions of period T, and α_k are n constants known as characteristic exponents of the solution. If all the α_k are purely imaginary, then the perturbations $\delta X_i(t)$ themselves will be periodic and bounded. If, however, some of the α_k are real and positive, then the

$\delta X_i(t)$ will grow exponentially with time. Discussions of the exact methods for determining the α_k in general, as well as their implications, can be found in Whittaker[3] or Minorsky[4]. This variational approach, due to Poincaré, is a rather universal one, but is clearly only a first-order approximation to the effects of arbitrary (finite) changes in all the variables. Specific applications of these methods to the determination of the first-order stability of solutions to the restricted three-body problem[5] are found in the work of Shearing[6] and Henon[7].

The limitations to the usefulness of this first-order theory are apparent. As long as we consider solutions with only an infinitesimal separation from the known periodic solution, we can definitely say (provided, of course, that we can directly integrate the variational equations (4)) whether the nearby solution will grow in size with increasing time, or whether it will remain infinitesimally "close". But what about solutions which are a finite distance from the periodic solution? Clearly the variational theory is only a local theory, whereas what we need is a global study of solutions of the equations of motion.

A first step in this direction was made by Liapunov[8] near the end of the nineteenth century. His so-called "second (or direct) method" yields conditions for "stability in the large", without the need to integrate the often difficult variational equations. His theory centers around the existence of certain algebraic functions (Liapunov V functions) of the n variables, which possess properties of definiteness of sign in different regions of phase-space. Liapunov's second theorem states that if there exists such a definite function $V(X_i)$ whose Eulerian derivative (i.e. a time derivative taken along a trajectory) is either zero or of opposite sign to V in some domain D, then the differential system of equation (1)

possesses a stable equilibrium around the singular point $X_i=0$. Weakening of the hypotheses produces several modified theorems for other "types" of stability. In the general case, however, his theorems do not specify any method for determining the function V, nor do they prove its existence. If such a function can be generated somehow, then it can be used to demonstrate stability of motions in the large or at least in definite regions. Although Liapunov's theorems have found extensive applications during the last 70 years, they still present a number of analytical problems which can be as difficult as those of the variational theory. But they do begin to tackle the basic problem of determining the global properties of solutions, as opposed to the strictly local properties.

The same period of history saw the emergence of a fundamentally different point of view about stability -- the topological approach of H. Poincaré[9]. He regarded the differential equations of motion as defining a transformation T^n of the phase-space onto itself. Specifically, the integration of the equations of motion takes initial coordinates on the manifold and maps them into final coordinates on the same manifold. It is not hard to imagine how simple regions of initial coordinates can become mapped onto quite complex, distorted regions on the manifold. Yet it is also conceivable that some particular points on the manifold could be transformed into themselves. Such points are called fixed points of the mapping T^n. In fact, Brouwer's remarkable fixed point theorem[4] asserts that every continuous transformation of a closed (n-dimensional) disk onto itself has at least one such fixed point.

The works of Poincaré in the field of topological approaches to stability are very extensive, but we need to mention here only one of his

last theorems, the so-called "geometric theorem"[10]. This theorem, which arose in connection with periodic solutions of the restricted three-body problem, concerns itself with any closed annular ring $0 < a \leq r \leq b$ in the $r\theta$-plane (a and b are fixed radii), and asserts that if a given transformation T^n of the annular ring onto itself satisfies certain conditions, then at least two points of this ring will be fixed under T^n. Those necessary conditions on T^n are that it must be one-to-one, continuous, and area-preserving, and that it advances points on the (inner) circle r=a while regressing points on the (outer) circle r=b. (A later extension of this theorem by Birkhoff[11] generalizes to the ring $0 < a \leq r$. If T^n advances points on the circle r=a and regresses all points $r \geq R > a$ by at least some angle $\theta_1 > 0$, then there will exist at least two fixed points of T^n in the open ring $a \leq r < R$.) This extremely remarkable geometric theorem of Poincaré has set the stage for all later topological investigations of stability.

Having isolated at least two fixed points of the mapping T^n, we may logically wish to know the general properties of the mapping T^n for points in any neighborhood of the invariant points just found. If we choose a (U,V) coordinate system on the manifold with the fixed point in question at the origin U=V=0, then we can investigate transformations T^n of the general form

$$\left\{ \begin{array}{l} U_1 = aU_o + bV_o + \cdots \\ V_1 = cU_o + dV_o + \cdots \end{array} \right\} \qquad (6)$$

where (U_1,V_1) is the map under T^n of some initial point (U_o,V_o) in a neighborhood surrounding the origin, and where a,b,c, and d are real constants satisfying $ad-bc > 0$. By studying the roots ρ_i of the

characteristic equation for the linear transformation above (e.g. see Minorsky):

$$\rho^2 - (a+d)\rho + (ad-bc) = 0$$

we find there are three basic types of such linear transformations. These three cases include

$$T_h^n: \quad \left\{ \begin{array}{l} U_1 = \rho U_o \\ V_1 = U_o/\rho \end{array} \right\}, \quad (\rho \neq \pm 1) \tag{7}$$

$$T_e^n: \quad \left\{ \begin{array}{l} U_1 = U_o\cos\theta - V_o\sin\theta \\ V_1 = U_o\sin\theta + V_o\cos\theta \end{array} \right\}, \quad (\rho = e^{i\theta}) \tag{8}$$

$$T_p^n: \quad \left\{ \begin{array}{l} U_1 = \pm U_o \\ V_1 = \pm V_o + aU_o \end{array} \right\}, \quad \left(\begin{array}{l} \rho = \pm 1 \\ a \neq 0 \end{array} \right). \tag{9}$$

The symbols h, e, and p designate respectively hyperbolic, elliptic, and parabolic mappings. That is, under repeated applications of one of these mappings, points near the original fixed point (U=V=0) move, or map, successively into other points whose locus is one of the three basic conic sections. Consequently we speak of hyperbolic (saddle), elliptic (vortex), and parabolic (nodal) fixed points under the general mapping T^n. (A fourth type of mapping exists if ρ_i is a complex root; the resulting motion is of a spiral nature, and the associated fixed point is called a focal point.)

In terms of our intuitive concept of stability we might guess the general stability properties of points "near" the original fixed point by reference to the basic type of T^n mapping under which that point is fixed. Thus elliptic points, plus spiral and parabolic points with nearby motions directed inwards to the point, ought to be relatively "stable", while all others ought to be basically "unstable". For example, the linear mapping

T_e^n successively maps an initial (neighboring) point along the locus of an ellipse whose major and minor axes will depend on the exact initial coordinates.

But the T^n transformations discussed above are strictly linear mappings. In general, nonlinear differential equations will possess nonlinear mappings T^n. Consequently any discussion of the possible stability or instability of a given fixed point of the mapping T^n will necessarily be of a more complex nature. Moreover, there are several additional theoretical and empirical results of the topological approaches of Poincaré and Birkhoff that complicate the general nonlinear problem. Birkhoff[12] has proved that inside any neighborhood of a given alliptic-type fixed point in phase-space there exist clusters of multiple fixed points. These multiple points are fixed under some integer multiple m of the original fixed point mapping T^n, i.e. are fixed points of the mapping T^{mn} (m successive applications of T^n). As we shall see later, for any particular value of the integer m there is an even number 2m of these T^{mn} multiple points, and they alternate around the T^{mn} cluster between elliptic-type and hyperbolic-type fixed points. To complicate matters even more, Bartlett[13] has shown, in a quantitative demonstration of Poincaré's theory of consequents[9], that the invariant curves issuing from and toward a T^n hyperbolic-type fixed point are, in general, oscillatory curves. (By invariant curve we mean a locus of points all of which are consequents, or maps under T^n, of themselves alone.) In fact, these hyperbolic invariant curves develop area-preserving oscillations of increasing amplitude as they approach the next hyperbolic-type point beyond the adjacent elliptic-type point.

It is this (denumerable) infinity of clusters of alternating T^{mn} fixed points and oscillating hyperbolic invariant curves which complicate the analysis of nonlinear mappings. In fact, this complex behavior suggests the possibility that all fixed points could be ultimately "unstable". For example, in any neighborhood of a given elliptic-type fixed point, no matter how small, one could always find regions containing hyperbolic-type fixed points of increasing multiplicity m. Points near these T^{mn} hyperbolic-type points (m of them) could be readily carried far away by the oscillating invariant curves issuing from (and coming into) the hyperbolic-type points. If successive mappings of these points under T^{mn} carry them out to infinity, then the original elliptic-type point would be "unstable".

The investigation of various forms of area-preserving mappings of annuli onto themselves has been a fruitful topological approach ever since the pioneering work of Poincaré. It is this same technique which forms the basis of several recent theorems on invariant curves and regions, published independently by Arnol'd[14] and Moser[15]. Moser's theorem is somewhat more general, and consequently we shall discuss his work. He first considers the annular region in the $r\theta$-plane defined by

$$0 < a \leq r \leq b \tag{10}$$

and the simple circular twist mapping:

$$\left\{ \begin{array}{l} \theta_1 = \theta_o + \alpha(r_o) \\ r_1 = r_o \end{array} \right\} \tag{11}$$

of that annular ring, where the function α satisfies

$$d\alpha/dr_o > 0 \quad . \tag{12}$$

This last requirement on $\alpha(r_o)$ means that the amount of the angular twisting

of the mapping always increases with radial distance from the origin of the polar coordinates. (Note that the sense of the twist is opposite to that of Poincaré.) It is clear that this simple mapping preserves circles by simply twisting them around counter-clockwise through an angle $\alpha(r_o)$.

Moser next considers a "small perturbation" of this simple circular twist mapping, of the form

$$\left\{ \begin{array}{l} \theta_1 = \theta_o + \alpha(r_o) + F(r_o, \theta_o) \\ r_1 = r_o + G(r_o, \theta_o) \end{array} \right\} \tag{13}$$

where F and G are assumed to be small and of angular period 2π radians. He then proves that for any $\epsilon > 0$, no matter how small, the above mapping possesses a smooth, closed invariant curve, lying inside an annular region, of the form

$$\left\{ \begin{array}{l} \theta = \theta' + p(\theta') \\ r = r_o + q(\theta') \end{array} \right\} \tag{14}$$

where the functions p and q also have an angular period of 2π radians and possess s continuous (partial) derivatives satisfying

$$|p|_s + |q|_s < \epsilon \ . \tag{15}$$

Moser also assumes that the following conditions hold:

i) Every closed curve near a circle:

$$r = f(\theta) = f(\theta + 2\pi) = \text{a constant} \tag{16}$$

intersects its mapped (image) curve at least twice;

ii) There exists a constant $C_o > 1$ such that

$$C_o^{-1} \leq d\alpha/dr_o \leq C_o \quad ; \tag{17}$$

iii) There exists a $\delta_o(\epsilon,s,C_o)$ and an $\ell(s)$ such that

$$\text{and} \quad \left\{ \begin{array}{c} |F|_o + |G|_o < \delta_o \\ \\ |\alpha|_\ell + |F|_\ell + |G|_\ell < C_o \end{array} \right\} \tag{18}$$

Finally he asserts that the mapping induced on the curve of equation (14) is given by

$$\theta_1' = \theta' + \alpha(r_o) \quad . \tag{19}$$

Moser later develops a formula for $\ell(s)$ and obtains the large value of ℓ=333! Thus the existence of only a (large!) finite number of partial derivatives of F,G, and α are necessary (in contrast to the theorems of Arnol'd which require infinitely many derivatives to exist).

Moser's theorem has an important bearing on the stability of solutions of differential equations. For if its necessary conditions for the mapping are met, then the theorem asserts that there exists a smooth, closed invariant curve of the mapping. This statement in turn means that the invariant curve and the interior region it bounds must <u>always</u> be preserved, even after an <u>infinite</u> number of mappings of the region onto itself. Consequently, points which lie initially anywhere <u>inside</u> the invariant region will always map into other points somewhere inside this region and thus will be absolutely stable (i.e. for an infinite time). Points initially <u>outside</u> this region may map anywhere outside, in particular to infinity, so that we can make no general (absolute) predictions about such points.

One method of studying Moser's contentions (and the general question of stability) is to pick a simple nonlinear differential equation which can be integrated in some closed form. We can then use a high-speed digital

computer to investigate its periodic and "almost-periodic" solutions to a high degree of accuracy. This arithmetical approach has been adopted in our research in order to avoid the accuracy limitations of ordinary numerical integration techniques. (We will, however, employ the latter approach for certain preliminary calculations.)

The non-autonomous (time-dependent) equation chosen, the "Cubic equation", arises in connection with the motion of charged particles in accelerators[16]. It has been studied numerically by Powell and Wright[17], and later by Bartlett[13] using the Illiac I computer. The dimensionless form of this "Cubic equation" is

$$\frac{d^2X}{dt^2} + p(t)\, X^3 = 0 \qquad (20)$$

where $p(t)$ is here chosen to be a periodic square-wave function of time, with a constant magnitude p_o and a fixed period τ, that is

$$\left\{ \begin{array}{ll} p(t) = p_o > 0 & \text{for } -\tau/4 < t \leq \tau/4 \\ p(t) = -p_o & \text{for } \tau/4 < t \leq 3\tau/4 \end{array} \right\} \qquad (21)$$

This equation can be easily integrated in a piecewise manner (i.e. over each half-period $\tau/2$ of the square-wave) to yield piecewise first integrals of the motion. These in turn can then be integrated once more to give a piecewise solution for $X(t)$ and $\dot{X}(t)$ in terms of Jacobian elliptic functions. Given initial phase-space coordinates $(X_i, \dot{X}_i)$ we can thus obtain the coordinates $(X_1, \dot{X}_1)$ at the end of the first quarter-period of the square-wave. Using these coordinates now as initial coordinates, we can calculate the coordinates $(X_2, \dot{X}_2)$ at the end of the next half-period of motion, and so on in steps of $\tau/2$ thereafter until we desire to stop. Thus a phase-space trajectory of period $n\tau$ can be constructed, where n is

some integer multiple of τ (i.e. an integral number of square-wave cycles). This trajectory, then, corresponds to a mapping $T^n(\tau)$ of the phase-space onto itself. We shall study the properties of this mapping and its multiples. A brief analysis of the possible solutions to equation (20) together with detailed methods for numerically calculating the piecewise trajectories above (i.e. the mappings $T^n(\tau)$) are given in the first appendix.

The object of this research will therefore be to analyze <u>experimentally</u> (i.e. by using computers) the mathematical contents of Moser's theorem for the above "Cubic equation". If we can assure ourselves of extreme precision in these computer calculations, then we ought to be able to locate and determine the precise shape and size of the closed invariant curves and regions, <u>if they exist</u>. It is hoped that these experimental methods will then be applicable to any nonlinear system of equations. If so, then a practical numerical understanding of the absolute stability of solutions for any particular nonlinear differential equations can be obtained easily and quickly.

II. CALCULATIONS

A. Exploratory mapping of the phase-plane

The analysis in the first appendix shows that we can utilize a digital computer for the rapid and accurate calculation of any desired solution of the original equation (20). That is, for any given initial coordinates $(X_i, \dot{X}_i)$ in phase-space we can calculate the subsequent trajectory for as many periods of the periodic function p(t) as we desire. The accuracy of these solutions will be limited chiefly by the capacity of the computer. A program (listed for reference in the second appendix) has been written in the machine language (NICAP) of the University of Illinois' Illiac II computer in order to obtain maximum (12-place) accuracy. (The Illiac II computer utilizes 52-bit words in the form of four quarter-words, and has a speed of up to twice that of the IBM-7094 computer.)

[It has also been convenient to write a simpler Fortran program (also included in the second appendix) for the direct numerical integration of equation (20) using a modified Runge-Kutta-Gill integration routine. This program, run on both the IBM-7094 and the Illiac II, has been highly useful for general exploratory investigations of solutions. Although the calculations made with this program are limited to about 6-place accuracy, they are helpful in ascertaining just which solutions require the highly accurate NICAP program. The program has the additional virtues of being short, simple to write, and compatible with IBM computers. Time-wise, however, the Fortran program is about 3 to 4 times slower than the NICAP program, in spite of the latter program's length and complexity (1250 NICAP instructions compared with 110 Fortran statements). On the average the NICAP program can calculate about 2200 periods of p(t) per minute of

computer time, while the Fortran program can compute only about 660 periods of p(t) per minute.]

An exploratory scan of solutions (in the phase-plane) was made on the Illiac I computer by Bartlett, who found that all fixed points in the phase-plane are either on the two coordinate axes or else are maps of these points[13]. A list of fixed points on the two axes for n=2,3,...,12 is reproduced in Table 1 for reference. These values are accurate only to about 3 decimal places (which is adequate for initial studies). As n gets larger the corresponding points fixed under $T^n(\tau)$ lie closer to the origin and closer to one another. We shall see that around any of these $T^n(\tau)$ fixed points there lie clusters of "satellite" multiple points fixed under the transformation $T^{mn}(\tau)$, where m is an integer.

Knowing the location of the simpler fixed points, we can proceed to investigate some of the properties of their associated solutions. Preliminary repeated mappings under $T^{11}(\tau)$ of points initially inside a relatively large neighborhood of the T^{11} elliptic fixed point on the +X-axis (at about $X_i = 1.667$) showed that the consequent (mapped) points generally return repeatedly to the same initial neighborhood. Few escape to infinity or wander very far from the initial neighborhood. Other T^n elliptic fixed points were similarly scanned, but none exhibited such an apparent "stability" of the repated mappings. Thus the remainder of this work will concern itself with a detailed analysis of the region near the T^{11} elliptic fixed point. A plot of the periodic orbit in phase-space that is associated with this T^{11} fixed point is shown in Figure 1. The (22) encircled points mark the end of each half-period arc of motion, while the T^{11} fixed point on the +X-axis (the initial conditions for the orbit) is enclosed by a small square.

Table 1

Approximate axis locations of some fixed points of the mapping $T^n(\tau)$, for n=2,3,...,12.

n	X-axis	$\bar{X}$-axis
2	3.4143	9.6012
3	3.1823	0.4591
4	2.387	0.3775
5	2.338	0.3579
6	2.1086	0.3088
7	2.058	0.1639
8	1.9106	0.1545
9	1.8506	0.1464
10	1.736	0.1259
11	1.667	0.1021
12	1.5777	0.09339

Figure 1. Periodic phase-space trajectory associated with the T^{11} elliptic fixed point on the X-axis.

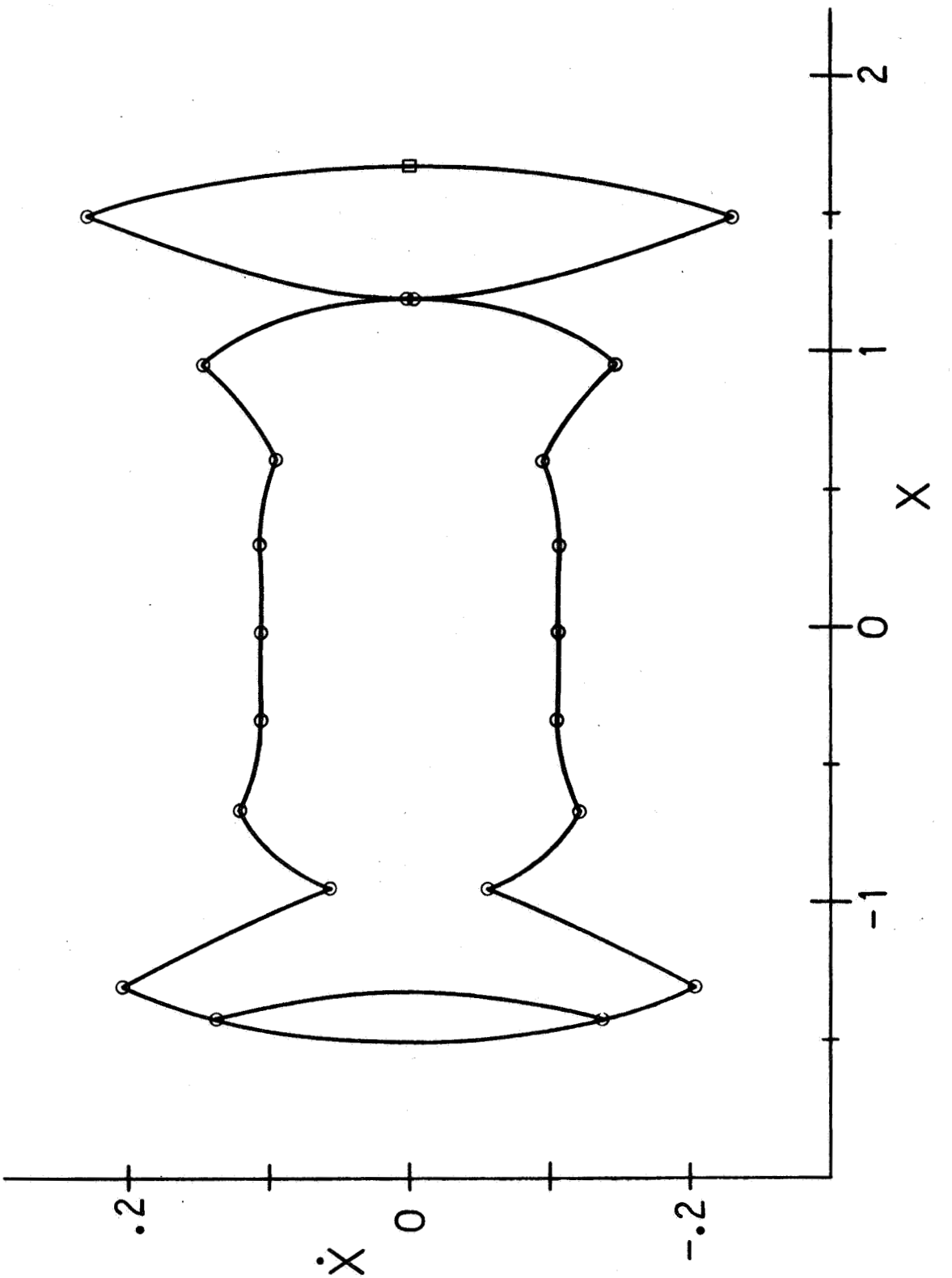
2
1
0
-1
X
.2
0
-.2
X

The X-axis near the point $X_i = 1.667$ was mapped for the multiples m=1,2,3,4, and 5 of the basic period $n\tau=11\tau$, and the results of the Runge-Kutta method are shown in Figure 2. Note the striking "twisted" character of these mappings, a feature that will play an increasingly important role. In the figure, E_1 marks the T^{11} fixed point, and the (+) superscripts on the letters A,B,C,D, and E indicate the curve is a map of the +X-axis for m=1,2,3,4, and 5 respectively. Each successive mapping is a twisted (rotated) version of the previous one, so that even by m=3 the plots become intricately twisted around each other. Sections get thrown outward and then return to intersect the axes again, more often the greater m is.

Yet a great deal of useful information can be obtained from this exploratory plot. First of all we observe that something in the structure of our nonlinear system is creating two wide "escape avenues" for points around the T^{11} fixed point. These begin in the neighborhoods of (1.66, 0.01) and (1.65,-0.01) and carry the mapped axis curves far away from the fixed point E_1. Already we have signs of what we would intuitively call "instability".

The other pieces of valuable information are the intersections of the various mapped axis curves with the X-axis and with each other. Curves E^+ and C^+ intersect the +X-axis and reveal fixed points for the T^{55} and T^{33} mappings respectively. Similarly E and C give fixed points for T^{55} and T^{33} on the -X-axis. Curves D^+ and B^+ intersect the -X-axis and locate points fixed under T^{88} and T^{44} respectively; the same applies for D and B intersecting the +X-axis. In addition, these curves cross each other. Curve A^+ intersects D^+ and so reveals a point fixed under $T^{44-11} = T^{33}$. Other T^{33} points arise from the following intersections: A with D, B^+ with E^+,

Figure 2. T^{11m} twist mappings of the X-axis around the T^{11} elliptic fixed point, for m=1,2,3,4, and 5.

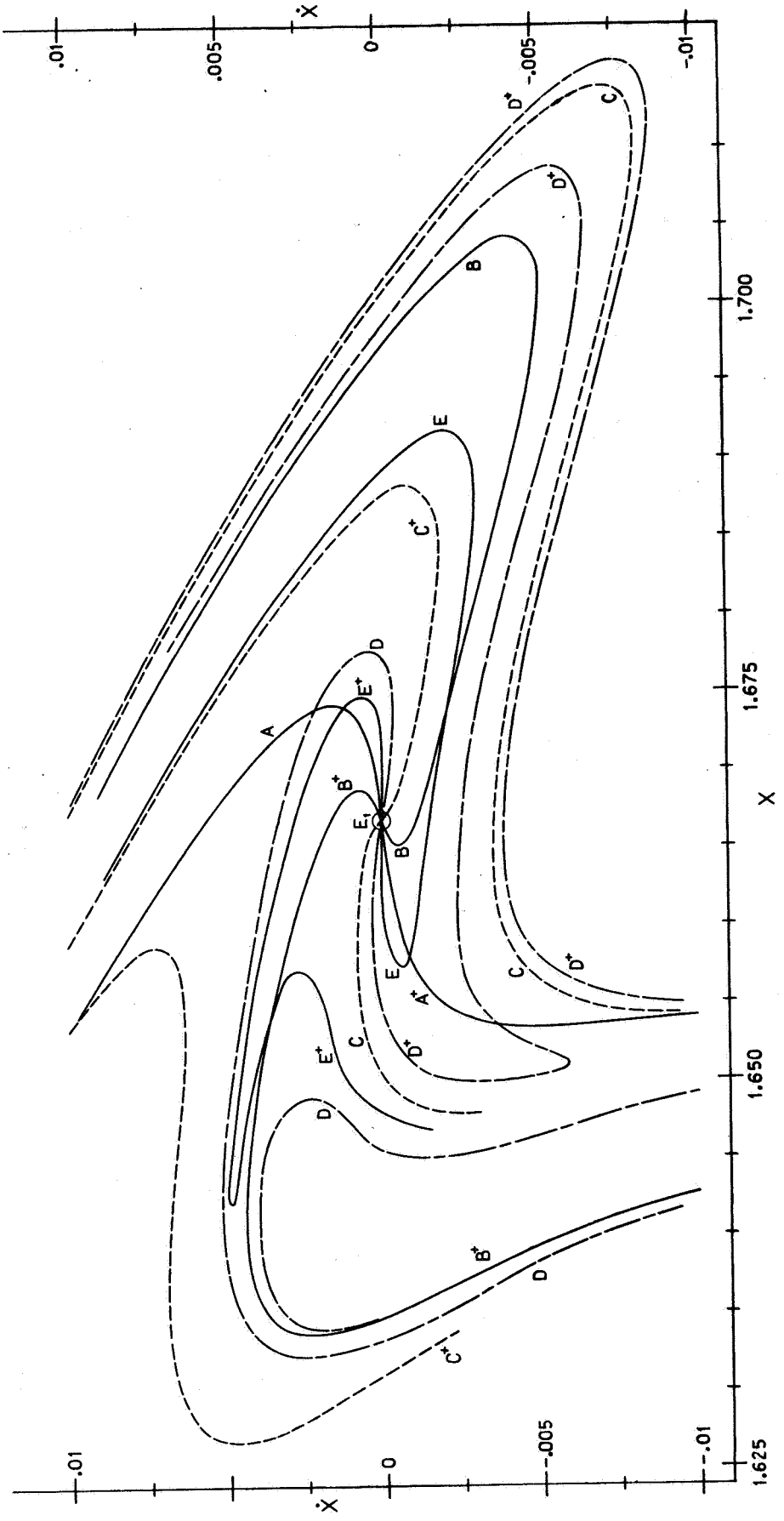
.01
.005
0
-.005
-.01
Ẋ
1.625
1.650
1.675
1.700
X
A
B
C
D
E
A*
B*
C*
D*
E*
E1

and B with E. The intersections of A with E^+ and A^+ with E yield points fixed under T^{88}.

Already we see some of the multiple (fixed) point structure of the T^{11} fixed point revealed to us in this simple scan. So far we have the approximate coordinates of 6 points fixed under T^{33}, two under T^{44}, two under T^{55}, and 4 under T^{88}. The 6 points fixed under $T^{33} = T^{3n}$ (for n=11) represent the totality of T^{3n} points which have been found in the cluster around the T^n fixed point. In simple cases we can expect 2m multiple fixed points of the mapping T^{mn} in a cluster around the T^n fixed point. Of these, m will be elliptic fixed points and m will be hyperbolic points, alternately spaced around the T^n fixed point.

B. Accurate mapping of the phase-plane

A finer scan, using the more accurate NICAP program for the Illiac II, resulted in accurate fixed point values for the T^{33} and T^{55} mappings. These values are listed in Table 2, along with the results of a later determination of the type of point (i.e. e or E stand for elliptic and h or H for hyperbolic-type fixed points). The points belonging to an e (or h) set for T^{33} and T^{55} are listed as the successive T^{11} transforms of the initial point on the X-axis. Approximate values for the two hyperbolic fixed points adjacent to the T^{11} elliptic fixed point on the X-axis are taken from the work of Bartlett[13].

To investigate the type of motion for points initially in a neighborhood of the basic T^n fixed point or its T^{mn} multiple points we can simply have the computer print out and plot the repeatedly mapped coordinates at intervals of n or mn periods. We can then draw a smooth curve through the locus of these successively mapped points and call this a

Table 2

Exact locations and designations of fixed points of the mapping T^{mn}, for n=11 and m=1,3,5.

n	X	$\mathring{X}$	Designation
11	1.666735430	0.0	E_1
11	1.6395	0.01690	H_1
11	1.6395	- 0.01690	H_2
33	1.687355697	0.0	e_1
33	1.653501571	$-3.641919791 \times 10^{-3}$	e_2
33	1.653501570	$+3.641919722 \times 10^{-3}$	e_3
33	1.650033472	0.0	h_3
33	1.673820978	$+2.109859576 \times 10^{-3}$	h_1
33	1.673820976	$-2.109859583 \times 10^{-3}$	h_2
55	1.672374290	0.0	e(1)
55	1.661880306	$-3.119288766 \times 10^{-4}$	e(3)
55	1.668547852	$+5.276790971 \times 10^{-4}$	e(5)
55	1.668547852	$-5.276791001 \times 10^{-4}$	e(2)
55	1.661880306	$+3.119288870 \times 10^{-4}$	e(4)
55	1.660868636	0.0	h(4)
55	1.671135787	$+3.399519824 \times 10^{-4}$	h(1)
55	1.665062836	$-4.802075374 \times 10^{-4}$	h(3)
55	1.665062836	$+4.802075326 \times 10^{-4}$	h(5)
55	1.671135787	$-3.399519730 \times 10^{-4}$	h(2)

stroboscopic mapping of the initial point. This curve will be approximately elliptical and closed if the initial point is "close" to an elliptic fixed point. If, on the other hand, the fixed point is hyperbolic, then this curve will depart rapidly from it. In either case the resulting stroboscopic curve is an invariant one, since any point on it will map into some other point on the same curve (its "consequent") under T^n. Applying this technique to points near the T^{33} and T^{55} fixed points, we find that for m = 3,5 the T^{11m} elliptic or hyperbolic point on the +X-axis lies respectively to the right or left of the original T^{11} elliptic fixed point. These results are listed in Table 2.

As we move away from the nearly elliptical motions close to an elliptic fixed point (such as e_1 of the T^{33} mapping), we find that many of the points sooner or later jump into regions which contain oscillating hyperbolic invariant curves and are then quickly lost to infinity. In making a stroboscopic scan of the X-axis, with $\theta_i = 0$ and $r_i \leq 0.040$, where r_i is now the initial radial distance from the T^{11} elliptic fixed point E_1 on the X-axis, we find that this sort of jumping behavior persists for all elliptic regions down to about $r_i = 0.0090$. Now, as we approach the T^{55} elliptic point e(1) on the X-axis, the motion becomes approximately cyclic every 5 multiples of the base period (11τ) of the mappings. Plotting every fifth point we obtain counter-clockwise stroboscopic motion around the T^{11} elliptic fixed point E_1. The periods for the completion of one stroboscopic revolution increase to infinite values as we cross the outer invariant curves of the adjacent T^{55} hyperbolic points. Inside these invariant curves the periods decrease to zero when we arrive at the T^{55} elliptic point e(1) itself. As we move to the left of this

point, they quickly get large again, become infinite as we cross the inner invariant curves of the adjacent T^{55} hyperbolic points, and then start decreasing.

These approximately closed, elliptical stroboscopic motions under T^{55} continue in a clockwise sense now, no matter how close we go toward E_1 (at least down to the distance $r_i = 10^{-8}$)! There seem to be no further hyperbolic "leakages" to infinity, even though we are crossing an increasingly denser set of clusters of alternating fixed points with multiplicities greater than 5. So it seems that we have found an invariant region of stability. For, once inside the invariant curves from the T^{55} hyperbolic points, at about $r_i = 0.005$, the endpoints of the T^{11} trajectories always remain inside this region, performing approximately closed, elliptical motions about E_1. A plot of these stroboscopic motions for initial X-axis points in the range $0.0002 \leq r_i \leq 0.0090$ (for $\theta_i = 0$ again) is shown in Figure 3. The five "islands" of locally elliptical motion under T^{55} separated by five "channels" of locally hyperbolic motion under T^{55} show up clearly, as does the transition from a counter-clockwise to a clockwise sense of stroboscopic revolutions. (As we move radially outward from the point E_1 the periods for the plotted stroboscopic revolutions increase from 120 to 1040 multiples of 11τ for the inner clockwise motions; then from 1060 to 200 and back to 1060 multiples for the "island" regions; and finally from 1140 to 90 multiples for the outer counter-clockwise motions shown.)

Thus the motion near the T^{55} cluster is "stable" while the motion near the T^{33} cluster is "unstable". We need to explain this difference in behavior. As will be seen later, the invariant curves from the

Figure 3. Stroboscopic trajectories of the mapping T^{55} around the T^{11} elliptic fixed point.

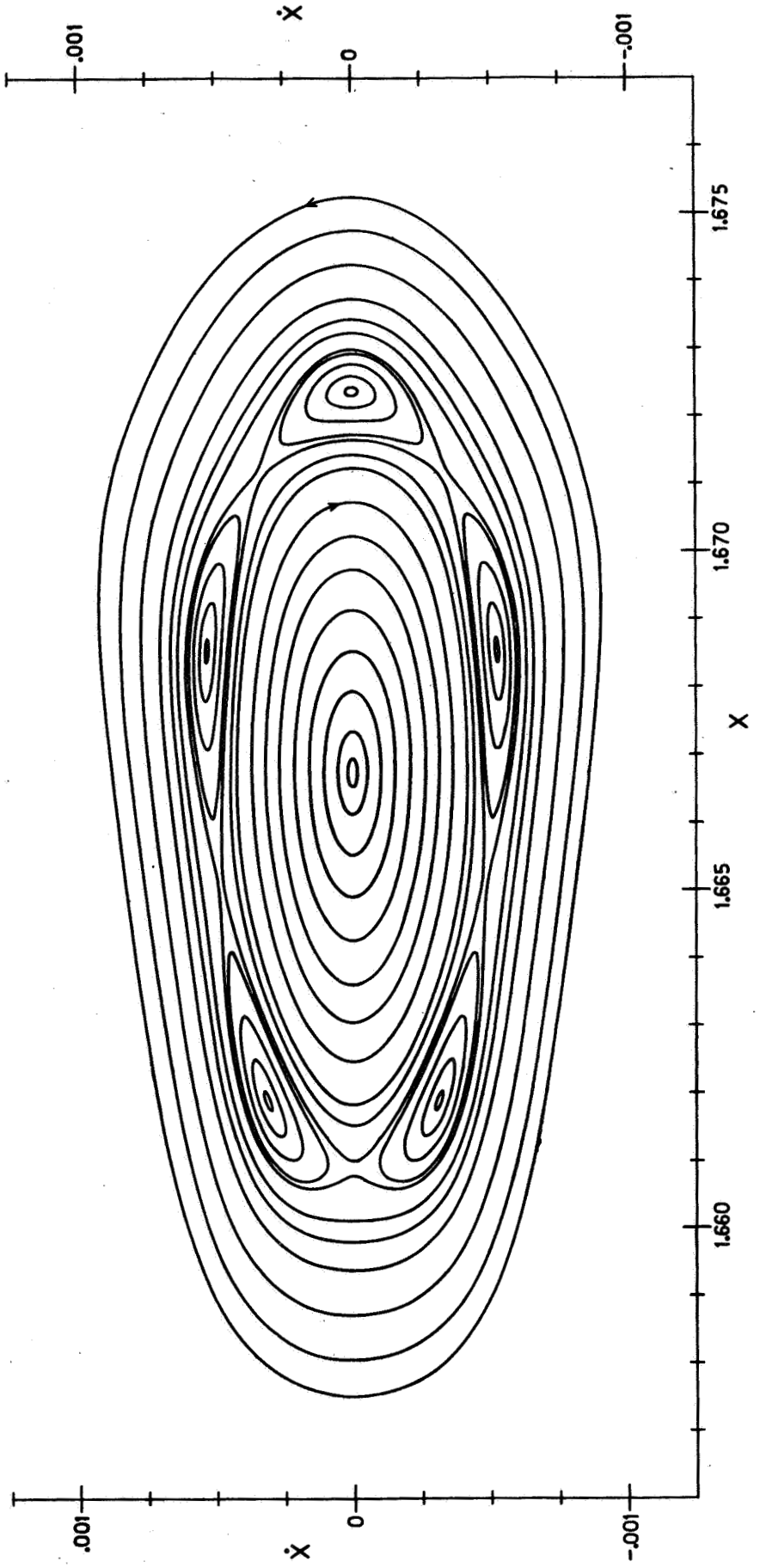
.001
0
-.001
Ẋ
1.675
1.670
1.665
1.660
X
.001
0
-.001
Ẋ

hyperbolic points of T^{33} have the general oscillation property (first demonstrated by Bartlett[13]). There do not appear to be any such oscillations of the T^{55} hyperbolic invariant curves in Figure 3. These hyperbolic invariant curves instead seem to join one another smoothly as they envelope the well-defined elliptic "islands". Perhaps, then, instability goes hand in hand with these oscillations, while stability is a result of the lack of such oscillations.

C. The mapping T^{11}

In order to see how the above apparently stable inner region coexists with the unstable outer regions, let us study the mappings for T^{11} in a region around the elliptic fixed point E_1 and large enough to include the two adjacent hyperbolic points H_1 and H_2. The invariant curves issuing from one hyperbolic point develop larger and larger oscillations as their overall motion carries them towards the nearest hyperbolic fixed points. This should hold true for both the inner and outer invariant curves, where we define "inner" as closer to the origin of our $\mathring{X}\mathring{X}$ coordinate system, and "outer" as farther away from that origin. In our case we find that the inner invariant curves move from H_2 toward H_1 with increasing oscillations, while the outer invariant curves move from H_1 to H_2. (A plot of similar hyperbolic invariant curves for the mapping $T^{12}(\tau)$ is shown in Figure 3 of reference 13).

To obtain these curves we need only pick initial points rather close to H_1 or H_2 and then map them repeatedly. From earlier discussions of motion near hyperbolic points we know that these points will move rapidly towards the invariant curves and be asymptotic to them. The initial points can be taken to be on a segment of the straight line from E_1 to H_2. At the end

of 11 periods the series of successive points will have been mapped into a new series of points forming the locus of the first mapped curve. This can be repeated for as many multiples m as desired, thus obtaining m mapped curves of the original straight line. If the range of initial radii is too small, these m curves will be disjoint. By choosing the initial interval just long enough, the m mapped curves will just overlap each other. We call one such barely overlapping mapped curve "one full oscillation" of the invariant curve. (Actually they will miss each other very slightly because two successive points on the initial straight line are at slightly different distances from the adjacent hyperbolic invariant curves.) These barely overlapping m curves can then be joined together smoothly to give a fairly accurate plot of the outgoing hyperbolic invariant curves.

In our calculations we use a section of the line between E_1 and H_2, at an angle of 211.85° to the +X-axis, with radii in the range $0.0300 \leq r_i \leq 0.0316$. Initially the scan can be in large increments of the r_i values (such as 5×10^{-5} or 10^{-5}), but eventually it becomes necessary to go to a finer grid with increments of 2×10^{-6} in r_i. The results of these mappings are plotted in Figure 4 as curve F, shown issuing from the point H_2 and moving upwards toward H_1. This is the "inner" invariant curve, as it passes to the left of E_1 (i.e. closer to the $X\mathring{X}$ origin). The outer invariant curve, plotted as curve G in Figure 4, is obtained by using a section of the line between H_1 and the point (1.716, 0.0). The angle of this line is 167.54° to the +X-axis, and the interval of initial radii covers the range $0.0750 \leq r_i \leq 0.0780$ in increments as small as 2×10^{-6}. Figure 4 also contains the reflections in the X-axis of curves F and G, labeled $\overline{F}$ and $\overline{G}$ respectively. From the time-reversal invariance of our

Figure 4. Hyperbolic invariant curves of the mapping T^{11} and their relations to those of the mapping T^{33}.

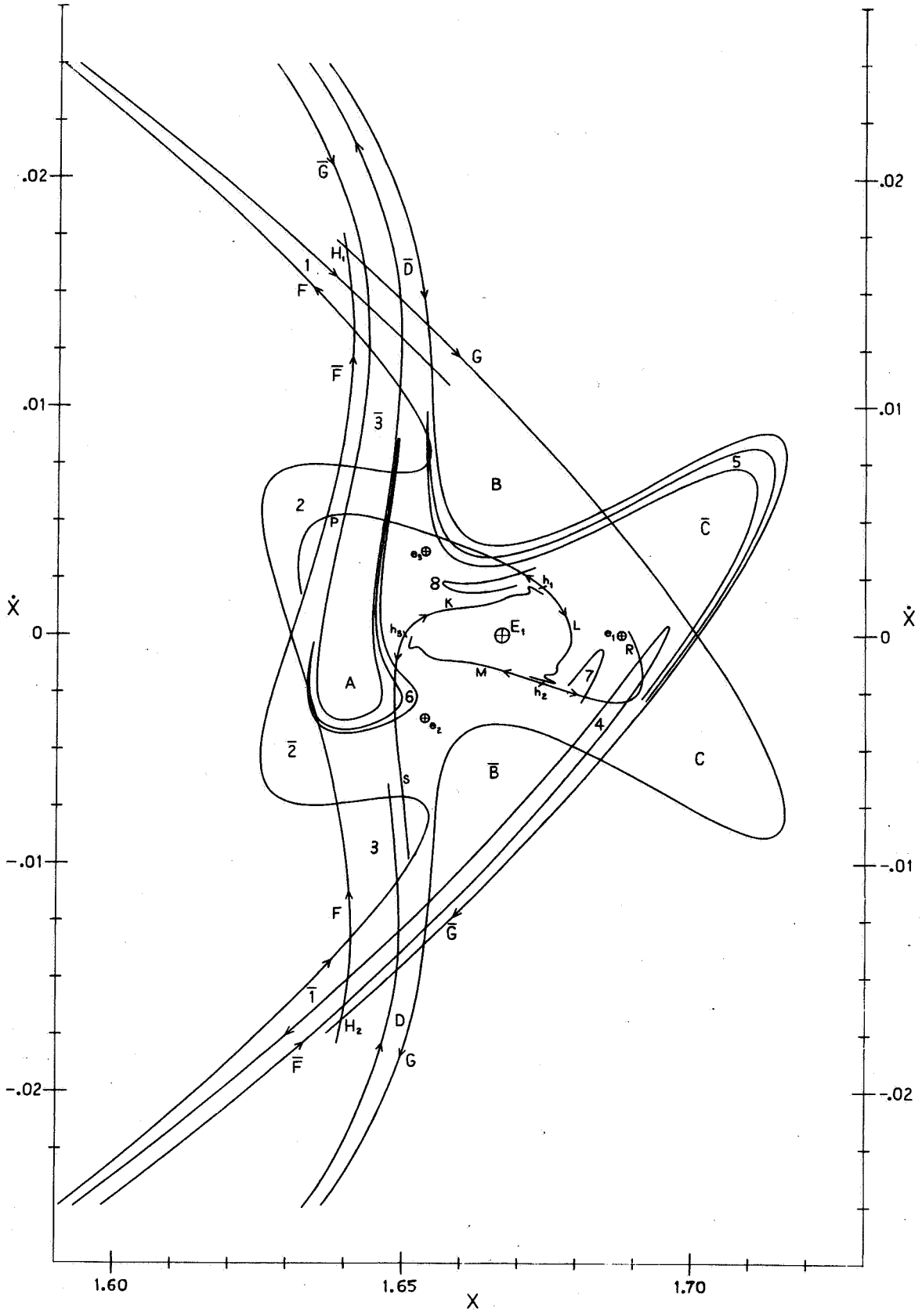
.02
.01
0
-.01
-.02
Ẋ
1.60
1.65
1.70
X
$\bar{G}$
H_1
1
F
$\bar{D}$
G
$\bar{F}$
$\bar{3}$
B
5
2
P
$\bar{C}$
$e_3\oplus$
8
h_3
K
L
h_5
$\oplus E_1$
$e_1\oplus$
R
M
7
h_2
A
6
$\oplus e_2$
4
$\bar{2}$
$\bar{B}$
C
S
3
F
$\bar{G}$
$\bar{1}$
H_2
D
$\bar{F}$
G

original equation we see that these curves are solutions not only for the motion with time running backwards, but also for the reversed motion originating at an infinite negative time and continuing with time running forwards toward t=0. Thus, for example, curve $\overline{F}$ shows a series of oscillations moving away from H_2 and becoming smoother as it approaches and intersects H_1 (as an inner invariant curve). Similarly $\overline{G}$ smooths out its oscillations as it moves away from H_1 to H_2 as an outer invariant curve.

Because of the "wild" oscillations in these curves, the "forward-going" invariant curves (F and G) do not join smoothly with their own reflections ($\overline{F}$ and $\overline{G}$), the "forward-coming" invariant curves. Instead they intersect one another (F with $\overline{F}$, and G with $\overline{G}$) an infinite number of times. The regions between successive intersections of F with $\overline{F}$ are labeled 1,2,3,...,8 when F is on the outside (with respect to E_1) of $\overline{F}$, and $\overline{1},\overline{2},\overline{3}$ when F is on the inside of $\overline{F}$ (these are reflections in the X-axis of the first set of areas). The regions between successive intersections of G with $\overline{G}$ are labeled A,B,C, and D when G is on the outside of $\overline{G}$; and $\overline{B},\overline{C}$, and $\overline{D}$ when G is on the inside of $\overline{G}$. By "inside" we now mean closer to E_1, while "outside" means farther away from E_1.

As the oscillations of the invariant curve F issuing from H_2 crowd in towards H_1, they become long and thin to conserve their phase-space area. By noting the directional arrows on the various sections of the curves F and $\overline{F}$ in Figure 4 we can see that all the points in region $\overline{1}$ will map into all of $\overline{2}$, then into all of $\overline{3}$, and so on into the <u>inside</u> of the hyperbolic invariant curves. But these points in $\overline{1}$ come from a longer, thinner oscillation $\overline{0}$ (not shown) that is closer to that incoming hyperbolic invariant curve which intersects H_2 from a direction exactly

opposite to the incoming curve $\overline{G}$. That is to say, these points may come from regions quite distant from E_1 and yet still get in close to E_1. Similarly we can see the fate of points within the "inner" region 6. They will map successively into regions 5,4,3,2, and 1 and then into a longer, thinner region which is closer to the outgoing hyperbolic invariant curve through H_1 (i.e. into a region which is a simple reflection of region $\overline{0}$ above, the "antecedent" of region $\overline{1}$). Thus these points initially within an inside region will soon escape to regions quite distant from their original region. In fact, as Bartlett has shown[13], these oscillating curves around the T^{11} fixed point E_1 will intersect similar invariant curves of the T^{10} mapping, so that some of the points in the region between these two sets of intersecting curves can be carried even further outward, eventually reaching infinity. The time-reversed motions will analogously bring points in from infinity to a region close to E_1.

This same discussion applies to the regions formed by the intersections of curves G and $\overline{G}$. Thus points from infinity can move into region $\overline{D}$ and then map into $\overline{C},\overline{B},\overline{A}$ (not shown), and so on into the inside of the invariant curves. Similarly, inside points within region A (or its unplotted antecedents) will map successively into regions B,C,D and then quickly move out directly to intersect the T^{10} hyperbolic oscillations. This is easy to visualize because region D lies outside that incoming hyperbolic invariant curve to H_2 which forms an outer bound to the (incoming) oscillations of curve $\overline{F}$. This shows indirectly that the outgoing oscillations of curve F also reach infinity via intersections with T^{10} oscillations. To see why, consider the reflected curve $\overline{F}$ coming in from the same distant regions reached by curve F. Points inside $\overline{1}$ will

map into $\overline{2},\overline{3}$, and so on. But notice that $\overline{3}$ intersects region A (as $\overline{4}$ will intersect B), so that points in the mutual intersection of regions $\overline{3}$ and A will map into B, then C,D, and so on out directly to the T^{10} oscillations. This may sound like a tautology, but nonetheless the observed facts are that points do escape from inner regions around E_1 to infinity.

We now have a mechanism whereby points may escape to infinity even when relatively close to an elliptic fixed point. Going back to Figure 4 we see that the inverse (time-reversed) maps of region 2 (i.e. regions 3,4, 5,6,...) should eventually fill a great deal of the space inside the inner and outer invariant curves because of their property of preserving phase-space areas. In principle we should be able to keep mapping region 2 backward in time or $\overline{2}$ forward in time, which in reality is how we actually make the maps (it is more convenient here to plot their reflections). Then in the limit perhaps we would end up with some envelope of the successively mapped regions which would coincide with some invariant inner region of stability.

Unfortunately we cannot do this in practice, for the mapped regions get progressively thinner and more convoluted. Region 5 is the last relatively complete region shown; under a time-reversed (inverse) mapping of T^{11} the section of region 5 lying inside region $\overline{C}$ gets "squirted" out to region $\overline{D}$, the antecedent of $\overline{C}$, and only the tip of the mapped region 6 re-enters the inside of the invariant curves. For the next few inverse maps we can only plot very small pieces of the mapped regions such as regions 7 and 8 in Figure 4. These small "hairpin" regions correspond to just a short segment of the inside portion of region 6 in the neighborhood of the bump near the number 6! We will therefore have to resort to some other approach in order to continue the investigation.

D. The mapping T^{33}

Since a knowledge of the oscillating invariant curves for T^{11} has helped us to explain the escape mechanism, let us next find these curves for T^{33}. (Referring to Figures 4 and 2 we note that the T^{11} oscillations already discussed have penetrated closer to E_1 than the cluster of T^{44} points, so we may bypass them and instead study the next cluster of points closer to E_1.) For this purpose we draw the line between e_1 and h_1 at an angle of 171.14° to the X-axis, and scan the line segment with initial radii in the range $0.0127 \leq r_i \leq 0.0135$ using increments of about 5×10^{-6}. Successive mappings then yield the hyperbolic invariant curves for T^{33}.

The invariant curve issuing from h_1 develops oscillations as it moves toward h_2, and is partially plotted as curve 2 in Figure 5. This curve 2 is not an inner invariant curve with respect to e_1 (i.e. is closer to our E_1 origin than is e_1), with its motion counter-clockwise about e_1. On the other hand the T^{11} invariant curve from H_1 is an outer invariant curve with respect to E_1 (i.e. is farther from the $X\text{-}\mathring{X}$ origin than is E_1), with clockwise motion about E_1.

By getting computer printouts of every 11τ periods we can easily obtain the T^{11} and T^{22} maps of curve 2 by plotting the points for $t=11\tau,44\tau,77\tau,\ldots$ and $t=22\tau,55\tau,88\tau,\ldots$ (since curve 2 comes from points at $t=0,33\tau,66\tau,\ldots$). The T^{11} transform of curve 2 is plotted as curve 3, while the T^{22} transform of curve 2 is shown as the more detailed curve 1. These curves and their mirror reflections in the X-axis (labeled $\overline{1},\overline{2}$, and $\overline{3}$) are <u>all</u> the "<u>inner</u>" T^{33} hyperbolic invariant curves (i.e. they lie closer to E_1 than e_1,e_2, or e_3 and so we designate them as "inner" with respect to E_1). To obtain the "outer" invariant curves (again outer with

Figure 5. Hyperbolic invariant curves of the mapping T^{33} and their relations to those of the mapping T^{55}.

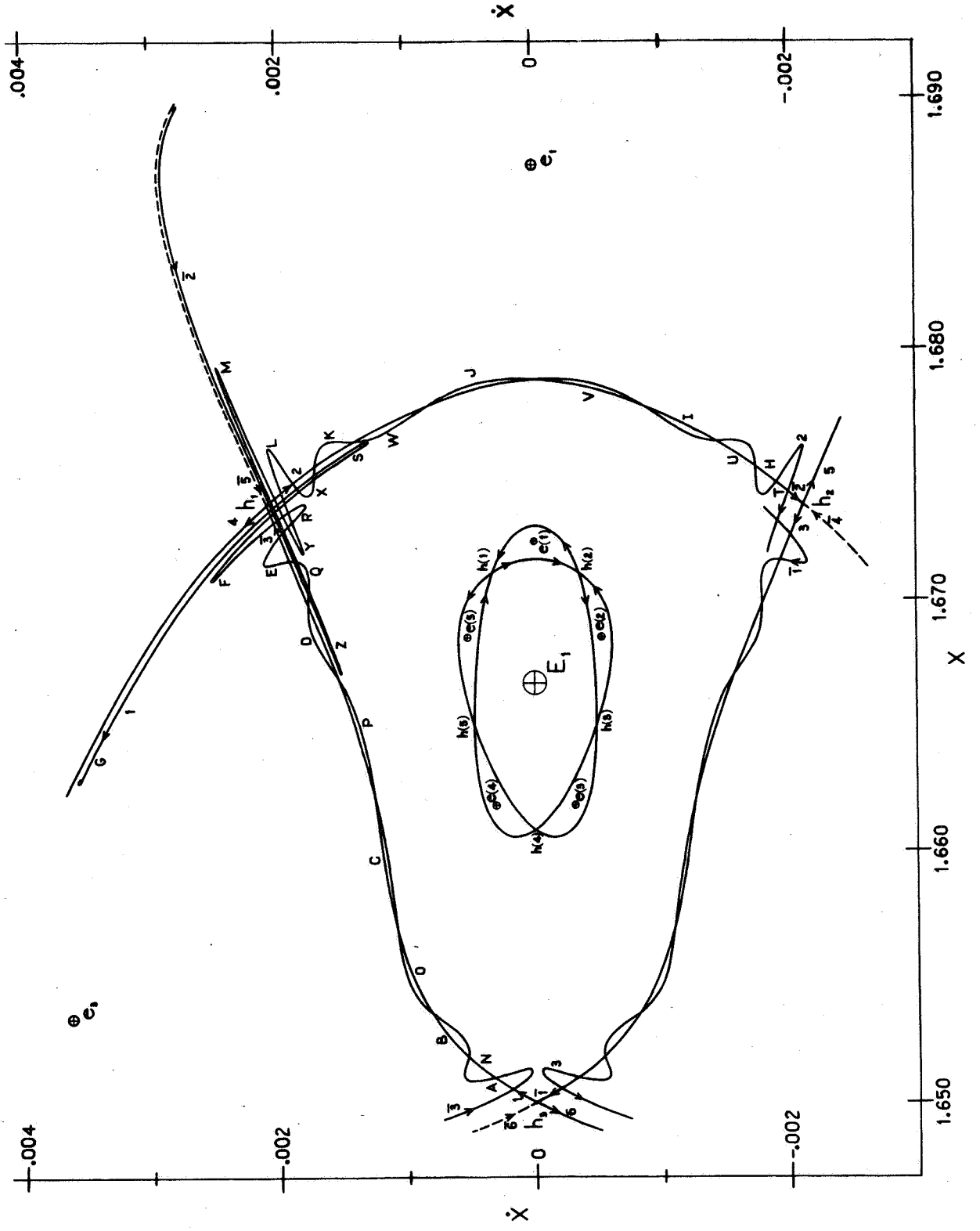
.004
.002
0
-.002
Ẋ
1.690
1.680
1.670
1.660
1.650
X
⊕e₁
⊕e₂
⊕E₁
h₁
h₂
h₃
h₄
h(1)
h(2)
h(3)
h(4)
h(5)
h(6)
⊕e(1)
⊕e(2)
⊕e(3)
⊕e(4)
⊕e(5)
A
B
C
D
E
F
G
H
I
J
K
L
M
N
O
P
Q
R
S
T
U
V
W
X
Y
Z

respect to E_1, as they extend farther from E_1 than e_1, e_2, or e_3), the easiest method is to pick several points along a short segment of the "inner" outgoing curve 1 which is very close to the T^{33} hyperbolic point h_3. Extending this short segment of curve 1 through h_3, we can then map points on this new extended straight-line segment of the "outer" outgoing invariant curve. The results are partially plotted as curve 6 in Figure 5. The T^{11} and T^{22} maps of this invariant curve are plotted as curves 4 and 5 respectively. The reflections of these 3 "outer" outgoing invariant curves are plotted as curves $\overline{4}, \overline{5}$, and $\overline{6}$, and complete the picture for all the T^{33} "outer" invariant curves (about E_1).

We shall discuss these intersecting oscillating invariant curves by comparing them to the picture for the T^{11} mapping. Looking at the intersections of curves 1 and $\overline{3}$ we can predict that points initially between the invariant curves in region A will map successively into region B,C, D,E,F,G,... outside the invariant curves along outgoing invariant curve 4. Similarly exterior points in region N will map into regions O,P,Q,R,S,... and become interior points. The same phenomena occur for the intersections of curves 2 and $\overline{2}$ or 3 and $\overline{1}$. For example, for the former, exterior points in region M (near the incoming invariant curve $\overline{5}$) map into interior points in region H via the regions L,K,J, and I. Interior points in region Y become exterior points in region T via regions X,W,V, and U. Here we are again using "interior" to mean closer to E_1, and "exterior" to mean farther away from E_1. Thus the term "exterior" here would be called "interior" (to the regions around e_1, e_2, or e_3) if we were investigating the stability of e_1, e_2, or e_3 rather than E_1. (In effect we have already investigated e_1 by observing that the T^{11} oscillations reach in close to it eventually.)

But now there are additional complications. Not only, for example, do curves 2 and $\overline{2}$ intersect one another, but their (inner) regions of mutual intersection are themselves intersected by curves $\overline{1}$ and 1 (issuing to and from the nearby T^{33} hyperbolic point h_3)! In the case of the T^{11} oscillations the nearest hyperbolic points to H_1 and H_2 are a good distance away along the cluster of 22 alternating T^{11} fixed points surrounding the XX origin. For T^{33} the nearest hyperbolic point to h_1 and h_2 is just the equivalent satellite multiple point h_3. This same pattern of mutual intersection of neighboring inner oscillations similarly occurs when curves 2 and $\overline{3}$ intersect the regions bounded by curves 3 and $\overline{1}$, or when curves 3 and $\overline{2}$ intersect the regions bounded by curves 1 and $\overline{3}$.

There are several important consequences of this mutual intersection property of the inner oscillations. One is that points from the 3 outer regions (bounded by the outer invariant curves) can get into the inner region, and vice versa. Consequently points from the outer region surrounding e_3, for example, can reach the inner region around E_1 (via curve $\overline{3}$) and then pass out to the outer region surrounding e_1 (via curve 2). These points might eventually reach the region of e_2, or even e_3 again by the same device. A second result is that the areas of the outer oscillations are considerably smaller (in proportion to the total "outer" area) than those for the T^{11} mapping. It thus seems unlikely that these oscillations will fill up the space around, for example, e_1 to the extent that the T^{11} oscillations did around E_1. But these outer oscillations have the same area as the inner oscillations, and so we are led to suspect empirically that the inner region around E_1 will be relatively free of inner oscillations from the T^{33} mapping crowding in toward E_1 (as they did for the T^{11} maps).

A third consequence is that some points will move around the periphery of the inner region for several entire stroboscopic revolutions before escaping to the outer regions. To see this let us consider points inside area Q of curve 1. Those points inside the rectangular area which is the mathematical intersection of regions Q and Z will map into the transforms of this area, i.e. the regions $R \cap Y$, $S \cap X$, and so on. But since these points lie inside region X, they will map subsequently into regions W,V,U,T, and so on into the outer regions. But let us now consider points inside the tip of region Q but not inside $Q \cap Z$. These will map into corresponding points in the inner tip of R,S, and so on. But the tip of S does not intersect W, so that the tip of the T^{11} map of S (call it S') will not intersect region V. (However a portion of S' will intersect region W, namely the T^{11} map of the region $S \cap X$, since X transforms into W.) The tip of each successive map of S' will move towards h_2 in this fashion, not intersecting regions U or T (which are transforms of V), and thus will remain on the inside. By the same token the tip will not intersect any of the inner regions I,H,... because these are transforms of regions L,K,J,... which in turn were not intersected by region S or its antecedents. (These calculations were in fact carried out, but are not shown in Figure 5 because of the difficulty of getting enough mapped points for a continuous curve.)

So the successively mapped tip will travel on toward h_2 on the inside, paralleling the inner oscillations of curve 2. Once close to h_2, the mapped tips enter the domain of tight oscillations of curve $\overline{1}$ as it moves left towards h_3. Now there are several alternatives. Since the tip of S' (too long and thin to be shown) extends below the X-axis at an angle $\neq 90°$, this tip of S' will intersect its own mirror image in the X-axis, $\overline{S'}$ (which is just the same inner oscillation of curve $\overline{1}$ as S'

is of curve 1). Now $\overline{S}'$ is the antecedent of $\overline{S}$, which in turn maps successively into regions $\overline{R},\overline{Q},\overline{P},\overline{O},\overline{N}$, and so on to the outer region. Thus if our mapped points in the tip of S' lie inside the region defined by $S' \cap \overline{S}'$, they will eventually go to the outer region along outgoing invariant curve 6. But if they still lie in the tip of S' and not inside $S' \cap \overline{S}'$, they will move from h_2 to h_3 on the inside, paralleling curve $\overline{1}$ but not intersecting it. So these points will then move around to the neighborhood of h_3 and into the influence of curve $\overline{3}$. There the same alternatives and processes will take place as above. Thus we can see that some points originally inside the region Q can move all the way around the inside periphery of the invariant curves, while others will gradually leak out near h_2 or h_3 (or h_1, h_2, or h_3 on the next revolution, etc.). Again because of the great stretching and twisting of each successive map of the inner oscillations, it is impractical to determine exactly which points (in a given initial region like Q) leak out and when, and which points circulate around the inside periphery and for how long. In principle it can be done.

But our main concern is with the vast majority of interior points that eventually leak to the outer regions around e_1,e_2, or e_3. To investigate this let us study both the T^{33} and the T^{11} mappings simultaneously. Referring back to Figure 4, the curves labeled K,L, and M are the 3 inner invariant curves of T^{33} plotted in Figure 5 as curves 1,2, and 3 respectively. The curves P,R, and S in Figure 4 are more complete plots of the 3 outer invariant curves of T^{33}, partially plotted in Figure 5 as curves 4,5, and 6 respectively. We recall from Figure 5 that the interior points which do escape to the outer regions do so by moving outward with the (outer) oscillations of curves 1,2, and 3, that is, along the general direction of the outer invariant curves 4,5, and 6 respectively. Looking

at Figure 4 we see the connecting link to infinity: the outer invariant curves P,R, and S (i.e. curves 4,5, and 6) intersect the time-reversed oscillations of the T^{11} mapping! Thus, in particular, interior points which escape (via curves 2 and 5 of Figure 5) along outer invariant curve R in Figure 4 will quickly intersect region 7 of the T^{11} mapping. In one more map of T^{33} (three more under T^{11}) these points will be inside region 4, and will then move successively under T^{11} through regions 3,2,1 to infinity. The same applies to points moving out along invariant curve S to intersect region 6, or those moving out along invariant curve P to intersect region 8. (Note the double intersection of R with 4, corresponding to similar double intersections of S with 6 and P with 5.)

A more detailed plot of the relationship between the T^{33} and T^{11} mappings is shown in Figure 6. Curve L is one of the oscillating T^{33} inner invariant curves (plotted in Figure 5 as curve 2). Curves $\overline{P},\overline{R}$, and $\overline{S}$ are incoming outer invariant curves (labeled $\overline{4},\overline{5}$, and $\overline{6}$ in Figure 5) which are simply reflections of the outgoing outer invariant curves P,R, and S of Figure 4. The directional arrows indicate the sense of the motion under T^{33}. Also plotted are the reflected regions $\overline{4},\overline{5},\ldots,\overline{14}$ of portions of the time-reversed T^{11} oscillations previously discussed. For example, $\overline{7}$ and $\overline{8}$ are reflections of regions 7 and 8 in Figure 4. Since these are reflections of time-reversed mappings themselves (for which 8 maps into 7 and so on as time goes forward), then the order of these mappings is clearly $\overline{4},\overline{5},\ldots\overline{14}$. (In fact, these are the original forward-going mappings obtained for T^{11}, and the regions plotted as $1,2,3,\ldots,8$ in Figure 4 are in reality themselves the mirror reflections of these original mappings.) The plot shows vividly how the inner T^{11} oscillations wrap themselves around the T^{33}

Figure 6. Hyperbolic invariant curves of the mapping T^{33} and their relations to those of the mappings T^{11} and T^{55}.

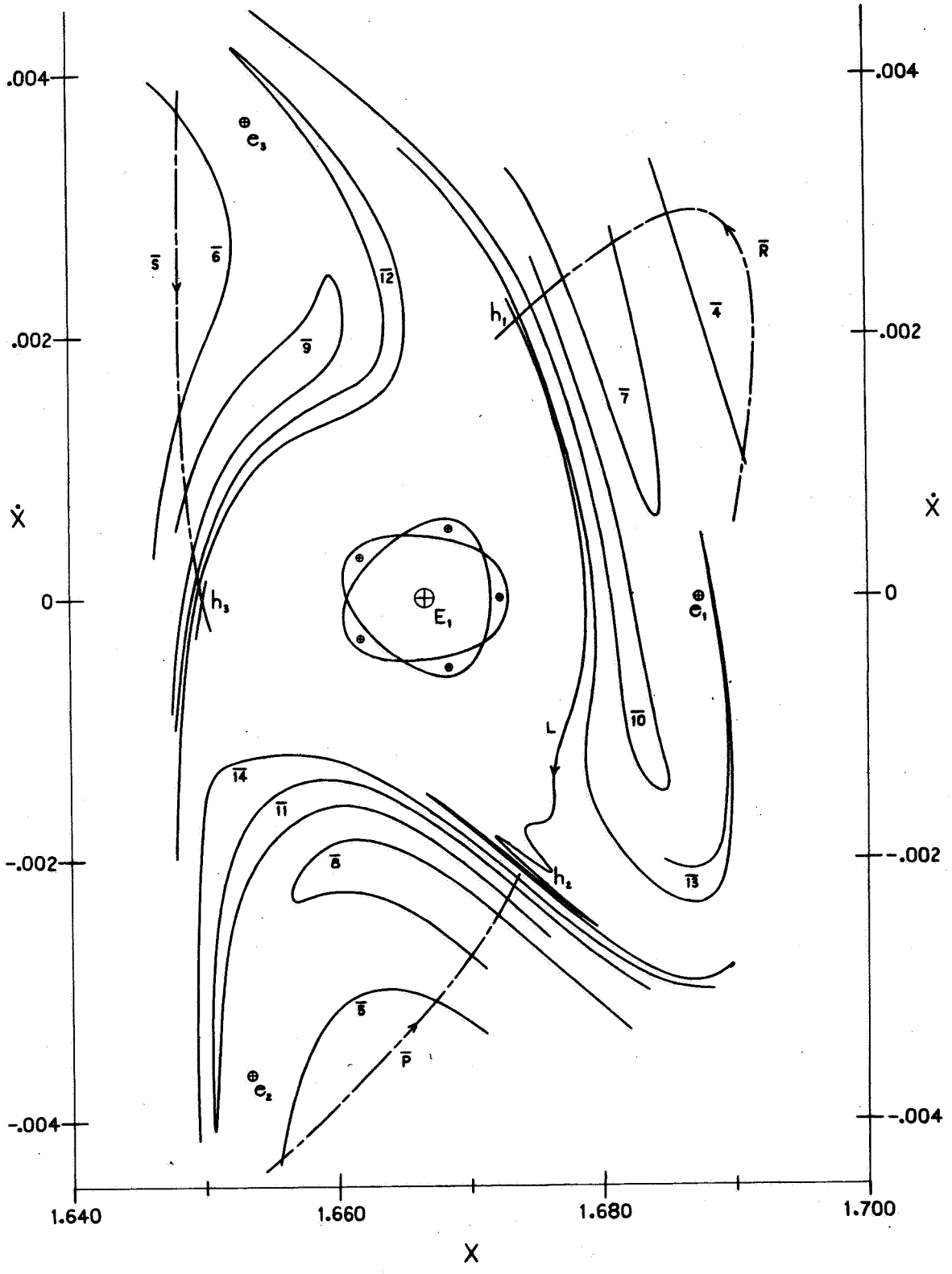
.004
.002
0
-.002
-.004
Ẋ
1.640
1.660
1.680
1.700
X
$\oplus e_3$
$\oplus E_1$
$\oplus e_1$
$\oplus e_2$
h_1
h_2
h_3
L
$\bar{R}$
$\bar{P}$
$\bar{4}$
$\bar{5}$
$\bar{6}$
$\bar{7}$
$\bar{8}$
$\bar{9}$
$\bar{10}$
$\bar{11}$
$\bar{12}$
$\bar{13}$
$\bar{14}$

elliptic fixed points in cycles of 3 (e.g. note the similarity and proximity of regions $\overline{5},\overline{8},\overline{11}$, and $\overline{14}$ as they wrap around e_2). It also shows that <u>in the limit</u> as $t \to \infty$ these T^{11} oscillations crowd in along $\overline{P},\overline{R}$, and $\overline{S}$ to the invariant curves of the T^{33} mapping (curves 1-6 in Figure 5, or curves K, L,M,P,R, and S in Figure 4). Finally, the plot clearly shows the 3 channels (along invariant curves P,R, and S) through which points can escape from the T^{33} mapping to the T^{11} mapping.

We therefore can understand the complete mechanisms for the escape of points from inside the T^{33} hyperbolic invariant curves out to infinity. The first link in the chain of mechanisms is the intersection of the hyperbolic invariant curves of the T^{33} and T^{11} mappings. The subsequent links are the intersections of the T^{11} mapping with the mapping of T^{10}, that of T^{10} with T^9, and so on out to T^1 and infinity. The key word is <u>intersection</u>.

E. <u>The mapping T^{55}</u>

We can now ask if the same mechanism allows escape from inside the T^{55} hyperbolic invariant curves. Our original stroboscopic calculations seemed to show smooth (non-oscillatory) behavior for T^{55}. The first strong indication that this behavior does occur has already been noted: the apparent inability of the T^{33} hyperbolic oscillations to fill up the region inside the T^{33} hyperbolic invariant curves and around E_1 (as do the T^{11} curves). Apparently the inner oscillations of the T^{33} invariant curves do not come close to the cluster of 10 fixed points of the T^{55} mapping, but instead stretch out thinner and thinner along the inside periphery of their mutual outer boundary, far away from the T^{55} invariant curves.

But to be positive of this apparent non-intersection of the T^{33} and T^{55} curves (just as for the T^{11} curves, we are here limited in practice

from mapping very many oscillations of the T^{33} curves) it is necessary to study the T^{55} invariant curves to a high degree of accuracy. The simplest approach is to study the inner invariant curve issuing from the T^{55} hyperbolic fixed point on the X-axis (h(4) in Table 2), analogous to curve 1 in Figure 5. The first step is to choose initial points on the X-axis very close to that hyperbolic fixed point as the origin of a polar coordinate system (with $r_i \leq 10^{-6}$ and $\theta_i = 0$). We can then make a stroboscopic plot of their subsequent motions under repeated mappings of T^{55}. These points will rapidly approach the outgoing hyperbolic curve, which is itself asymptotic to a short straight-line segment through h(4). Knowing the angle this asymptote makes with the X-axis, we can then map a segment of this radial line for many successive applications of T^{55}.

In our particular case the asymptote makes an angle of about 15.9° with the X-axis, and the range of initial radii used is $7.00 \times 10^{-7} \leq r_i \leq 8.15 \times 10^{-7}$ with increments as small as 2×10^{-9}. Once again it is useful to print out our coordinates every 11 periods, so that we can plot the invariant curve issuing from the original hyperbolic point h(4) <u>or</u> from any of the other 4 hyperbolic points which are transforms of it (see Table 2). In particular the choice of the invariant curve issuing from h(3) is convenient because its oscillations (if they exist) would crowd into the asymptote to h(4) which has already been determined above.

The results of these calculations differ strikingly from those for the T^{11} or T^{33} invariant curves. First of all there is a pronounced increase in the stroboscopic period of the motion. Whereas points on the T^{11} or T^{33} invariant curves cover most of the distance between alternate hyperbolic points in 4 or 6 multiples of the basic mapping (11τ or 33τ),

points on the T^{55} invariant curves require more than 100 multiples of the basic mapping of 55τ periods. Secondly, as points in the original radial segment near h(3) slowly approach h(4), they do develop a small irregular "scatter", undoubtedly due to the accumulation of truncation and inversion errors after so many successive mappings by the computer. [Note that 100 maps under T^{55} correspond to 5500 periods of τ, or 11,000 half-period calculations. Now each of these calculations involves 9 or 10 computational steps such as basic arithmetic operations, square roots, and elliptic function interpolations and inversions. These latter computations in turn involve separate subprograms with many calculational steps themselves (on the order of 10 to 100). Thus each final plotted point may require some 10^6 or 10^7 arithmetic operations! If the computer truncation error is in the thirteenth decimal place (as it is on the Illiac II computer), then this error might accumulate constructively for 10^6 operations or more and hence show up in even the seventh decimal place. In our calculations the scatter shows up in the <u>eighth</u> decimal place, entirely consistent with the predictable errors.]

However, there is no tendency of the T^{55} invariant curves to develop any <u>regular</u> pattern of oscillations analogous to the T^{11} or T^{33} invariant curves. The 46 circled points in Figure 7 are results of the $442^{\underline{nd}}$ successive application of the T^{11} mapping to <u>each</u> of 46 points on the original radial segment through h(4) (with $\theta_i = 15.9°$ and $7.00 \times 10^{-7} \leq r_i \leq 8.15 \times 10^{-7}$). These circled points are the results using an elliptic function inversion-routine error of $E = 10^{-12}$, while those points inside squares are the results for $E = 10^{-11}$. The smooth continuous curve is a quadratic, least-squares computer fit of the 46 circled points for

Figure 7. Computer fluctuations over the 442$^{\underline{nd}}$ "oscillation" of one hyperbolic invariant curve of the mapping T^{55}.

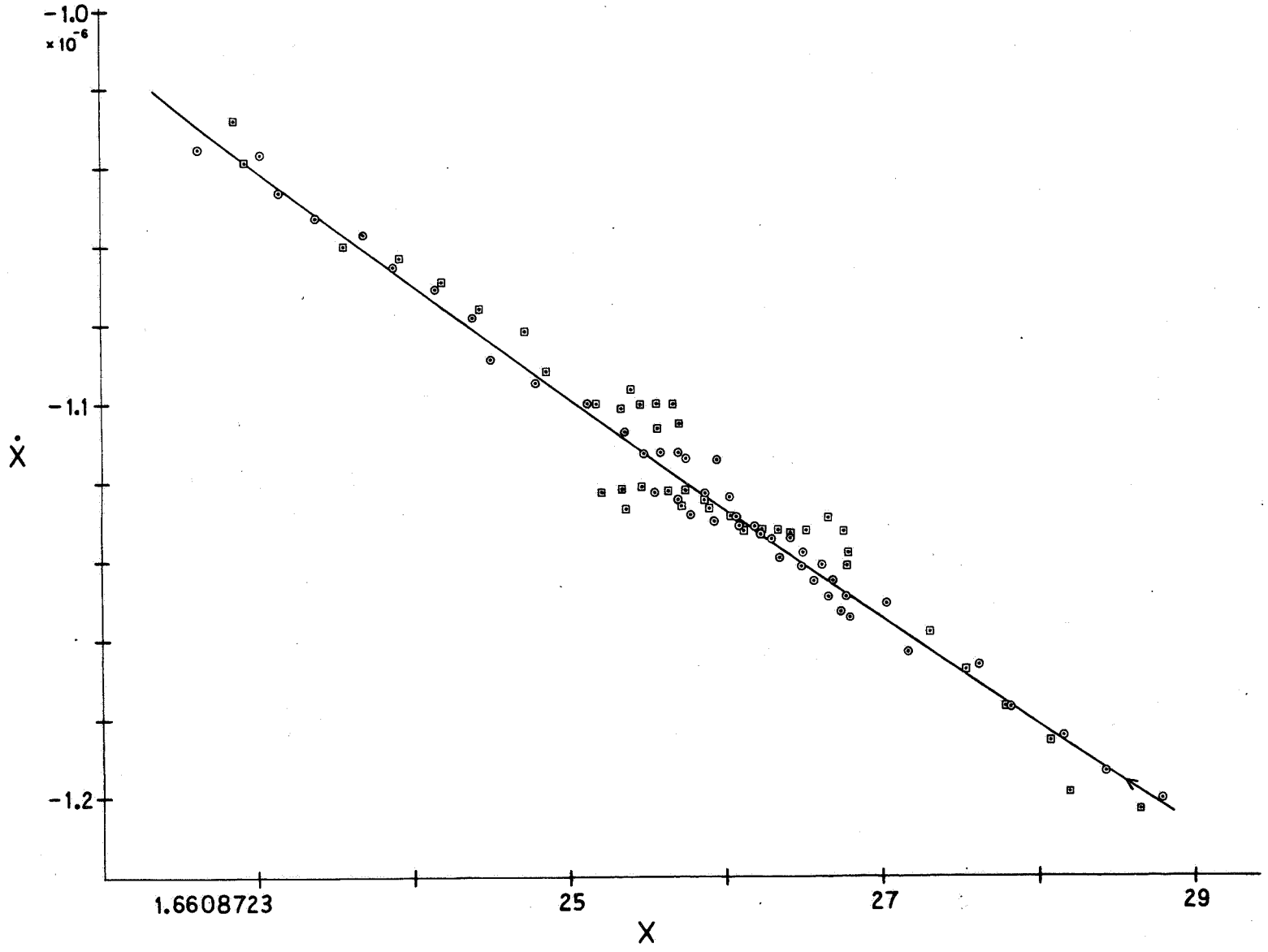
-1.0
× 10⁻⁶
-1.1
-1.2
Ẋ
1.6608723
25
27
29
X

$E = 10^{-12}$ (the best possible accuracy for the inversion routines). This plot clearly shows the nature and magnitude of the random scatter of mapped points. Also, this mapped section does indeed correspond to a "full period of an oscillation" of the T^{55} invariant curve. For, the first circled point in the lower-right corner of Figure 7, which is a map of the point with $r_i = 7.00 \times 10^{-7}$, transforms under T^{55} into a point lying below and to the right of the last circled point in the upper-left corner of the plot, a map of the point with $r_i = 8.15 \times 10^{-7}$. That is, the stroboscopic mapping of the original radial segment at the end of the $447^{\underline{th}}$ successive application of T^{11} overlaps the $442^{\underline{nd}}$ mapping of the same original radial segment. This overlapping of the ends of the mapped segment with the next T^{55} map of that segment is what we mean by a "full period of one oscilllation" of the T^{55} invariant curve.

The most convincing contrast between the behavior of this T^{55} invariant curve and that of the T^{11} or T^{33} invariant curves is the phase-space area occupied by any one oscillation of the mapping. Using Figures 4 and 5 we can measure the phase-space area enclosed by one of the T^{11} or T^{33} oscillations, for example, region 3 in Figure 4 and region E in Figure 5. For the randomly scattered points of the T^{55} invariant curve in Figure 7 we can simply connect all points in a piecewise (discontinuous) fashion and then measure the area of the largest areal fluctuation. The results are

$$\left\{ \begin{array}{lll} T^{11}: & A_{11} \cong 5.65 \times 10^{-5} & (\dot{X}\dot{X} \text{ units}) \\ T^{33}: & A_{33} \cong 1.4 \times 10^{-7} & (\dot{X}\dot{X} \text{ units}) \\ T^{55}: & A_{55} \cong 8 \times 10^{-17} & (\dot{X}\dot{X} \text{ units}) \, . \end{array} \right\} \qquad (22)$$

Now the ratio $(A_{11}/A_{33}) \cong 400$, so that if we use this same ratio for (A_{33}/A_{55}) we might expect $A_{55} \cong 10^{-10}$ ($X\dot{X}$ units). What we actually find is that A_{55} is 10^6 times smaller than this area, suggesting that A_{55} is almost, if not exactly, zero. In fact, recalling that computer truncation errors may build up to 10^{-8} in both X and $\dot{X}$ after long periods of time, we see that the product of the predictable errors in X and $\dot{X}$ agrees with the largest areal fluctuation found for the T^{55} mapping.

Having thus determined, to the 10^{-12} accuracy of the Illiac II computer, that there exist no oscillations in the T^{55} hyperbolic invariant curves, we can now look at the composite picture of all of the T^{55} hyperbolic invariant curves. The (inner) invariant curve issuing from h(3) approaches h(4) via the radial asymptote to h(4) which makes an angle of $360° - 15.9° = 344.1°$ to the X-axis. In what follows we assume that our point lies an infinitesimal distance from the true mathematical invariant curve, and that we can perform our T^{55} mappings with extreme precision. After repeated applications of T^{55}, our point slowly emerges near the outer invariant curve at an angle around $180° - 15.9° = 164.1°$. Referring to the stroboscopic map of the region shown in Figure 3 we see that the point will now move around the outside of the fixed point e(4) and will then proceed into fixed point h(5). But now it will move towards the X-axis and along an inner invariant curve. It will next go around e(5) on the inside and then head out into h(1). Next the point will cross the X-axis with an intercept $(X_r,0)$ to the right of e(1) and then proceed to h(2). In like manner the point will move inside e(2), through h(3), outside e(3), through h(4), inside e(4), through h(5), outside e(5), through h(1), then cross the X-axis with an intercept

$(X_\ell, 0)$ to the left of e(1), next pass through h(2), and finally move outside e(2) and return to h(3) along the same initial invariant curve. This motion represents one complete stroboscopic revolution.

Therefore the union of the forward-going and the forward-coming (reflected) invariant curves is in reality <u>one</u> continuous, smooth curve with an angular period of 4π radians. It simultaneously bounds the inner region as well as the 5 outer "islands" of T^{55} elliptic fixed points. This curve, then, is what we may properly call the <u>continuous doubly-periodic invariant curve</u> of the T^{55} mapping.

Determining curves which lie very close to this T^{55} invariant curve is an easy matter on the computer. We now make long-period stroboscopic mappings under T^{55} of a series of points in an interval of the X-axis which brackets the inner invariant curve intercept $(X_\ell, 0)$. From our initial stroboscopic scan of the X-axis (see Figure 3) we see that the region in question has a radius $r_i \cong 5 \times 10^{-3}$ for $\theta_i = 0$ (again using E_1 as origin of our polar coordinates). From Figure 3 it is clear that initial points with $X_i < X_\ell$ will move stroboscopically in a clockwise sense about E_1, always sticking to the inner periphery of the envelope of the T^{55} invariant curves. On the other hand, points with $X_i > X_\ell$ will move stroboscopically in a counter-clockwise sense around e(1), defining the "island" curves about the elliptic point. (Note that if we print out every T^{11} map of these points with $X_i > X_\ell$ we will simultaneously obtain the other 4 "island" curves as transforms of the original one around e(1).)

We can now take successively finer grids of initial points around the suspected X_ℓ value and calculate for about 300 mappings of T^{11} (about all that is needed before "island" motions separate from inner-region motions).

It is then an easy matter to narrow the interval down as close to X_ℓ as the errors in computation will permit. The result of this scan is the following bracketed interval for X_ℓ:

$$1.671665069 = X_{\ell 1} < X_\ell < X_{\ell 2} = 1.671665070 \ . \qquad (23)$$

Setting $X_i = X_{\ell 1}$ and applying T^{55} successively, we obtain an approximately closed curve very close to the envelope of the inner T^{55} invariant curves, as suggested by its long stroboscopic period of 2610 multiples of 11τ. Similarly by setting $X_i = X_{\ell 2}$ and now applying T^{11} repeatedly, we can obtain the 5 approximately closed curves around the 5 "islands" (we find each has a stroboscopic period of 1060 multiples of 11τ). We might note that from the mapping of the initial point $X_i = X_{\ell 2}$ (after about 530 multiples of 11τ) we can obtain an approximate value for the outer invariant curve intercept X_r of the X-axis. We find this value to be $X_r \cong 1.672981475$. (In polar coordinates about E_1, with $\theta=0$, this outer intercept has $r_r \cong 0.00624605$; likewise the inner intercept X_ℓ has $r_\ell \cong 0.00492964$.)

The resulting 6 disjoint "closed" curves, lying very close to the T^{55} hyperbolic invariant curves, are plotted in Figure 5, with directional arrows for the motion indicated on a few. The five T^{55} elliptic fixed points are plotted and labeled, while the labeled positions of the five T^{55} hyperbolic points show up clearly between the five elliptic points. The same curves are plotted in Figure 6 as one continuous closed curve, i.e. as the closed invariant curve of the T^{55} mapping, to an accuracy better than the width of the lines in the figure. This closed curve thus bounds the invariant region of stability which we have been seeking.

III. CONCLUSIONS

A. Summary of results; an application

Let us summarize the results of our detailed calculations. There does exist to the 10^{-12} accuracy of the Illiac II computer a closed region of phase-space which surrounds the T^{11} elliptic fixed point (E_1) on the X-axis and which is invariant under successive T^{55} mappings of the phase-space onto itself. Many points initially outside this region will escape to infinity after a finite number of T^{55} mappings. Some points are stable for a long time but eventually escape to infinity also, so that they can be considered to lie in a "twilight zone" that surrounds the invariant region. The outer T^{33} invariant curves oscillate and intersect the inner T^{11} oscillating invariant curves, so that points can move from near the T^{33} fixed points about E_1 into the T^{11} oscillations and escape to infinity.

However in our particular case the mutual intersection of oscillating invariant curves which correspond to multiples of the basic (T^{11}) mapping terminates at the T^{33} level. The inner oscillations of the T^{33} mapping do not intersect the outer hyperbolic invariant curves of the T^{55} mapping which apparently have no oscillations. The union of all the T^{55} hyperbolic invariant curves is actually one continuous closed curve with an angular period of 4π radians. This curve bounds a stable region around the T^{11} elliptic fixed point E_1.

This region of stable motions consists of 6 cells: a large inner region, plus 5 smaller "islands" which surround the 5 elliptic fixed points of the mapping T^{55}. The inner region has a generally flat elliptical shape but has 5 distinct bulges toward the 5 hyperbolic points of T^{55}. Points initially inside this inner region always remain inside the

region under successive applications of the mapping T^{11}. They execute clockwise, almost-elliptical motions under successive mappings of T^{55}.

For the purpose of comparison let us arbitrarily select the inner, almost-elliptical motion generated by successive T^{55} mappings of the initial point with $\theta_i = 0$, $r_i = 0.0045$, which is just inside the inner hyperbolic invariant curves of the T^{55} mapping. Next let us match an ellipse to this motion at two points on the curve, for example at 0° and 90°. Identifying the radii at these two angles with the semi-major and semi-minor axes of the ellipse respectively, we calculate the corresponding "standard" eccentricity to be $e_s = 0.995635$. The actual deviations of the mapped motions from a "standard" ellipse which has an eccentricity e_s are obtained by calculating the ratio of the mapped radius r_1 at some angle θ_1 to the polar radius r_e of a standard ellipse for the same angle θ_1. This standard ellipse is completely specified by $e_o = e_s$ and a_o values. We then use the initial radius r_i at $\theta_i = 0$ for the semi-major axis a_o. The value of r_e at the mapped angle θ_1 is given by the equation

$$r_e(\theta_1) = a_o \sqrt{\frac{1-e_o^2}{1-e_o^2 \cos^2\theta_1}} \quad . \tag{24}$$

We now stroboscopically map the initial point $\theta_i = 0$, $r_i = r_\ell = 0.004929639$ in order to obtain a curve $r_1(\theta_1)$ very close to the inner invariant curves of T^{55} which bound the inner cell. A plot of the results for the ratio r_1/r_e as a function of θ_1 around this mapped curve (using $a_o = r_i = r_\ell$) is shown in Figure 8. This plot shows a large 19% deviation in the direction of h(4), 15.8% deviations toward h(1) and h(2), and 9.7% deviations toward h(3) and h(5). Minimum deviations are about 2% in the directions

Figure 8. Deviation from a standard ellipse of a curve very close to the union of inner hyperbolic invariant curves of the mapping T^{55}.

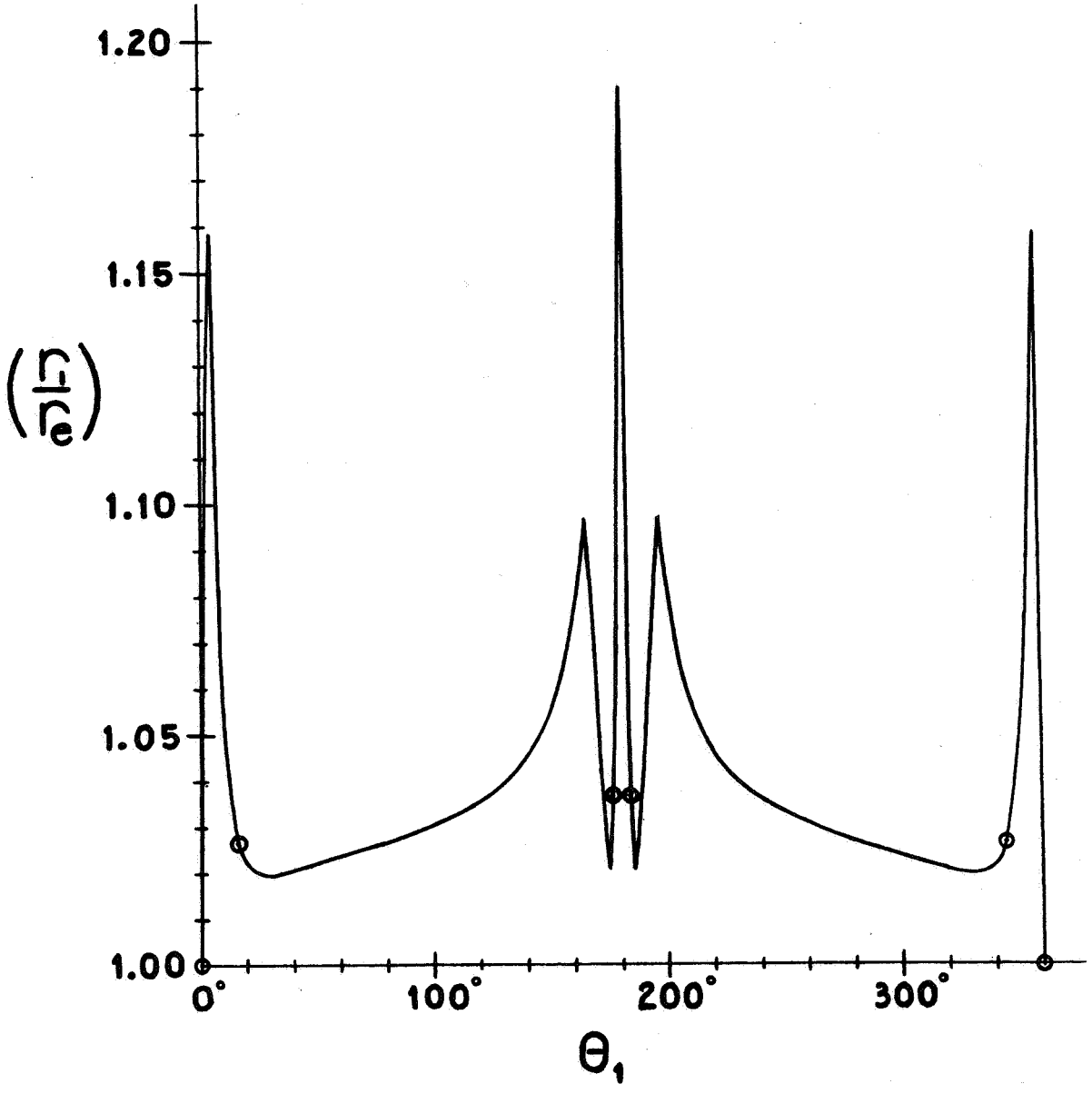
1.20
1.15
1.10
1.05
1.00
$\left(\frac{\sigma}{\sigma_e}\right)$
0°
100°
200°
300°
θ_1

of e(2), e(3), e(4), and e(5). (The values of r_1/r_e for these T^{55} elliptic points are indicated by small circles.) Thus, very close to the outer edge of the inner invariant cell the mapped motions deviate from our very flat standard ellipse for all non-zero angles. Nevertheless the concept of a standard ellipse does constitute a good way of comparing a wide range of mapped motions around E_1.

Points lying initially inside any one of the 5 "island" regions will always remain inside that particular "island" for successive mappings of T^{55}, but will jump discontinuously through all 5 "island" regions under the mapping T^{11}. Under T^{55} the mapped motions will be counter-clockwise and nearly elliptical in each of the 5 "islands". It is therefore clear that we can break up our original invariant region into 6 cells possessing separate invariance properties and predictable stroboscopic motions under T^{55}. But because these same 6 cells are also bounded by one continous closed invariant curve, we can say that there is <u>one invariant region with a doubly-periodic boundary</u>.

These results can be applied to a totally different type of problem, the numerical search for additional integrals of motion (see, for example, the work of Bozis[18] on the restricted three-body problem). Hénon and Heiles[19], in an earlier general search, plotted disjoint curves which in reality are stroboscopic trajectories around various T^{mn} satellite fixed points (e.g. their Figure 5 is exactly analogous to our Figure 3). They studied these disjoint curves for a wide range of values of the energy E (they considered motions under a general nonlinear potential). Interpreted in the light of our results, their work shows that the particular T^{mn} cluster of satellite multiple points which bounds the invariant region(s) <u>depends on the energy E</u>. Their plots for lower energies demonstrate that

the T^{3n} satellite fixed points bound the invariant region(s), whereas at higher energies the T^{5n} points form the boundary. At still higher energies the invariant regions get smaller and smaller, undoubtedly involving T^{mn} points with very large m. (One of the figures in the paper of Bozis shows a multiplicity of m = 37!)

Hénon and Heiles refer to their closed curves (i.e. the stroboscopic trajectories) around the central point and around the outlying "islands" as disjoint "isolating third integrals of the motion". Points, with puzzling random (or jumping) behaviors, which lie outside these curves are referred to as points on the "ergodic trajectories in the sea between the islands" (i.e. where the third integral is non-isolating). Our work shows that these points are following completely predictable trajectories, as long as the global T^{mn} mappings are known. It is also clear that the invariant region(s) we have found are just those regions where an "isolating third integral of the motion" exists. In fact, the bounding invariant curve of our 6 invariant cells is a graphic example of such an "isolating integral of the motion", for it exhibits a functional relationship between X, $\dot{X}$, and t for successive stroboscopic (integrated) motions. Thus the application of our methods not only will yield the invariant curves and regions of stability (for a given equation with given parameter values), but also will exhibit simultaneously the regions of phase-space in which "isolating integrals of the motion" exist. In reality, these two concepts are equivalent.

B. Applicability of Moser's theorem to the T^{55} mapping

Since the delineation of a locally stable invariant region for our equation has involved much computer time, it would be desirable to utilize

any general mathematical methods available for the reduction of the time required. To this end we shall discuss the applicability of a recent theorem of Moser[15]. Our exploratory mappings of the X-axis (a few of them are shown in Figure 2) are highly suggestive of properties which might be necessary conditions for stroboscopic stability. The most obvious one is the property of twist mappings of the phase-plane, where the angles of the mapped points increase monotonically with radial distance from the given fixed point. In Figure 2 we see that this property holds for all the mappings T^{11m} (for m=1,2,3,4,5) as long as we stay moderately close to E_1 (within, roughly, an elliptical region with $e_o = e_s$ and semi-major axis $a_o \leq 0.0100$). As we get farther away from E_1 the twisting gets much more complicated, so that a monotonically increasing T^{11m} twist mapping may no longer exist. For example, for the T^{44} mapping of the X-axis to the right of E_1 (curve D^+) we see that the condition of equation (12) is not satisfied for a small region around (1.652, -0.005). This region lies just outside the T^{33} elliptic fixed point e_2 (which is located by the intersection of curves D^+ and A^+). Therefore, it appears that some type of a twist mapping property does exist in the interior of an elongated irregular region bounded, roughly, by the 6 fixed points of the T^{33} mapping.

The maps of Figure 2 indicate the general regions in which a T^{11m} twist mapping appears to exist, but these regions are much more extensive (in area) than the known invariant regions of Figures 5 and 6. There seems to be no clue here that the T^{55} invariant curves form the boundary of the invariant region. So let us examine in detail the general region of the T^{55} fixed points, where we know that an invariant region exists. Since the inner stroboscopic motions are clockwise and almost-elliptical

(see Figure 3), let us make a T^{55} mapping of a set of concentric ellipses and radiating straight lines about and through the point E_1. The maps of these initial curves and lines are shown in Figure 9. The eccentricity of the initial ellipses is $e_o = e_s = 0.995635$. The values of the initial semi-major axes a_o are 10×10^{-4}, 30×10^{-4}, and 45×10^{-4} to 125×10^{-4} in steps of 10×10^{-4}. The angles θ_o of the initial straight lines are indicated near their T^{55} maps. Evidently a T^{55} twist mapping condition does hold throughout this range of initial semi-major axis values. Again, however, there does not appear to be any readily visible indication of the actual existence of an invariant region for $a_o \cong 50 \times 10^{-4}$.

For $a_o \cong 100 \times 10^{-4}$ the mapped curves deviate considerably from their initial elliptical shapes, especially for the initial angles around 0°, 165°, and 215°. Referring to the plots of the T^{33} mappings (Figures 5 and 6), we see that the three prominent directions for "bulging" of the T^{55} twist maps in Figure 9 are toward the 3 hyperbolic "escape channels" of the T^{33} mapping (i.e. along its 3 outgoing outer invariant curves). These bulges, signs of impending escape to infinity via the T^{33} and T^{11} oscillating invariant curves, begin to show up faintly in the mapped curves of Figure 9 at about $a_o = 85 \times 10^{-4}$, but not noticeably before that. So once again we find no striking behaviors of the mappings which might indicate the <u>precise</u> location of the invariant region around E_1.

Moser[15] has demonstrated the theoretical existence of invariant curves and regions for mappings which are small perturbations of the <u>circular</u> twist mapping. Our mappings are very flat <u>elliptical</u> twist mappings, but we can change our scale so that the minor axis of our elliptical motions approximately equals the major axis (e.g. we can adjust

Figure 9. T^{55} mappings of initially concentric standard ellipses and radiating straight lines around the T^{11} fixed point.

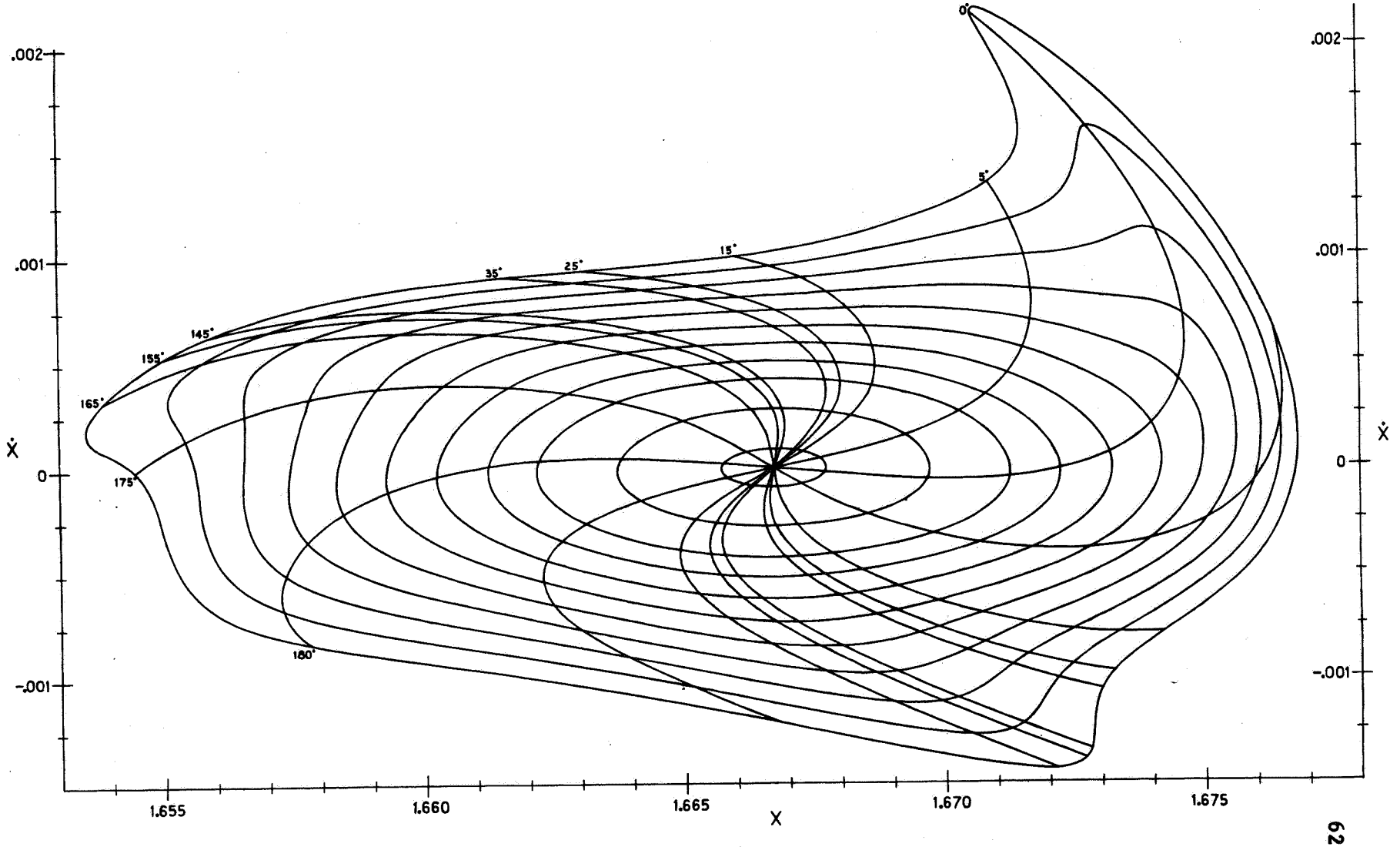
.002
.001
0
-.001
Ẋ
0°
5°
15°
25°
35°
145°
155°
165°
175°
180°
1.655
1.660
1.665
1.670
1.675
X

the value of p_o in equation (20)). An equivalent procedure is to choose a particular standard ellipse, map its points, and compare the resulting locus (i.e. the image curve) with the original ellipse. This procedure is precisely the one which we followed in order to obtain Figure 9.

Now let us see if Moser's conditions apply to the T^{55} mapping. The computations for Figure 9 show that the image curve and the initial curve (a standard ellipse) generally intersect each other four times. Thus Moser's first condition (equation (16)) is satisfied. In order to check his other conditions (equations (17) and (18)) we would first have to exhibit his functions $\alpha(r_o)$, $F(r_o,\theta_o)$, and $G(r_o,\theta_o)$. From equations (13) we see that this can be done directly by calculating the increments

$$\Delta\theta = (\theta_1-\theta_o) = \alpha(r_o) + F(r_o,\theta_o) \qquad (25)$$

and

$$\Delta r = (r_1-r_o) = G(r_o,\theta_o) \ , \qquad (26)$$

where (r_o,θ_o) is the initial point and (r_1,θ_1) is the mapped point, for a whole series of initially concentric ellipses. (Recall from equation (24) that e_s, a_o, and θ_o uniquely determine the $r_o = r_e$ coordinates of points on the initial standard ellipse.) By plotting the $\Delta\theta$ increment versus θ_o we obtain the angular dependence of the F function (for one a_o value) plus one value of the α function. Similarly a plot of Δr versus θ_o yields the angular dependence of the G function for one a_o value. By repeating this process for many initial ellipses with different initial semi-major axes a_o (keeping e_s constant) we can obtain α, F, and G as functions of a_o for various values of θ_o.

Before examining these functional dependences in detail, let us write down a more convenient elliptical analog of Moser's twist mapping,

using different functional symbols:

$$\theta_1 = T^n(\theta_o) = \theta_o + \beta(a_o, e_o) + R(a_o, e_o, \theta_o) \tag{27}$$

and

$$r_1 = T^n(r_o) = r_o + S(a_o, e_o, \theta_o) \tag{28}$$

where a_o and e_o are the semi-major axis and the eccentricity respectively of an ellipse close to its image curve which lies within some elliptical annular region. Note that the variable r_o (or r_1) can be expressed in terms of the basic variables a_o (or a_1) and e_o by using equation (24).

Because of the three variables now (a_o, e_o, and θ_o), the task of exhibiting the functions β, R, and S is greatly complicated. If, however, we set $e_o = e_s$ for convenience, then we have the simpler problem of mapping concentric initial ellipses and radial straight lines and determining the functional dependences as before. Using the data from the plots in Figure 9 we can calculate the basic T^{55} mapping increments

$$\Delta\theta = (\theta_1 - \theta_o) = \beta(a_o, e_s) + R(a_o, e_s, \theta_o) \tag{29}$$

and

$$\Delta r = (r_1 - r_o) = S(a_o, e_s, \theta_o) \tag{30}$$

as functions of a_o or θ_o (for $e_o = e_s$). Now in contrast to the previous discussion of methods for obtaining Moser's functions (α, F, and G), we find it more convenient to first calculate $\Delta\theta$ and Δr as functions of a_o for various fixed initial values of θ_o (i.e. for a series of different initial straight lines).

The results of these calculations for $\Delta\theta$ and Δr are plotted in Figures 10 and 11 respectively. The dashed curves in both figures (for $\theta_o = 15°$ and 95°) are plots of $\Delta\theta$ or Δr versus r_o. The solid curves (for

Figure 10. Angular T^{55} mapping increment $\Delta\theta$ as a function of the semi-major axis a_o of an initial standard ellipse, for several initial angles θ_o.

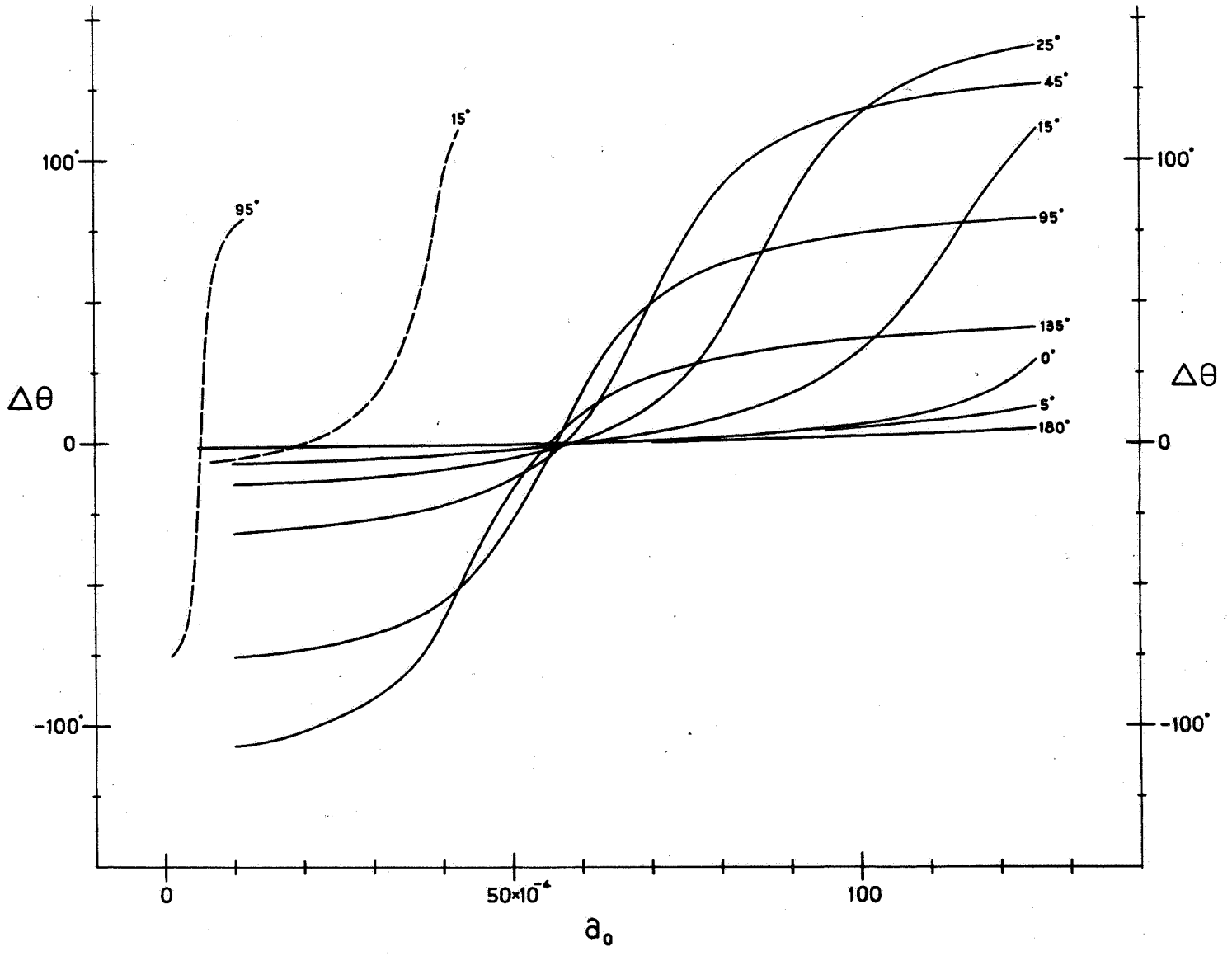
25°
45°
15°
95°
135°
0°
5°
180°
15°
95°
100°
-100°
0
Δθ
0
50×10⁻⁴
100
a_0

Figure 11. Radial T^{55} mapping increment Δr as a function of the semi-major axis a_o of an initial standard ellipse, for several initial angles θ_o.

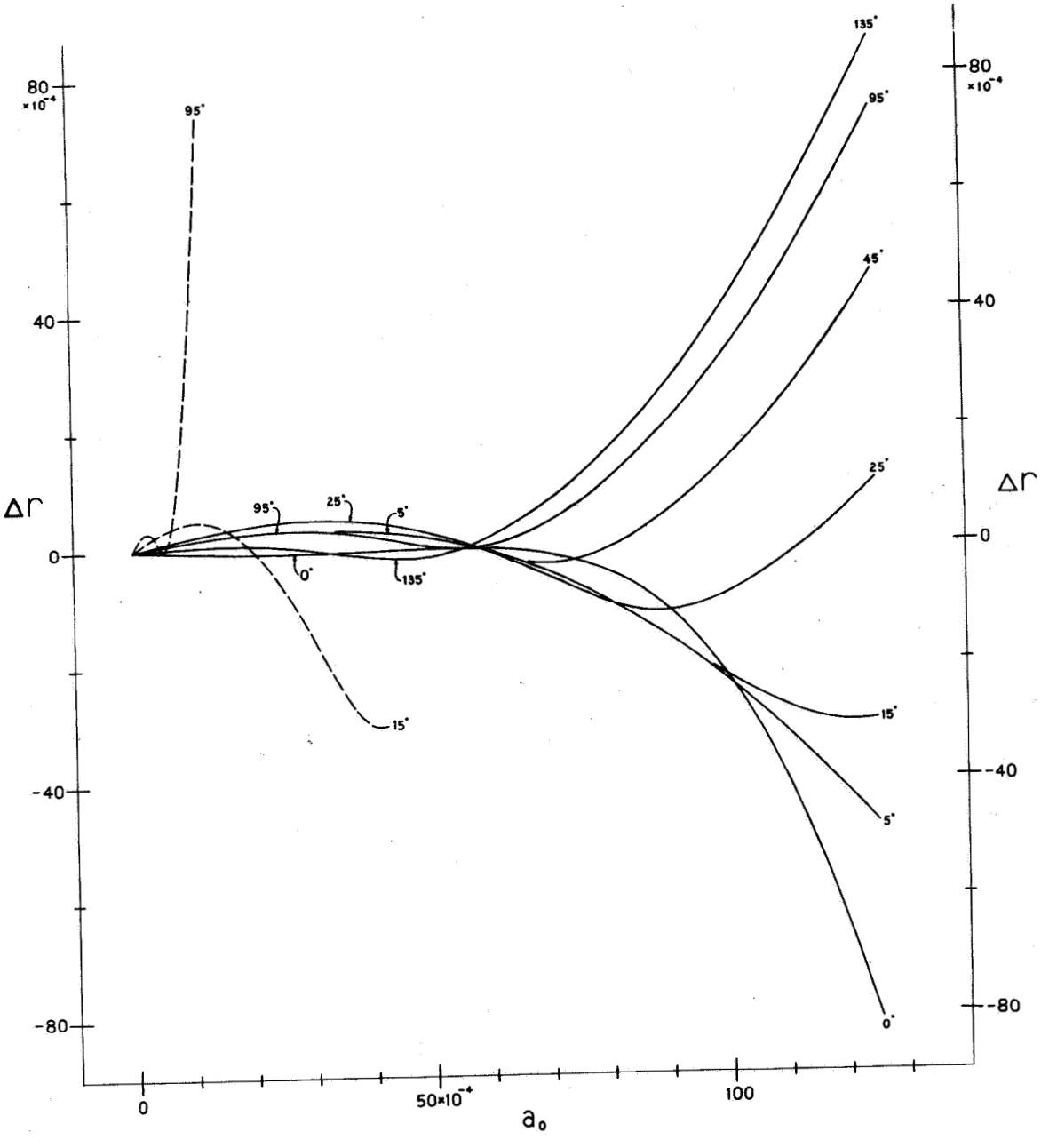
80
×10⁻⁴
40
0
-40
-80
Δr
95°
95°
25°
5°
0°
135°
15°
135°
95°
45°
25°
15°
5°
0°
0
50×10⁻⁴
100
a₀

θ_o = 0°,5°,15°,25°,45°,95°,135°, and 180°) are plots of $\Delta\theta$ or Δr versus a_o. We immediately see that plotting the increments $\Delta\theta$ or Δr versus a_o gives a spectrum of curves that can be easily compared, whereas plotting versus r_o does not.

Referring now to the solid curves in Figure 10, we notice that the $\Delta\theta$ function is smooth and differentiable over the full range $0 < a_o < 125 \times 10^{-4}$, well beyond the known invariant region at $a_o \cong 50 \times 10^{-4}$. The $\Delta\theta$ function is always negative for the inner region $0 < a_o < 55 \times 10^{-4}$, always positive for the outer region $60 \times 10^{-4} < a_o < 125 \times 10^{-4}$, and is monotonically increasing over the full range. The first two features correspond to the known (opposite) directions of the stroboscopic motions for the two regions. The small region between the inner and outer regions corresponds to the cluster of T^{55} fixed points, where the sense of the motion changes sign at different a_o values depending on the angle θ_o (e.g. compare a straight line through e(1) with one through h(1)).

The function β is ordinarily obtained by plotting $\Delta\theta$ versus θ_o for various fixed initial values of a_o, and is the <u>angularly independent</u> part of each of these curves. Now the $\Delta\theta$ function is approximately symmetric about θ_o = 180°, so we might use the $\Delta\theta$ intercepts at θ_o = 0° or 180° as the value of $\beta(a_o)$ for each curve, provided they are <u>identical</u> (β is just like an additive constant for all θ_o values). If they are not identical, then the function β contains some angular dependence (and there is no exact symmetry about θ_o = 180°). One way to check this possibility is to compare the θ_o = 0° and 180° curves in Figure 10 for the full range of a_o values. For the <u>inner</u> region we find that these two curves always differ from one another by less than 0.1° in the ordinate $\Delta\theta$. Both curves

increase almost linearly from about $\Delta\theta \cong -1.25°$ for $a_o = 10 \times 10^{-4}$ to about $\Delta\theta \cong -0.3°$ for $a_o = 50.5 \times 10^{-4}$. For the outer region we find that the two curves differ widely from one another by as much as 24° for $a_o = 125 \times 10^{-4}$. They still increase monotonically.

Hence we may conclude that for the inner region the function β is a small, negative, almost linearly increasing function of a_o, with approximately no angular dependence. For the outer region β is a rather large, positive, increasing function of a_o, with very definite angular dependence.

The function $R(a_o, e_s, \theta_o)$ for the inner region is a negative, monotonically increasing function of a_o for all angles θ_o. For this inner region we see that for fixed a_o values, $\Delta\theta$ first decreases with increasing θ_o and then increases again. In other words the second derivative of $\Delta\theta$ with respect to θ_o is positive for all θ_o and all a_o in this region. For the outer region the conclusions are not so definite because of the angular dependence of β (which decreases as θ_o increases). Here R is a positive function of a_o which increases with increasing a_o, except for $\theta_o \lesssim 15°$ when the reverse is true. Scanning the angular dependence we observe that the second derivative of $\Delta\theta$ with respect to θ_o is now negative for all θ_o when $a_o < 80 \times 10^{-4}$. When $a_o > 80 \times 10^{-4}$ this derivative is still negative for most values of θ_o, but it does develop a pronounced positive region for $0 < \theta_o \lesssim 15°$.

Let us now turn to the solid curves for Δr versus a_o in Figure 11. Analogous to the $\Delta\theta$ function, the $\Delta r = S(a_o, e_s, \theta_o)$ function appears to be smooth and differentiable over the full range $0 < a_o < 125 \times 10^{-4}$, again well beyond the known invariant region. Now, however, the function takes on both positive and negative values inside each region, depending on

the θ_o value. There is also no striking pattern of monotonicity of the function over the two regions. We can only say that the function $S(a_o, e_s, \theta_o)$ has a varied (continuous) dependence on a_o in both regions. For the inner region we notice that the function Δr is generally positive and rather small for all angles θ_o. In fact the values of Δr range between $+5.1 \times 10^{-4}$ and -1.3×10^{-4} for all values of θ_o (when a_o is in the inner region). For the outer region the fluctuation of Δr with varying θ_o values is markedly greater. For example, for $a_o = 125 \times 10^{-4}$ the range of values for Δr is $+86 \times 10^{-4}$ to -81×10^{-4}. Thus we can conclude that for the inner region the function S is nearly independent of the angle θ_o, whereas for the outer region it is strongly dependent on both a_o and θ_o.

All of these results for the behavior of our β, R, and S functions (or Moser's α, F, and G functions if we convert to the polar coordinates r, θ exclusively) can be summarized in the following relations for the two regions discussed above:

Inner (Invariant) Region

$$T^{55}: \left\{ \begin{array}{l} \theta_1 = \theta_o + \beta(a_o, e_s) + R(a_o, e_s, \theta_o) \\ r_1 = r_o + S(a_o, e_s, \theta_o) \end{array} \right\} \tag{31}$$

$$\left. \begin{array}{l} \text{where} \quad \beta < 0 \ , \quad R < 0 \ , \quad |\beta| \ll |R| \\ \text{with} \quad d\beta/da_o > 0 \ , \quad d^2\beta/da_o^2 \cong 0 \\ \text{and} \quad \partial R/\partial a_o > 0 \ , \quad \partial^2 R/\partial \theta_o^2 > 0 \ , \quad \partial^2 S/\partial \theta_o^2 \cong 0 \ ; \end{array} \right\} \tag{32}$$

Outer (Non-invariant) Region

$$T^{55}: \left\{ \begin{array}{l} \theta_1 = \theta_o + \beta(a_o, e_s, \theta_o) + R(a_o, e_s, \theta_o) \\ r_1 = r_o + S(a_o, e_s, \theta_o) \end{array} \right\} \tag{33}$$

$$\left. \begin{array}{l} \text{where} \quad \beta > 0 \,, \quad \partial\beta/\partial\theta_o < 0 \,, \quad \partial\beta/\partial a_o > 0 \\ \text{and} \quad R > 0 \,, \quad \partial R/\partial a_o > 0 \,, \quad \partial^2 R/\partial\theta_o^2 < 0 \quad \text{for} \quad \theta_o \gtrsim 15° \end{array} \right\} \tag{34}$$

We are now in a position to check the applicability of Moser's second and third conditions (equations (17) and (18)) to our T^{55} mapping. First of all, it is clear that β (or α) is a monotonically increasing function of a_o over the full range of a_o values plotted. The value of $d\beta/da_o$ is positive and approximately constant in the inner region, while $\partial\beta/\partial a_o$ is positive, increasing and bounded in the outer region. Therefore if we choose any number greater than the upper bound of $\partial\beta/\partial a_o$ as the constant C_o in equation (17), then Moser's second condition will be satisfied by our T^{55} mapping over the open interval $0 < a_o < 125 \times 10^{-4}$.

In order to check Moser's third condition we first observe that both the R and S functions are bounded and continuous over the open interval $0 < a_o < 125 \times 10^{-4}$. Thus we can choose some finite value of δ_o which is greater than the sum of the absolute bounds of the R and S functions. From the smooth, continuous behavior of the β, R, and S functions we can estimate the sum of the absolute values of the $\ell = 333^{\underline{rd}}$ partial derivatives of these three functions as approximately zero, and in any case less than the value of C_o chosen above. Hence Moser's third condition is satisfied by our T^{55} mapping over the open interval $0 < a_o < 125 \times 10^{-4}$.

Because all of Moser's conditions are satisfied, we may conclude that invariant closed curves and regions will exist somewhere within the

standard ellipse having $a_o = 125 \times 10^{-4}$ and $e_s = 0.995635$. Indeed we have already found an invariant region which is bounded by the union of the hyperbolic invariant curves of the T^{55} mapping and which is located approximately within the standard ellipse having $a_o = 50 \times 10^{-4}$. However we have also seen that points outside the latter ellipse but still inside the larger ellipse having $a_o = 125 \times 10^{-4}$ do escape to infinity in a finite time. Since Moser's conditions apply to this outer, unstable (non-invariant) region as well, we conclude that Moser's conditions are not sufficient to locate the invariant region precisely.

The empirical properties summarized in equations (31) through (34) exhibit several distinctions between the inner invariant region and the outer non-invariant region for the T^{55} mapping. For example, the transition of β from a linear to a nonlinear function and the abrupt change of magnitude and functional dependences of S may be possible theoretical clues to the exact location of the invariant region. At this point it should be noted that exhibiting the β, R, and S functions involves as much work as actually locating the invariant region accurately. But an adequate theorem would definitely be valuable for rigorously proving the actual invariance of the region.

C. Summary of methods

Having shown that invariant regions of stability do exist, and that at present they can be located most readily by using a computer, let us now summarize our practical, empirical methods for exhibiting the existence and form of the invariant curves.

The first step is to find the fixed points by scanning the phase-plane in some systematic fashion, such as repeatedly mapping a grid or mesh

of points. If these mappings are superimposed on the original grid, their intersections will yield all the fixed points in the phase-space. For this work a computer program based on numerical integration (e.g. a Runge-Kutta-Gill routine) should be quite adequate.

Next we can look for invariant regions around any particular one of these fixed points. If $T^n(\tau)$ refers to the mapping under which the given point is fixed, then we can apply this mapping a number of times m in succession to <u>each</u> of a series of points along an axis through the fixed point (e.g. m=5 or 10 times). This initial scan can be rather coarse, but should cover a reasonable neighborhood around the fixed point (for example, a radial range of perhaps 10^{-8} to 10^{-2} or more). Now for <u>each</u> value of m plot the locus of that particular $m^{\underline{th}}$ map of the entire series of points along the axis. If the original point is strongly unstable, then the maps of points along the axis will jump about discontinuously and may quickly reach infinity (even for m=2 or 3). But if the mapped loci of the axis points seem to possess some form of a general elliptical <u>twist</u> mapping of that axis, then look for any repeating patterns in the <u>successive T^n mappings</u> of <u>each</u> initial axis point by itself. For example, do the radii or especially the <u>angles</u> of the mapped points seem to exhibit similarities every m cycles of the mapping T^n? If so, for what regions? If not, make a finer grid and scan closer to the original fixed point; increase the number m of successive T^n mappings of each point.

If a pattern eventually emerges, it will probably be indicative of precisely which $m^{\underline{th}}$ cluster of $T^{mn}(\tau)$ satellite multiple points of the original fixed point bounds the invariant region (and which hyperbolic invariant curves make up the doubly-periodic invariant curve around that

region). If no pattern ever emerges, even though the mappings are quasi-stable, then the original point is probably an elliptic point which is nevertheless unstable. Again we should stress that the appearance of an elliptical twist mapping around an elliptic fixed point seems to be a necessary (but not necessarily sufficient) condition for the existence of an invariant region. The appearance of a definite pattern in cycles of every M mappings of T^n seems to be the chief indicator of the particular mapping $T^{Mn}(\tau)$ which exhibits the seemingly necessary twist mapping conditions.

To obtain the invariant region more accurately, we can first scan all our initial T^{mn} twist maps of the axis for all mutual intersections to see whether or not we already may have found any of the 2M fixed points of the T^{Mn} mapping of the axis. If not, we will have to make a crude mapping of the axis for points whose radii coincide approximately with the outer bounds of the region which exhibits the M-fold mapping patterns. In any case, once approximate values for the two T^{Mn} fixed points on the axis are found, their exact location can be determined as accurately as desired by taking successively finer and finer grids of initial points. By making repeated T^n mappings of both of these points for a total of (M-1) times each, the entire cluster of 2M alternating hyperbolic and elliptic T^{Mn} satellite fixed points can be located. These will bound the invariant region.

We now make some preliminary short-period T^{Mn} stroboscopic mappings (perhaps for 50 to 100 strobe periods) of a series of points on the axis and inside the cluster of T^{Mn} satellite points. These mappings will show the elliptical character of the inner motions, plus the sense of

their stroboscopic rotations (which reverse outside the region). If, in fact, we map a coarse grid of inner axis points which extend towards the T^{Mn} elliptic fixed point on that axis, we will find that those grid points farthest from the T^{Mn} fixed point will move nearly elliptically around the inner region in one direction. Grid points closer to the T^{Mn} fixed point will move outward around that elliptic fixed point itself, in an opposite sense. By taking finer and finer grids we can locate (to the accuracy of the computer) the approximate borderline between these motions. Now, longer-period stroboscopic mappings (e.g. for 500 to 1000 strobe periods of T^{Mn}) of two points on opposite sides of this borderline will trace out both the inner union of hyperbolic invariant curves (if we use T^{Mn} printouts), plus all the outer hyperbolic invariant curves surrounding the M elliptical cells or "islands" (if we use T^{n} printouts). The union of these (M+1) curves will be the one continuous doubly-periodic invariant curve of T^{Mn} which bounds the invariant region, in the limit that our two initial points approach the inner invariant curve.

All of the preceding steps can be carried out quickly and efficiently utilizing only a moderately accurate computer and a numerical integration routine (such as our Fortran program included in the second appendix). In special cases some numerical analysis may be necessary to obtain sufficient accuracy for the longer-period stroboscopic mappings (needed to generate the actual closed invariant curve). But in general the preceding methods should enable one to easily and relatively accurately determine the invariant regions and hence the stroboscopic stability of any particular solution (fixed point) of a particular differential equation.

If more detailed proof of the stroboscopic stability of a particular

solution is desired, then we must study carefully the hyperbolic invariant curves of all T^{mn} mappings (at least up to m=M) of a global region around our particular fixed point. By mapping the inner and outer hyperbolic invariant curves "layer by layer" (i.e. for consecutive values of m), we can check for intersections of these consecutive T^{mn} invariant curves. Thus we can gradually exhibit the mechanisms or "channels" whereby points can escape to infinity from regions close to our particular fixed point. After "peeling off" each successive "layer" until we reach one layer whose T^{Mn} hyperbolic invariant curves do not intersect those of the next outer layer, we can conclude that the escape mechanism no longer holds for this layer. (That is, the hyperbolic invariant curves of the T^{Mn} mapping develop no oscillations with which to carry points out to infinity.)

To explicitly demonstrate the non-oscillatory behavior of these T^{Mn} hyperbolic invariant curves would require more accuracy still. However, this seems not to be important for our conclusion that the union of the hyperbolic invariant curves of the T^{Mn} mapping isolated above will therefore form the continuous, closed, doubly-periodic boundary of an invariant region of absolute stroboscopic stability.

IV. APPENDIX -- ANALYSIS

A. Integration of the equations of motion

The first integral of equation (20), when $p=p_o$ and X_a is an intercept on the X-axis, is simply

$$(dX/dt)^2 + \tfrac{1}{2}p_o X^4 = \tfrac{1}{2}p_o X_a^4 > 0 \quad . \tag{35}$$

A half-period of motion described by this equation in phase-space is an arc of a quasi-ellipse which intersects the X-axis at X_a and is concave inward. Similarly when $p=-p_o$ and X_b is another X-axis intercept, the first integral of equation (20) is

$$(dX/dt)^2 - \tfrac{1}{2}p_o X^4 = -\tfrac{1}{2}p_o X_b^4 < 0 \quad . \tag{36}$$

A half-period of motion described by this equation in phase-space is an arc of a quasi-hyperbola which intersects the X-axis at X_b and is concave outward. Finally when $p=-p_o$ and $\dot{X}_c$ is an intercept on the $\dot{X}$-axis, the first integral of equation (20) is

$$(dX/dt)^2 - \frac{1}{2}p_o X^4 = \dot{X}_c^2 = \frac{1}{8}p_o c^4 > 0 \quad . \tag{37}$$

where c is a real constant. Again a half-period of the motion is an arc of a quasi-hyperbola which now intersects the $\dot{X}$-axis at $\dot{X}_c$ and is also concave outward. Notice that a transition must occur between the last two types of quasi-hyperbolic motion whenever $\dot{X}^2 - \tfrac{1}{2}p_o X^4 = 0$, i.e. when

$$\dot{X} = \pm \sqrt{p_o/2}\; X^2 \quad . \tag{38}$$

The motion described by this last equation consists of two parabolas through the origin in phase-space. It reveals that the origin is a parabolic (nodal) fixed point of equation (20).

Equations (35), (36), and (37) above can be reduced to a standard form

$$\dot{q}^2 = \tfrac{1}{2}p_o C_i (1-q^4) \qquad (39)$$

where C_i is X_a, X_b, or c respectively. This standard form can be integrated in terms of the Jacobian elliptic functions snu, cnu, and dnu. This integration has been done by Bartlett[13], and the resulting solutions for the three basic types of motion considered above are reproduced here.

Quasi-Elliptic Case (QE Motion):

$$X = X_a \text{ cnu} \qquad (40a)$$

$$\dot{X} = -\sqrt{p_o}\, X_a^2 \text{ snu dnu} \qquad (40b)$$

$$u = \sqrt{p_o}\, X_a\, t \qquad (40c)$$

Quasi-Hyperbolic Case I (QH I Motion):

$$X = X_b/\text{cnu} \qquad (41a)$$

$$\dot{X} = \sqrt{p_o}\, X_b^2 \text{ snu dnu}/\text{cn}^2 u \qquad (41b)$$

$$u = \sqrt{p_o}\, X_b\, t \qquad (41c)$$

Quasi-Hyperbolic Case II (QH II Motion):

$$X = \sqrt{c^2/2}\ \text{snu}/(1 + \text{cnu}) \qquad (42a)$$

$$\dot{X} = \sqrt{p_o/2}\ c^2\ \text{dnu}/(1 + \text{cnu}) \qquad (42b)$$

$$u = \sqrt{p_o}\ c\ t \qquad (42c)$$

A number of theoretical predictions based on these results can be made about the general properties of the motion[13], but we will not dwell on them here. Instead we will go directly to the more specific problem of numerically calculating many highly accurate solutions $(X(t),\dot{X}(t))$ from any arbitrary set of initial conditions $(X_i,\dot{X}_i)$.

B. Jacobian elliptic functions

The first obvious problem in doing our numerical calculations is one of obtaining accurate tables of the Jacobian elliptic functions snu, cnu, and dnu. Each of these functions can be written as products and quotients of the four Jacobian Theta functions, which in turn are expressible as infinite series. The resulting formulas, taken from the Smithsonian Elliptic Function Tables[20], are reproduced here for reference.

$$\text{snu} = \frac{\theta_3(0,q)}{\theta_2(0,q)} \quad x \quad \frac{\theta_1(v,q)}{\theta_o(v,q)} \tag{43}$$

$$\text{cnu} = \frac{\theta_o(0,q)}{\theta_2(0,q)} \quad x \quad \frac{\theta_2(v,q)}{\theta_o(v,q)} \tag{44}$$

$$\text{dnu} = \frac{\theta_o(0,q)}{\theta_3(0,q)} \quad x \quad \frac{\theta_3(v,q)}{\theta_o(v,q)} \tag{45}$$

where

$$\theta_o(v,q) = 1 - 2q\cos 2\pi v + 2q^4\cos 4\pi v - 2q^9\cos 6\pi v + \ldots \tag{46}$$

$$\theta_1(v,q) = \sin\pi v - q^2\sin 3\pi v + q^6\sin 5\pi v - q^{12}\sin 7\pi v + \ldots \tag{47}$$

$$\theta_2(v,q) = \cos\pi v + q^2\cos 3\pi v + q^6\cos 5\pi v + q^{12}\cos 7\pi v + \ldots \tag{48}$$

$$\theta_3(v,q) = 1 + 2q\cos 2\pi v + 2q^4\cos 4\pi v + 2q^9\cos 6\pi v + \ldots \tag{49}$$

with

$$v = u/2K \tag{50}$$

and

$$\left\{ \begin{array}{l} K = 1.854074677301372\ldots \\ q = 0.04321391826377225\ldots \\ \pi = 3.14159265358979323846\ldots \end{array} \right\} . \tag{51}$$

Since highly accurate routines exist for the calculation of the circular functions used above, these formulas are admirably suited to a high-speed, highly accurate digital computer such as the Illiac II.

In our work, tables for the elliptic functions snu, cnu, and dnu are calculated and stored by the computer in terms of the "angular" argument b, where

$$u = K(b/90) \tag{52}$$

so that

$$v = b/180 \ . \tag{53}$$

The tables are calculated for the first quadrant values of b (i.e. for $0.0 \leq b \leq 90.0$) in steps of 0.1 in b. Using the periodic properties of the elliptic functions (e.g. snu and cnu are analogous to sinu and cosu, with K playing the role of $\pi/2$) and using the first quadrant tables calculated above, we can easily obtain any of the elliptic functional values for the full range $0 \leq u \leq 4K$. For example, it will be necessary to calculate and store a table of values of the function

$$S(u) = snu/(1 + cnu) \tag{54}$$

for the range $0 \leq u \leq 3K/2$. For the range $0 \leq u \leq K$ it is a trivial calculation. For the range $K < u \leq 3K/2$ the table is assembled by calculating the function snu/(1-cnu) starting with the u=K end of the first quadrant tables and going backwards toward u=K/2 (i.e. b=45.0). These results are then stored as S(u) starting at u=K and going forwards toward u=3K/2 (i.e. b=145.0).

At this point we should remark that if only a <u>few</u> values of the elliptic functions are needed, it would be most efficient to use equations (43) through (53) <u>each</u> time the need arose. However for an inordinately

large number of required values (e.g. as many as 10^5 per trajectory, as in the present work), it becomes more efficient time-wise to construct relatively small, accurate tables and then use an accurate (nonlinear) interpolation routine. In this work we make use of a Lagrange six-point (equal interval) interpolation routine[21], which has an average execution time of 375 microseconds per entry on the IBM-7094 computer. This method utilizes the three nearest table entries on each side of the input value of u and then interpolates the (elliptic) functional value corresponding to u from a sixth-order fit of the 6 tabulated functional values. The results are then nearly as accurate as if they had been calculated from the original infinite series expressions. It should be noted that this method allows us to use relatively small tables (our tables contained 900 entries for the range $0 \leq u \leq K$) and still obtain highly accurate interpolations. For a small computer memory core this efficiency is essential.

C. Inversion of elliptic functions

A second major problem which we will face in the actual calculations is that of obtaining accurate values for the inverted Jacobian elliptic functions. Instead of using the obvious elliptic integrals (i.e. the formal inversions of the elliptic functions) to calculate still more tables, we will consider several alternatives which are more efficient with regard to saving time and memory core. One alternative is to adapt a Lagrangian six-point (unequal interval) interpolation routine to the calculations. This approach is the desirable one for highest accuracy and overall efficiency. In the present work, however, it has been more expedient to follow a different approach, one of approximation and iteration. From equations (40a,b,c), (41a,b,c), and (42a,b,c) for the three different types of motion

it is seen that we only have to invert cnu (for both QE and QH I Motions) and the S(u) = snu/(1+cnu) function (for QH II Motion only).

Given some value of cnu_i which we wish to invert in order to obtain u_i, let us quickly scan our cnu table and determine between which two entries our value of cnu_i lies. Then let us choose the one with the smaller b value, call it $b_o = 90u_o/K$ (where $u_o < u_i$ is the nearest smaller value of u, with $cnu_o > cnu_i$ the nearest larger value of cnu). Now let us write a Taylor expansion for cnu_i about the point cnu_o. Using the properties of the elliptic functions[22] we obtain

$$cnu_i = f_o - g_o\Delta - 1/2\ f_o^3\Delta^2 + 1/2\ g_o f_o^2\Delta^3 + 1/8(f_o^5 - 2f_o g_o^2)\Delta^4 + \ldots \tag{55}$$

where

$$\left\{ \begin{array}{l} f_o = cnu_o \\ g_o = snu_o\ dnu_o \\ \Delta = (u_i - u_o)\ . \end{array} \right\} \tag{56}$$

For the first approximation we neglect all nonlinear terms and obtain

$$\Delta_1 = (f_o - cnu_i)/g_o\ . \tag{57}$$

Neglecting terms beyond Δ^2 and using Δ_1 in the second-order term, we obtain the second-order approximation

$$\Delta_2 = \Delta_1 - (f_o^3\Delta_1^2)/2g_o\ . \tag{58}$$

Similarly we obtain the third-order approximation

$$\Delta_3 = \Delta_2 + \tfrac{1}{2}f_o^2\Delta_2^3 - (f_o^6\Delta_1^3)/2g_o^2 + (f_o^5\Delta_1\Delta_2^3)/2g_o + \ldots\ . \tag{59}$$

Given cnu_i and having chosen the nearby smaller base value u_o we can readily calculate first Δ_1, then Δ_2, and finally Δ_3. The third-order approximation

for u_i is then

$$u_{i3} = u_o + \Delta_3 \quad . \tag{60}$$

In the second case of inversion, if we are given a value for the function $S(u_i) = snu_i/(1+cnu_i)$ and we wish to invert it to obtain u_i, we can proceed as follows. We first make a Taylor expansion about the point u_o (chosen as before with $u_o < u_i$, but now with $S(u_o) < S(u_i)$) and obtain

$$S(u_i) = f_o + g_o\Delta + \tfrac{1}{4}f_o^3\Delta^2 + \tfrac{1}{4}f_o^2g_o\Delta^3 + (3f_og_o^2 + 3f_o^5/4)\Delta^4/24 + \ldots \tag{61}$$

where now

$$\left\{ \begin{array}{l} f_o = snu_o/(1+cnu_o) = S(u_o) \\ g_o = dnu_o/(1+cnu_o) \\ \Delta = (u_i - u_o) \ . \end{array} \right\} \tag{62}$$

Analogous to the case of the cnu_i inversion, we can invert this expansion by means of successive approximations to obtain

$$\Delta_1 = (S(u_i) - f_o)/g_o \tag{63}$$

$$\Delta_2 = \Delta_1 - (f_o^3\Delta_1^2)/4g_o \tag{64}$$

$$\Delta_3 = \Delta_2 - \tfrac{1}{4}f_o^2\Delta_2^3 + (f_o^6\Delta_1^3)/8g_o^2 + (f_o^5\Delta_1\Delta_2^3)/8g_o + \ldots \ . \tag{65}$$

Given $S(u_i) = snu_i/(1+cnu_i)$ we can readily calculate Δ_1, then Δ_2, and finally Δ_3, yielding the third-order approximation for u_i as in equation (60).

In the special case that $u_o = 0$ or $u_o = K$ (the ends of the table) we can simplify our original expansions for cnu_i and $S(u_i)$ given in equations (55) and (61). Recalling that sn0=0 and cn0=dn0=1, we obtain the third-order expressions

$$u_{i3} = \sqrt{2(1 - cnu_i)} \qquad \text{for } u_o = 0 \ , \tag{66a}$$

and $$u_{i3} = K - \sqrt{2}\ cnu_i \qquad \text{for } u_o = K\ ; \tag{66b}$$

also $$u_{i3} = 2S(u_i) \qquad \text{for } u_o = 0\ , \tag{67a}$$

and $$u_{i3} = K - \sqrt{2}\ (1 - \sqrt{2S(u_i)-1}\ ) \qquad \text{for } u_o = K\ . \tag{67b}$$

Before we start the calculations we can see that our above successive approximations for the Δ_i in the case of the cnu_i inversion do not converge as $u_o \to 0$. This divergence is due to the presence of snu_o in the denominators of all of the expressions. Since the approximations are increasingly accurate toward the middle of the tables, it is clear that we must devise an accurate (converging) approximation for the case $u_o \to 0$ in the cnu_i inversion. To this end we make use of a direct expansion for cnu in powers of u[22]:

$$cnu = 1 - \tfrac{1}{2}u^2 + u^4/8 - 3u^6/80 + \ldots\ . \tag{68}$$

Forming the quotient

$$R(u) = \frac{1 - cnu}{1 + cnu} = \frac{\tfrac{1}{2}u^2 - u^4/8 + 3u^6/80}{2 - \tfrac{1}{2}u^2 + u^4/8 - 3u^6/80} \tag{69}$$

and performing the indicated long-division, we obtain

$$R(u) = \frac{1 - cnu}{1 + cnu} = \frac{u^2}{4} + \frac{u^6}{320} + \frac{7u^8}{1280} + \ldots\ . \tag{70}$$

If we drop all terms higher than u^2 we get the first-order approximation for u_i^2 to be

$$u_{i1}^2 = 4(1 - cnu_i)/(1 + cnu_i)\ . \tag{71}$$

Inserting this value in the two higher-order terms in equation (70) and solving for the resulting approximation, we obtain

$$\tfrac{1}{2}u_{i2}^2 = R(u_i) - R^3(u_i)/5 - 7R^4(u_i)/5 - \ldots \quad . \qquad (72)$$

When $u_i \to 0$ both sides of the last equation converge to zero, so that we have a valid expression for small u_i in terms of the given cnu_i value. When u_i gets larger, this expression will become decreasingly accurate. On the other hand, our original equations for cnu_i inversion (equations (56) to (60)) will become increasingly accurate. Clearly there will be some crossover point between the accuracies of the two inversion methods, and we will need to know this point if we are to use <u>both</u> methods for the full range of the table values. To find this crossover point we must do some hand calculations (faster than writing a small computer program in this case). We can select, for example, an integral value of b_i and then take the <u>accurate</u> table value for the associated $cnu_i = cn(Kb_i/90)$. Next we can <u>invert</u> this cnu_i value using <u>both</u> inversion methods. These results for u_{i3} (or u_{i2}) can then be compared with the <u>original</u> value of $u_i = (Kb_i/90)$. Thus we can tabulate the error $\Delta b = |b_i - b_{i3}|$ as a function of the original b_i for both inversion methods. A semi-log plot of these results is shown in Figure 12. Curve B is the error plot for the original inversion method, while curve A is for the second method for small angles. From this plot we find the crossover value of b_i as

$$b_c = 18.2 \quad . \qquad (73)$$

In our calculations we use the original cnu_i inversion method (equations (56) to (60)), for $b_i > 18.2$ and the second inversion method of equation (72) for $b_i \leq 18.2$. Note that the maximum error in u_{i3} will then be about 10^{-6} when $b_i = b_c$.

Figure 12. Numerical errors arising in two methods for the inversion of Jacobian elliptic functions.

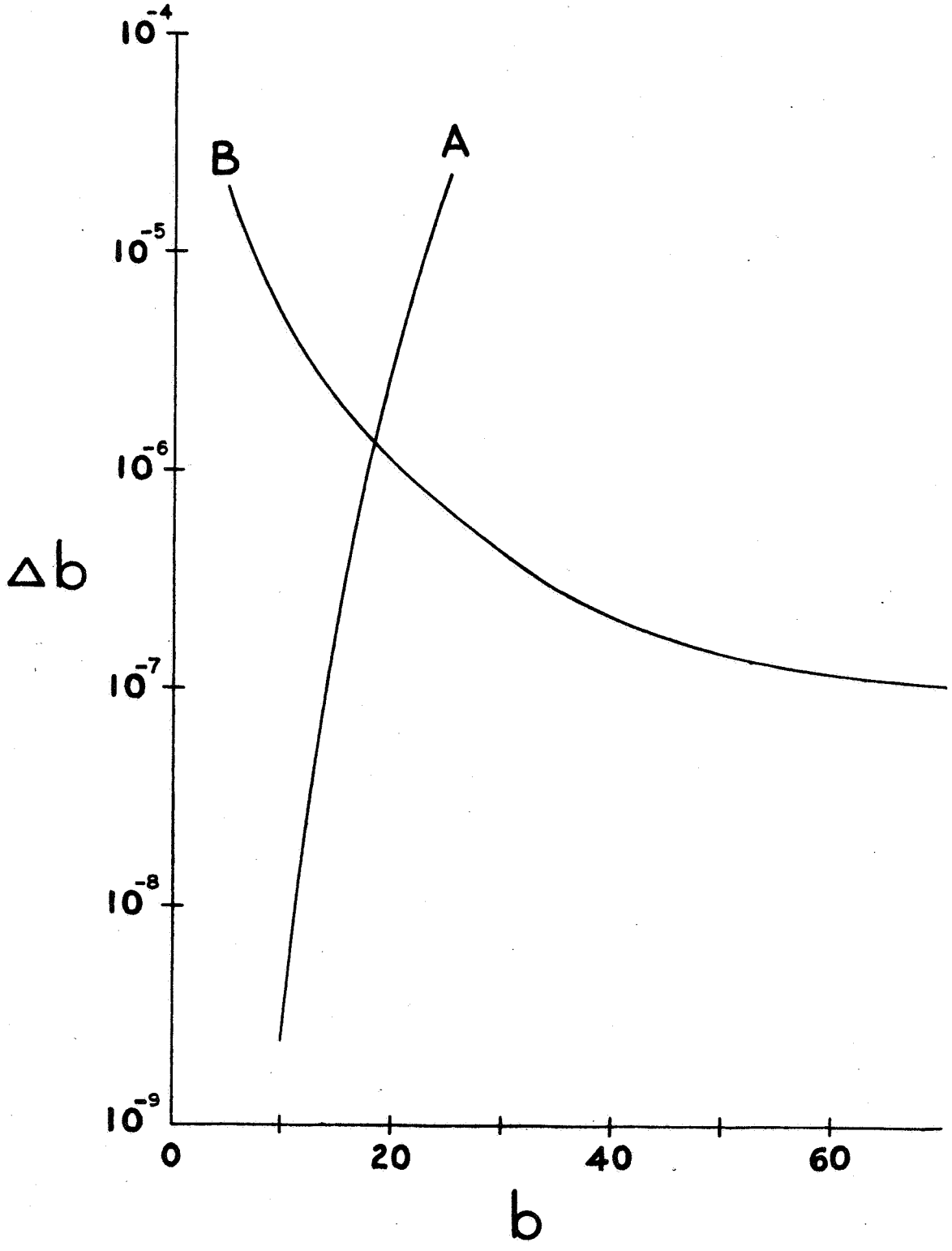
10^{-4}
10^{-5}
10^{-6}
10^{-7}
10^{-8}
10^{-9}
B
A
Δb
0
20
40
60
b

In order to obtain more accurate inversions than the above u_{i3}, we now add an iteration process. After inverting cnu_i or $S(u_i)$ to obtain the approximate value of u_{i3} (or u_{i2}) we turn around and calculate the corresponding value of cnu_{i3} or $S(u_{i3})$ using the accurate Lagrangian interpolation routine and our original tables. The resulting value can then be compared with the given value of cnu_i or $S(u_i)$ that we initially tried to invert. If $|cnu_{i3} - cnu_i| \leq E$ or $|S(u_{i3}) - S(u_i)| \leq E$, where E is some preset error limitation, then we can regard u_{i3} (or u_{i2}) as close enough to u_i for our purposes. In our work we eventually set $E = 10^{-12}$.

However, if the error is greater than E we can make a new estimate for u_i by expanding cnu_i or $S(u_i)$ in a Taylor series about u_{i3} or u_{i2}, namely

$$cnu_i = cnu_{i3} - snu_{i3}dnu_{i3}\,(u_i - u_{i3}) + \ldots \tag{74}$$

and

$$S(u_i) = S(u_{i3}) + \left(\frac{dnu_{i3}}{1 + cnu_{i3}}\right)\,(u_i - u_{i3}) + \ldots . \tag{75}$$

Solving each of these equation for u_i we obtain

$$u_{i4} = u_{i3} + \frac{(cnu_{i3} - cnu_i)}{snu_{i3}dnu_{i3}} + \ldots \tag{76}$$

and

$$u_{i4} = u_{i3} + \frac{(S(u_i) - S(u_{i3}))\,(1 + cnu_{i3})}{dnu_{i3}} + \ldots \tag{77}$$

as the next approximations for the inversions of cnu_i and $S(u_i)$ respectively (provided that u_{i3} or u_{i2} are not zero). This procedure can be repeated over and over again until the desired accuracy is achieved. In practice it has not been necessary to use these corrections more than once.

Although the previous analysis should be complete and contain no sources for computational errors (greater than 10^{-12}), one final error did arise. This error manifested itself in the eighth decimal place after about 10^5 quarter-period calculations, but only for a few random initial conditions. Its effects were observed as random discontinuities in certain plots that should have been smooth ones. After many careful hand-calculations, the error was tracked down to the random truncation error in the 13^{th} decimal place by the Illiac II computer! This seemingly insignificant computer "fact-of-life" has overwhelming effects on the cnu_i inversion process when cnu_i is very close to one. If under QE or QH I motion we have $X_i \cong X_a$ or X_b within about one part in 10^{13}, then the ratio $cnu_i = X_i/X_a$ or $cnu_i = X_b/X_i$ will be about 1.0 to the same accuracy. But the computer would sometimes call this exactly 1.000..., while at other times it would truncate it to $0.999... = 1 - 10^{-13}$ (this is at the limit of its accuracy). Again this may seem inconsequential, but when we look at the inversions of these slightly different cnu_i values we find that $cn^{-1}(1.0) = 0.00$ while $cn^{-1}(1.0 - 10^{-13}) \cong 10^{-7}$. So suddenly we see the cause of the random discontinuities!

To overcome this problem we refer back to equations (35) and (36) for X_a and X_b in terms of the initial coordinates X_i and $\dot{X}_i$. Factoring these expressions and expanding them by means of the binomial theorem, we obtain respectively

$$X_a = X_i(1+\delta)^{\frac{1}{4}} = X_i(1 + \tfrac{1}{4}\delta - 3\delta^2/32 + \ldots) \tag{78}$$

and

$$X_b = X_i(1-\delta)^{\frac{1}{4}} = X_i(1 - \tfrac{1}{4}\delta + 5\delta^2/32 - \ldots) , \tag{79}$$

where

$$\delta = 2\dot{X}_i^2/p_o X_i^4 \ll 1 . \tag{80}$$

From equations (40a) and (41a) we obtain

$$\text{cnu} = X_i/X_a = (1 - \tfrac{1}{2}\delta + 3\delta^2/32 - \ldots) \quad \text{for QE} \tag{81}$$

and

$$\text{cnu} = X_b/X_i = (1 - \tfrac{1}{2}\delta + 5\delta^2/32 - \ldots) \quad \text{for QH I} . \tag{82}$$

Thus to first-order in δ (fourth-order in X_i) we obtain for <u>both</u> QE and QH I motions

$$\text{cnu} \cong 1 - \tfrac{1}{2}\delta \quad . \tag{83}$$

Since our given value of cnu_i differed from 1.0 by about 10^{-13}, the above approximation to first-order in δ is justified. Note that this value for cnu_i requires $u_o = 0$ in our cnu_i inversion routines. Then using equation (66a) for u_{i3} when $u_o = 0$ we obtain

$$u_{i3} = \sqrt{2(\tfrac{1}{2}\delta_i)} = \sqrt{\delta_i/2} \tag{84}$$

or

$$u_{i3} = \pm \dot{X}_i/(\sqrt{p_o}\, X_i^2) \quad (\text{for } u_o = 0). \tag{85}$$

Thus whenever

$$1.0 \geq \text{cnu}_i \geq \text{cn}(K/900) \tag{86}$$

(where cn(K/900) is the first table entry for b = 0.1), the value of u_{i3} would be calculated <u>directly</u> from $(X_i, \dot{X}_i)$ using equation (85), thus bypassing the regular inversion routines.

D. <u>Piecewise calculations</u>

Let us now turn to the actual procedures for the numerical calculations. In order to limit the amount of computations involved, we first choose fixed numerical values for our two parameters p_o and τ, namely

$$p_o = 0.037 \quad \text{and} \quad \tau = 6.0 \ . \tag{87}$$

These are arbitrarily chosen values, but they will generate solutions which can be scaled (both in phase-space and in time) in order to yield solutions for other values of p_o and τ. For more general equations with non-scaling parameters, or for non-integrable equations which possess some constants of the motion (e.g. the energy), we would have to use different values for those parameters or constants of the motion and calculate all the corresponding solutions. A complete representation of the structure of periodic solutions to the equations could then be obtained by plotting the phase-space trajectories for many different values of the parameters or constants of the motion. Treating these parameters then as continuous variables, we could thus generate sets of "eigensurfaces" of solutions in phase-parameter space[23]. But for our equation (20) we need select only one value for the parameters.

Since our numerical calculations will begin at t=0, it is clear from our definition of p(t) in equation (21) that for the first quarter-period ($\tau/4 = 1.5$) we will have $p(t) = p_o > 0$ and hence a quasi-elliptical (QE) motion. Then for the next half-period ($\tau/2 = 3.0$) we will have $p(t) = -p_o < 0$ and hence a quasi-hyperbolic (QH I or QH II) motion. Next will follow another half-period of QE motion, and so on for as long as we wish to calculate. A simple index counter can be employed to keep track of the sign of p(t) as a function of the number of quarter-periods of elapsed time. Note that we could have defined p(t) so that $p(0) = -p_o$ instead of $+p_o$ simply by shifting our p(t) by a half-period in time. Then the motion would have begun as QH I or QH II motion for the first quarter-period. We have arbitrarily chosen p(t) here so that we will begin with QE motion at t=0.

Before presenting a summary of the program logic for the computer calculations, it will be to our advantage to discuss in detail a few typical solutions for the possible motions. These will then illustrate the various features of the computational techniques. Let us first choose some set of initial coordinates $(X_i, \dot{X}_i)$ in our two-dimensional phase-space, for t=0. (In our program we make use of the polar coordinates r_i and θ_i as input variables, where $X_i = r_i \cos\theta_i$ and $\dot{X}_i = r_i \sin\theta_i$.) Specifically, let us choose this initial phase-space point to lie somewhere in the first quadrant and near the positive X-axis. This choice is not necessary in the general calculations.

Using the initial coordinates $(X_i, \dot{X}_i)$ we can calculate the X-axis intercept X_a from the first integral for QE motion, given in equation (35). The result for $X_i \neq 0$ is

$$X_a = +(2\dot{X}_i^2/p_o + X_i^4)^{\frac{1}{4}} \geq X_i \ . \tag{88}$$

(The case when $X_i = 0$ is discussed in the next section.) Next, using equations (40c) and then (40a) we can compute the <u>time</u> it would take to go from $(X_i, \dot{X}_i)$ to $(X_a, 0)$, namely

$$t_a = \left(\sqrt{p_o}\ X_a \right)^{-1} \ cn^{-1}(X_i/X_a) \geq 0 \ . \tag{89}$$

Now if $t_a = 1.5$ then the initial QE motion would just be completed at $(X_a, 0)$. If, however, $t_a < 1.5$ then the motion will continue on beyond (below) the X-axis for a time interval $t_1 = (1.5 - t_a) > 0$. To find the final coordinates (when t = 1.5) we simply use (40c) and then (40a) and (40b). Thus

$$X_1 = X_a \ cnu_1 > 0 \tag{90a}$$

$$\dot{X}_1 = -\sqrt{p_o}\ X_a^2 \ snu_1 dnu_1 < 0 \tag{90b}$$

where

$$u_1 = \sqrt{p_o}\, X_a\, t_1 > 0 \quad . \tag{90c}$$

If instead $t_a > 1.5$ then the QE motion will fall short of (or above) the X-axis by the time interval $t_1 = (1.5 - t_a) < 0$. With $t_1 < 0$ we clearly have $u_1 < 0$ also. From the symmetry properties of the elliptic functions (sn(-u) = -snu; cn(-u) = cnu; dn(-u) = dnu) we see that for $u_1 < 0$ we have $X_1 > 0$ and also $\dot{X}_1 > 0$. The magnitudes of X_1 and $\dot{X}_1$ are found by using equations (90a) and (90b). These coordinates, then, are simply a reflection in the X-axis of the coordinates of the motion for an equal but positive interval of t_1. Indeed, inspection of our original equation (20) readily reveals that it is <u>invariant</u> under the time-reversed operation $t \to -t$, as well as under the space reflection operation $X \to -X$, or under both simultaneously. This invariance follows from equation (20) plus the symmetry property p(t) = p(-t) built into our periodic square-wave function in equation (21).

Now that we have determined our phase-space coordinates $(X_1, \dot{X}_1)$ at the end of the first quarter-period, we can calculate the next half-period of quasi-hyperbolic motion. From equations (36) and (37) we see that it will be either QH I or QH II motion depending on our new initial coordinates $(X_1, \dot{X}_1)$ satisfying the conditions:

$$|\dot{X}_1| < \sqrt{p_o/2}\, X_1^2 \qquad \text{for QH I motion} \tag{91}$$

or

$$|\dot{X}_1| > \sqrt{p_o/2}\, X_1^2 \qquad \text{for QH II motion.} \tag{92}$$

Note that if $|\dot{X}_1| = \sqrt{p_o/2}\, X_1^2$ then the motion is parabolic (see the discussion of equation (38)).

Let us assume first that the motion is QH I. Paralleling the QE calculations we first find the intercept X_b on the X-axis

$$X_b = +(X_1^4 - 2\dot{X}_1^2/p_o)^{\frac{1}{4}} \leq X_1 \quad . \tag{93}$$

The time to go from $(X_1,\dot{X}_1)$ to $(X_b,0)$ would be

$$t_b = \left(\sqrt{p_o}\ X_b\right)^{-1} \mathrm{cn}^{-1}(X_b/X_1) \geq 0 \quad . \tag{94}$$

If $t_b = 3.0$ then the QH I motion would be completed at the point $(X_b,0)$. But if $t_b < 3.0$ then the motion will go beyond (above) the X-axis for a time interval $t_2 = (3.0 - t_b) > 0$. The final coordinates (when $t = 1.5 + 3.0 = 4.5$) will thus be

$$X_2 = X_b/\mathrm{cnu}_2 > 0 \tag{95a}$$

$$\dot{X}_2 = \sqrt{p_o}\ X_b^2\ \mathrm{snu}_2\mathrm{dnu}_2/\mathrm{cn}^2u_2 > 0 \tag{95b}$$

where

$$u_2 = \sqrt{p_o}\ X_b\ t_2 \quad . \tag{95c}$$

Similarly if $t_b > 3.0$ the motion will fall short of (or below) the X-axis for a negative time interval t_2. The final coordinates will still be calculated from the above equations, but now $\dot{X}_2 < 0$.

For the next half-period the motion will be QE again. The calculations for $(X_3,\dot{X}_3)$ will take the same form as equations (88), (89), and (90) except that $(X_i,\dot{X}_i)$ will be replaced by $(X_2,\dot{X}_2)$ and that (from now on) we must subtract t_a from 3.0 instead of 1.5. Thus in the present case we must calculate $t_3 = (3.0 - t_a)$. If $(X_2,\dot{X}_2)$ had been in the first quadrant, then we would obtain $X_3 > 0$, $\dot{X}_3 < 0$ for $t_3 > 0$ (or $\dot{X}_3 > 0$ for $t_3 < 0$). If $(X_2,\dot{X}_2)$ had been in the fourth quadrant, a different result would be obtained:

$(X_3, \dot{X}_3)$ would be in either the fourth or the third quadrant. We will return to this case in the next section of this appendix.

But first let us consider the next half-period of quasi-hyperbolic motion to be QH II motion starting from initial coordinates $(X_3, \dot{X}_3)$. Let us for the moment assume $X_3 > 0$ and $\dot{X}_3 < 0$ (which required $t_3 > 0$ plus the initial requirement that $X_2 > 0$, $\dot{X}_2 > 0$). We proceed in a manner similar to the QE and QH I cases already discussed above. First we calculate the constant c^2 from the first integral for QH II motion, equation (37):

$$c^2 = \pm(8\dot{X}_3^2/p_o - 4X_3^4)^{\frac{1}{2}} \quad . \tag{96}$$

Notice that the absolute value of the $\dot{X}$-axis intercept $\dot{X}_c$ will be given by

$$|\dot{X}_c| = \sqrt{p_o c^4/8} < |\dot{X}_3| \quad . \tag{97}$$

The time to go from $(X_3, \dot{X}_3)$ to $(0, -|\dot{X}_c|)$ would be

$$t_c = \left(\sqrt{p_o}\, c\right)^{-1} f^{-1}\left(\sqrt{2}\, X_3/c\right) > 0 \tag{98}$$

where as before

$$f(u) = snu/(1 + cnu) \quad .$$

(As mentioned before it is convenient to tabulate the function f(u) for $0 \leq u \leq 3K/2$ in order to facilitate taking its inverse.) If $t_c = 3.0$ then the QH II motion would be completed at $(0, -|\dot{X}_c|)$. If however $t_c < 3.0$ then the motion will go beyond (or to the left of) the $\dot{X}$-axis by a time interval $t_4 = (3.0 - t_c)$ which is positive. The final coordinates for this motion will be

$$X_4 = -\sqrt{c^2/2}\ \mathrm{snu}_4/(1 + \mathrm{cnu}_4) < 0 \qquad (99a)$$

$$\dot{X}_4 = -\sqrt{p_o/2}\ c^2\ \mathrm{dnu}_4/(1 + \mathrm{cnu}_4) < 0 \qquad (99b)$$

where

$$u_4 = \sqrt{p_o}\ c\ t_4 > 0 \qquad (99c)$$

and where the minus signs have been chosen to agree with QH II motion originating in the fourth quadrant (see the following section of this appendix). If $t_c > 3.0$ the motion will fall short (or to the right) of the $\dot{X}$-axis for a negative time interval t_4. The final coordinates will still be calculated from the above equations, but now $X_4 > 0$.

E. Final coordinate signs

Now that we have discussed several typical motions for a particular set of initial coordinates, it is clear that one problem remains to be solved. That problem is the unambiguous determination of signs for the final coordinates of the QE, QH I, or QH II motions originating in any arbitrary quadrant of the phase-plane.

The simplest way to calculate the final coordinates from any initial coordinates is first to calculate the absolute values of all quantities (e.g. $|\dot{X}_c|$, $|t_c|$, $|t_4|$, $|X_4|$, and $|\dot{X}_4|$ for the last case discussed). Then we can attach the appropriate signs. These signs can be determined a priori from a consideration of the general properties of motion. Let us look at QE motion first. This motion is described in clockwise quasi-elliptic arcs about the origin, concave inward (see equation (88)). Thus if $(X_i, \dot{X}_i)$ is in the first or third quadrant (i.e. if $X_i \dot{X}_i > 0$) then the motion will be towards the X-axis, with an intercept X_a. Thus the results outlined in

equations (88) to (90) will hold. That is, the sign of X_1 will equal the sign of X_i, while the sign of $\dot{X}_1$ will be equal or opposite to the sign of $\dot{X}_i$ according as $|t_a| > 3.0$ (or 1.5 in the first step only) or $|t_a| < 3.0$. In the special cases where $(X_i,\dot{X}_i)$ is on the $\pm$X-axis, then we will have $\dot{X}_1 < 0$ for $X_i > 0$, and $\dot{X}_1 > 0$ for $X_i < 0$.

If $(X_i,\dot{X}_i)$ is in the second or fourth quadrants (i.e. if $X_i\dot{X}_i < 0$) then the motion will be in clockwise arcs away from the X-axis, with an X-axis intercept X_a now in <u>past</u> time. Thus $|t_a|$ is just the time it would have taken to go from $(X_a,0)$ on the axis to $(X_i,\dot{X}_i)$. Therefore the <u>total</u> time from the X-axis to the final point $(X_1,\dot{X}_1)$ will be the sum $t_1 = (3.0 + |t_a|)$. To get the time it would take to go from $(X_i,\dot{X}_i)$ to the $\dot{X}$-axis (i.e. the axis towards which the motion is directed), we can subtract $|t_a|$ from the <u>total</u> time T_a it would take for a point to go from the X-axis initially to the $\dot{X}$-axis finally under QE motion. To find T_a we use equation (90a) and see that for $X_1 = 0$ (on the $\dot{X}$-axis finally) we must have $cnu_1 = 0$ or $u_1 = \sqrt{p_o}X_aT_a = K$. From equation (88) it is clear that for $\dot{X}_i = 0$ (on the X-axis initially) we have $X_a = X_i$. Thus the <u>maximum</u> time T_a between axes under QE motion will be

$$T_a = K/\left(\sqrt{p_o}\ X_i\right) . \qquad (100)$$

We can therefore conclude that the sign of X_1 will be equal or opposite to the sign of X_i corresponding to $(T_a - |t_a|) > 3.0$ or $(T_a - |t_a|) < 3.0$. The sign of $\dot{X}_1$ will generally remain the same as the sign of $\dot{X}_i$, unless the motion goes beyond the next quadrant, i.e. unless $(2T_a - |t_a|) < 3.0$. In the special cases that $(X_i,\dot{X}_i)$ is on the $\pm\dot{X}$-axis we see that $|t_a| = T_a$ above, so that $t_1 = (3.0 + T_a)$. Then for $\dot{X}_i < 0$ we will generally have $X_1 < 0$ (unless $2T_a < 3.0$, in which case $X_1 > 0$), while the sign of $\dot{X}_1$ will be equal or opposite to the sign of $\dot{X}_i$ corresponding to $T_a > 3.0$ or $T_a < 3.0$. For $\dot{X}_i > 0$

the results for the sign of $\dot{X}_1$ will still hold, but in general we now will have $X_1 > 0$ (unless $2T_a < 3.0$, in which case $X_1 < 0$).

Next let us consider QH I motion. This motion is described in counter-clockwise quasi-hyperbolic arcs about the origin, concave outward (see equation (93)). Thus if $(X_i,\dot{X}_i)$ is in the second or fourth quadrants (i.e. if $X_i\dot{X}_i < 0$) then the motion will be towards the X-axis, with an intercept X_b. Thus the results for the final coordinates will be those given in equations (93) to (95), with the following signs. The sign of X_2 will equal the sign of X_i, while the sign of $\dot{X}_2$ will be equal or opposite to the sign of $\dot{X}_i$ corresponding to $|t_b| > 3.0$ or $|t_b| < 3.0$. There is no possible sign change for X_2 (as there is for QE motion) since the QH I motion is outward and asymptotic to the characteristic straight lines of the quasi-hyperbola. On the other hand, if $(X_i,\dot{X}_i)$ is in the first or third quadrants (i.e. if $X_i\dot{X}_i > 0$) or if it is on the $\pm$X-axis (the $\pm\dot{X}$-axis is excluded by equation (91)) then the motion will be away from the X-axis, with the intercept X_b now in past time. That is, $|t_b|$ will be the time it would take to go from $(X_b,0)$ on the X-axis to $(X_i,\dot{X}_i)$. Therefore the total time to move from the X-axis to the final point $(X_2,\dot{X}_2)$ will be $t_2 = (3.0 + |t_b|)$. Clearly the signs of X_2 and $\dot{X}_2$ will be equal to those of X_i and $\dot{X}_i$ respectively (if $\dot{X}_i = 0$, then $\dot{X}_2 > 0$ for $X_i > 0$, while $\dot{X}_2 < 0$ for $X_i < 0$).

Finally let us consider QH II motion. This motion is described in clockwise arcs about the origin, concave outward (see equation (97)), with its intercept $(\dot{X}_c)$ now on the $\dot{X}$-axis. Thus for $(X_i,\dot{X}_i)$ in the second or fourth quadrants the motion is towards the $\dot{X}$-axis. Analogous to the $X_i\dot{X}_i < 0$ case for the QH I motion, the sign of $\dot{X}_4$ will equal the sign of $\dot{X}_i$, while the sign of X_4 will be equal or opposite to the sign of X_i corresponding to

$|t_c| > 3.0$ or $|t_c| < 3.0$. Again it is impossible for the sign of $\dot{X}_4$ to differ from the sign of $\dot{X}_i$ because the QH II motion arcs outward towards infinity. If now $(X_i, \dot{X}_i)$ is in the first or third quadrants or if it is on the $\pm\dot{X}$-axis (the $\pm X$-axis is excluded by equation (92)), the motion will be away from the $\dot{X}$-axis, and so $|t_c|$ will be the time to go from $(0, \dot{X}_c)$ on the $\dot{X}$-axis to $(X_i, \dot{X}_i)$. Thus the total time to move from the $\dot{X}$-axis to the final point $(X_4, \dot{X}_4)$ will be $t_4 = (3.0 + |t_c|)$. Again, the signs of X_4 and $\dot{X}_4$ will be equal to those of X_i and $\dot{X}_i$ respectively; if $X_i = 0$, then $X_4 > 0$ if $\dot{X}_i > 0$ while $X_4 < 0$ if $\dot{X}_i < 0$.

In conclusion, it can be seen that the calculation of the final coordinates of the motion is best done by computing only the magnitudes of the necessary quantities. Then a logical sign routine based on the above results can be constructed. A simple test of the product $(X_i \dot{X}_i)$ plus a determination of the type of motion involved will then simply and easily fix the signs of the final coordinates. (Recall that the motion is QE if $p(t) > 0$, and QH I or QH II according to equations (91) and (92) when $p(t) < 0$.) A summary of all these sign results together with the piecewise computational steps previously discussed are given in the beginning of the next appendix.

V. APPENDIX -- PROGRAMS

A. Summary of piecewise calculations and sign routines

Initial Tests: $p(t) = +p_o$ QE Motion

$$|X_a| = + (2\dot{X}_i^2/p_o + X_i^4)^{\frac{1}{4}}$$

$$|t_a| = (|X_a| \sqrt{p_o})^{-1} \, cn^{-1} \, (|X_i|/|X_a|)$$

$$|u_1| = \sqrt{p_o} \; |X_a| \; |t_1|$$

$$|X_1| = |X_a| \; cn|u_1|$$

$$|\dot{X}_1| = \sqrt{p_o} \; X_a^2 \; sn|u_1| \; dn|u_1|$$

$$T_a = K/(|X_i| \sqrt{p_o})$$

Case I: $(X_i \dot{X}_i) > 0$

Use: $t_1 = (3.0^* - |t_a|)$ in third equation above;

Set: Sign X_1 = Sign X_i if $t_1 < T_a$,

or Sign X_1 = -Sign X_i if $t_1 > T_a$;

Set: Sign $\dot{X}_1$ = Sign $\dot{X}_i$ if $t_1 < 0$ or $t_1 > 2T_a$,

or Sign $\dot{X}_1$ = -Sign $\dot{X}_i$ if $0 < t_1 < 2T_a$.

Case II: $\dot{X}_i = 0$

Use: $t_1 = 3.0^*$ in third equation above;

Set: Sign X_1 = Sign X_i if $T_a > 3.0^*$,

or Sign X_1 = -Sign X_i if $T_a < 3.0^*$.

Subcase 1: $X_i > 0$

Set: $\dot{X}_1 < 0$ if $2T_a > 3.0^*$,

or $\dot{X}_1 > 0$ if $2T_a < 3.0^*$.

Subcase 2: $X_i < 0$

Set: $\dot{X}_1 > 0$ if $2T_a > 3.0^*$,

or $\dot{X}_1 < 0$ if $2T_a < 3.0^*$.

Case III: $X_i = 0$

Use: $t_1 = (3.0^* + T_a)$ in third equation above;

Set: Sign $\dot{X}_1$ = Sign $\dot{X}_i$ if $T_a > 3.0^*$,

or Sign $\dot{X}_1$ = -Sign $\dot{X}_i$ if $T_a < 3.0^*$.

Subcase 1: $\dot{X}_i < 0$

Set: $X_1 < 0$ if $2T_a > 3.0^*$,

or $X_1 > 0$ if $2T_a < 3.0^*$.

Subcase 2: $\dot{X}_i > 0$

Set: $X_1 > 0$ if $2T_a > 3.0^*$,

or $X_1 < 0$ if $2T_a < 3.0^*$.

Case IV: $(X_i \dot{X}_i) < 0$

Use: $t_1 = (3.0^* + |t_a|)$ in third equation above ;

Set: Sign X_1 = Sign X_i if $t_1 < T_a$,

or Sign X_1 = -Sign X_i if $t_1 > T_a$;

Set: Sign $\dot{X}_1$ = Sign $\dot{X}_i$ if $t_1 < 2T_a$,

or Sign $\dot{X}_1$ = -Sign $\dot{X}_i$ if $t_1 > 2T_a$.

Return to Initial Tests

*(Use 1.5 instead of 3.0 for the first quarter-period of QE motion, plus the last quarter-period of the motion if the total period of the solution is to be an integer multiple of the period τ).

Initial Tests: $\left\{ \begin{array}{l} p(t) = -p_o \\ |\dot{X}_i| < \sqrt{p_o/2}\ X_i^2 \end{array} \right\}$ QH I Motion

$$|X_b| = + (X_i^4 - 2\dot{X}_i^2/p_o)^{\frac{1}{4}}$$

$$|t_b| = (|X_b| \sqrt{p_o})^{-1} \ cn^{-1}(|X_b|/|X_i|)$$

$$|u_2| = \sqrt{p_o}\ |X_b|\ |t_2|$$

$$|X_2| = |X_b|/cn|u_2|$$

$$|\dot{X}_2| = \sqrt{p_o}\ X_b^2 \ (sn|u_2|dn|u_2|)/cn^2|u_2|$$

Case I: $(X_i \dot{X}_i) > 0$

Use: $t_2 = (3.0 + |t_b|)$ in third equation above ;

Set: Sign X_2 = Sign X_i

and Sign $\dot{X}_2$ = Sign $\dot{X}_i$.

Case II: $\dot{X}_i = 0$

Use: $t_2 = 3.0$ in third equation above;

Set: Sign X_2 = Sign X_i

and $\dot{X}_2 > 0$ if $X_i > 0$,

or $\dot{X}_2 < 0$ if $X_i < 0$.

Case III: $X_i = 0$

Excluded (QH II Motion Only).

Case IV: $(X_i \dot{X}_i) < 0$

Use: $t_2 = (3.0 - |t_b|)$ in third equation above;

Set: Sign X_2 = Sign X_i

and Sign $\dot{X}_2$ = -Sign $\dot{X}_i$ if $t_2 > 0$,

or Sign $\dot{X}_2$ = Sign $\dot{X}_i$ if $t_2 < 0$.

Return to Initial Tests

Initial Tests: $\left\{ p(t) = -p_o \right.$; $\left. |\dot{X}_i| > \sqrt{p_o/2}\, X_i^2 \right\}$ QH II Motion

$$|c| = + (8\dot{X}_i^2/p_o - 4X_i^4)^{\frac{1}{4}}$$

$$|t_c| = (|c| \sqrt{p_o})^{-1} \; f^{-1} \; (\sqrt{2}\,|X_i|/|c|)$$

where $f(u) \equiv snu/(1 + cnu)$

$$|u_4| = \sqrt{p_o}\; |c|\; |t_4|$$

$$|X_4| = \sqrt{c^2/2}\; sn|u_4|/(1 + cn|u_4|)$$

$$|\dot{X}_4| = \sqrt{p_o/2}\; c^2\, dn|u_4|/(1 + cn|u_4|)$$

Case I: $(X_i \dot{X}_i) > 0$

Use: $t_4 = (3.0 + |t_c|)$ in fourth equation above;

Set: Sign $\dot{X}_4$ = Sign $\dot{X}_i$

and Sign X_4 = Sign X_i.

Case II: $\dot{X}_i = 0$

Excluded (QH I Motion Only).

Case III: $X_i = 0$

Use: $t_4 = 3.0$ in fourth equation above;

Set: Sign $\dot{X}_4$ = Sign $\dot{X}_i$

and $X_4 > 0$ if $\dot{X}_i > 0$,

or $X_4 < 0$ if $\dot{X}_i < 0$.

Case IV: $(X_i \dot{X}_i) < 0$

Use: $t_4 = (3.0 - |t_c|)$ in fourth equation above;

Set: Sign $\dot{X}_4$ = Sign $\dot{X}_i$

and Sign X_4 = -Sign X_i if $t_4 > 0$,

or Sign X_4 = Sign X_i if $t_4 < 0$.

Return to Initial Tests

B. NICAP program for the Illiac II

Opening routines (only one entry per run)

Calling of library subroutines for input/output, Lagrangian 6-point interpolation, arctangent, square root, cosine and sine functions;

SYSETC, TLOOP, QUAD1, QUAD2: Calculation and storage of Jacobian elliptic function tables (snu = SNARRY, cnu = CNARRY, dnu = DNARRY, and f(u) = snu/(1 + cnu) = SBYC).

Main program (EFPR3)

Input/output controls, various counters;

EFPRA: Conversion from input polar to cartesian coordinates.

ELOOP: Preparation for entry into QE Motion Loop.

H1LOOP: Preparation for entry into QH I Motion Loop.

H2LOOP: Preparation for entry into QH II Motion Loop.

OP: Output options with final coordinates, e.g. conversion back to polar coordinates, calculation of special functions such as $\Delta\theta$, Δr, and the ratio r_1/r_e = RUCRIN.

Subroutines

ELLIP: Calculations for QE Motion.

HYP1: Calculations for QH I Motion.

HYP2: Calculations for QH II Motion.

NVERS1: cnu = CNARRY inversion (both methods).

NVERS2: f(u) = SBYC inversion.

LOOKUP, LKAUX, AUXLK: Preparation of data for using the library subroutine for the six-point Lagrangian interpolation of the tables (i.e. for the direct lookup of off-table values).

SIGNEA: Final coordinate sign routine for QE Motion.

SIGN1A: Final coordinate sign routine for QH I Motion.

SIGN2A. Final coordinate sign routine for QH II Motion.

STXCAL: Special subroutine to calculate the statistical properties of certain functions (e.g. RUCRIN) for large numbers of solutions.

RDUM: Counter routine to allow recycling of calculations for multiples m of the basic mapping period n.

Input parameters

XPERM: The X-coordinate of the point to be used as the origin of the polar coordinates.

XDPERM: The $\dot{X}$-coordinate of the point to be used as the origin of the polar coordinates.

AMJOUT, AMJIN: The semi-major axes of two ellipses which form the outer and inner boundaries respectively of the (elliptical) annular region under study.

ECOUT, ECIN: The eccentricities of these two (outer and inner, respectively) bounding ellipses.

AMJOR: The semi-major axis a_o corresponding to the initial point in phase-space being mapped.

DELRAD: An increment in a_o if a regular series of a_o values is desired.

RADFIN: The final a_o in the desired series of a_o values (may equal AMJOR).

PHINP: The original angle θ_o corresponding to the initial point in phase-space being mapped.

DELPHI: An increment in θ_o if a regular series of θ_o values is desired.

ECCEN: The fixed eccentricity e_o corresponding to the initial point in phase-space being mapped.

XMAX: The maximum value of X which a final coordinate is allowed to attain.

N: The integer number of periods of τ of the basic mapping (printout every N periods).

M: The integer number of multiples of the basic period N (M lines of printout of N periods apiece).

P: The number of incremented values for θ_o (the number of times DELPHI is added for a given a_o; DELRAD is controlled by RADFIN).

Output parameters

M11: The running counter for the number of multiples m of the basic period n.

RUCRIN: The ratio of the mapped radius r_1 at the angle θ_1 to the radius r_e of a standard ellipse (specified by AMJOR and ECCEN) at the same angle θ_1.

LARGEG: The ratio of the mapped radius r_1 to the original radius r_o.

F: Moser's $\Delta\theta$ function = $(\theta_1-\theta_o)$.

SMALLG: Moser's Δr function = (r_1-r_o).

RAD: The mapped radius r_1 about (XPERM, XDPERM).

PHI: The mapped angle θ_1 about (XPERM, XDPERM).

XF: The mapped X-coordinate X_1.

XDF: The mapped $\dot{X}$-coordinate $\dot{X}_1$.

Q: The running counter for the number of increments P in the initial angle θ_o.

```
PRINT
READ
LAG6
ATAN1
SQR1
COS1
SIN1
SYSETC
*
*       M0      PAGE COUNT.
*       M2      'LOOPS'.
*       M4      FIXED POINT NUMBER, 'N'.
*       M5      ORBITS, 'M'.
*       M6      'P'.
*       M7      'Q'.
*       M8      USED ONCE ONLY, TO START OFF-AXIS IN ELLIP.
*       M9      SAME AS M5 (M), BUT USED IN CALCULATIONS.
*       M10     SAME AS M6 (P), BUT USED IN CALCULATIONS.
*       M11     OUTPUT COUNT.
*
        CALL    SYSETC
        DECQL   ,,IGNORE,
        CAD     K
        DIV     900.
        STR     SCALE
        CAD     15,3,
        STU     SNARRY          TABLE OF SN, CN, AND DN.

        ADD     1.
        STR     CNARRY          SET INITIAL TABLE VALUES

        STR     DNARRY
        CAD     PSZ

        CALL    SQR1
        STR     RPSZ
*
*
*   RED     RED     RED     RED     RED     RED     RED     RED
        CSM     0,900           LOOP COUNTER.
        LFR     2,Q             F2 = Q = QFAST
        CAD     QFAST
        MPY     F1
        STU     F3
        SFR     3,Q2
        MPY     F3
        STU     Q4              Q**4 = Q4
        MPY     F1
        STU     Q6              Q**6 = Q6
```

```
        MPY     F1
        MPY     QFAST
        STU     Q9              Q**9 = Q9

        MPY     F1
        MPY     F3
        STU     Q12             Q**12 = Q12

        ADD     Q6
        ADD     Q2

        ADD     1.              Q12+Q6+Q2+1
        STR     CQ              GOES TO CQ

        CAD     Q9
        ADD     Q4

        ADD     QFAST
        ADD     10,3,2048       Q9+Q4+Q+1/2
        STR     AQ              GOES TO AQ
        LFR     3,RINCR
TLOOP   CAT     RFAST
        CALL    COS1
        MPY     Q               *Q
        STU     F5              TO F5
        CAD     RFAST
        MPY     6.
        CALL    COS1
        MPY     Q9              * Q9
        STU     F6              TO F6
        CAD     RFAST
        MPY     4.
        CALL    COS1
        MPY     Q4              *Q4
        ADD     10,3,2048       1/2
        SUB     F5              -QCOS(RINCR)-Q9*COS(6*RINCR)
        SUB     F6
        MPY     CQ
        STR     BNQCQ           TO BNQCQ
        CAD     RFAST
        MPY     5.

        CALL    SIN1
        MPY     Q6              * Q6
        STR     F5              TO F5
        CAD     RFAST
        MPY     3.
```

```
        CALL    SIN1
        MPY     Q2              * Q2
        STU     F6              TO F6
        CAD     RFAST
        MPY     7.
        CALL    SIN1
        MPY     Q12             *Q12
        STU     F7              TO F7
        CAD     RFAST
        CALL    SIN1
        ADD     F5              Q6SIN(5*RINCR)
        SUB     F6              -Q2SIN(3*RINCR)
        SUB     F7              -Q12SIN(7*RINCR)
        MPY     AQ              *(Q9+Q4+Q+1/2)

        DIV     BNQCQ           BY Q4COS(4*RINCR)+1/2-
        STR     SNARRY+M0+901   ELLIPTIC SINE.

        MPY     FQ              1 -(SNU*SIN(RINCR))
        STR     F5              -Q6SIN(5RINCR)  ROOTED
        CAD     1.

        SUB     F5
        CALL    SQR1
        STR     CNARRY+M0+901   ELLIPTIC COSINE.
        CAD     2.              2 - Q6SIN(5*RINCR) * 1/2
        SUB     F5              ROOTED
        DIV     2.
        CALL    SQR1

        STR     DNARRY+M0+901   ELLIPTIC TANGENT.
        CAD     RINCR
        ASC     RFAST           INCREMENT R...
        CJU     M0,TLOOP        AND LOOP.
        CSM     0,901

        CAM     1,SNARRY
        CAM     2,CNARRY

QUAD1   CAD     2,1,
        ADD     1.
        VID     1,1,
        STR     SBYC+M0+901
        CJU     0,QUAD1

        CSM     0,801
        CAM     1,SNARRY+899
```

```
         CAM     2,CNARRY+899
QUAD2    CSB     2,,
         ADD     1.
         VID     1,,
         STR     SBYC+MO+1702

         SBM     1,1
         SBM     2,1

         CJU     0,QUAD2
         FIL
*     MAIN PROGRAM---(E)LLIPTIC (F)IXED (P)OINT, (R)ED---
*
*     LOOPS = MODIFIER 2
*
EFPR3    CAM     1,READIN
         CALL    READ
         CAM     1,CTOFF
         CALL    READ
         CAM     1,PRINTN
         CALL    PRINT
         CAM     1,CTOFFP
         CALL    PRINT
         CSM     0,41                PAGE COUNTER.
         LFR     5,SETUP
         CRN     4,12
         CSM     4                   FIXED POINT NUMBER.
         CSM     5,M5                TOTAL NUMBER OF ORBITS.

         CAM     7,1                 SET INITIAL VALUE OF Q.
         SFR     5,SETUP             SAVE INPUT COUNTERS.

         CSM     9,M5
         CAM     10,M6

         CAM     11                  SET INITIAL VALUE OF M(6)
         SFR     6,COUNT             3,COUNT = 0.
         CAD     15,3,
         STU     AVRUC
         STU     RMRUC

         STU     AVG
         STU     RMG

EFPRB    CAM     1,HEAD
         CALL    PRINT
```

```
         CAD     PHINP
         STR     PHIIN
EFPRA    CALL    RDUM
         DECQL   AMJOR,ECCEN,PHIIN,RADIN
         CAD     PHIIN
         DIV     180.
         STR     F3
         CALL    COS1
         MPY     RADIN
         ADD     XPERM
         STR     XINP
         STR     XIN
         STR     XINS
         STR     XF
         CAD     F3
         CALL    SIN1
         MPY     RADIN
         ADD     XDPERM
         STR     XDINP
         STR     XDIN
         STR     XDINS
         STR     XDF
         CAD     15,3,
         STU     F

         STU     SMALLG

         STU     LARGEG
         ADD     1.

         STR     RUCRIN
         CAD     RADIN

         STR     RAD
         CAD     PHIIN

         STR     PHI
         CAM     1,OUT

         CALL    PRINT
         CSM     LOOPS,1
         CSM     8,1                    FIRST ELLIPTIC ENTRY.
ELOOP    CALL    ELLIPA
         CALL    OP
         CJU     LOOPS,ELOOP
         CSM     LOOPS,2
         CAM     8
         CAD     X
         CAV     XMAX
```

```
         TP      CXMAX          PRINT X, XD, THEN READ IN NEW
         CAD     X

         MPY     F1
         STR     F3
         CAD     PSZ

         DIV     2.
         CALL    SQR1

         MPY     F3
         CAV     XC
         TN      H2LOOP

H1LOOP   CALL    HYP1A
         CALL    OP
*
*
         CJU     LOOPS,H1LOOP
         CSM     LOOPS,2
         TRA     ELOOP
H2LOOP   CALL    HYP2A
         CALL    OP
*
*
         CJU     LOOPS,H2LOOP
         CSM     LOOPS,2
         TRA     ELOOP
OP       SFR     4,OPBSS        SAVE RETURN.
         CJZ     LOOPS,OPC      JUMP IF ON SECOND LOOP TO OUTP
         CAD     XZERO
         STR     XIN
         CAD     XCZERO

         STR     XCIN
         CAD     TBY4
         ASC     T
         CJU     4,OPX          JUMP IF NO OUTPUT IS DESIRED.
         LDM     4,SETUP        RESET OUTPUT COUNTER.
         CAD     X
         SUB     XPERM
         STR     DELX
         CAD     XC
         SUB     XCPERM
         STR     DELXC
         CAD     RAC
         STR     RADOLD
         CAD     PHI
         STR     PHIOLD
```

```
        CAD     DELX
        MPY     F1
        STR     F0
        CAD     DELXD
        MPY     F1
        ADD     F0
        CALL    SQR1
        STR     RAD
        CAD     DELXD
        DIV     DELX
        CALL    ATAN1
        MPY     180.
        DIV     PI
        STR     PHI
        CALL    PHIST
        LFR     6,COUNT
        ADM     11,1                    INCREMENT RUNNING COUNTER (M11)
        SFR     6,COUNT
        CALL    RDUM
        DECQL   AMJOR,ECCEN,PHI,RADNEW
        CAD     RAD
        DIV     RADNEW
        STR     RUCRIN
        ASC     AVRUC
        CAD     RUCRIN
        MPY     F1
        ASC     RMRUC

        CALL    RDUM
        DECQL   AMJOUT,ECOUT,PHI,ROUT
        CALL    RDUM
        DECQL   AMJIN,ECIN,PHI,RIN
        CAD     RAD
        SUB     ROUT
        TU      OPG.
        CAD     15,3,
        STU     LARGEG

        TRA     OPF
OPG     CAD     RAD

        SUB     RCUT
        DAV     15,3,
        STR     F2
        CAD     ROUT
```

```
        SUB     RIN

        CAV     15.3.
        STR     F3
        MPY     F2
        MPY     2.
        STR     F7
        CAD     RAD

        SUB     RIN
        CAV     15.3.
        ADD     F2
        SUB     F3
        DIV     F7
        STR     FQ
        CAD     RAD
        SUB     ROUT
        MPY     FQ
        STR     LARGEG
OPF     CAD     PHI

        SUB     PHIOLD
        TP      OPD

        ADD     360.
OPD     STR     F

        CAD     RAD
        SUB     RADOLD

        STR     SMALLG
        CAD     X

        STR     XF
        CAD     XC

        STR     XDF
        CAD     LARGEG

        ASC     AVG
        CAD     LARGEG

        MPY     F1
        ASC     RMG
        JNM     0,OPE
        CAM     1,HEAD          HEAD TOP OF PAGE.
        CALL    PRINT
```

```
        CSM     0,44            OUTPUT PAGE COUNTER.
OPE     CAM     1,OUT
        CALL    PRINT
        ADM     0,2             UPDATE PAGE COUNTER.
        CAD     X
        CAV     XMAX
        TP      CXMAX           PRINT X, XD, THEN READ IN NEW C
        CJZ     5,OPA
OPX     LDM     3,OPBSS         RESTORE RETURN.
        LDM     LOOPS,OPBSS     RESTORE LOOP COUNTER.
        JLH     3,,             EXIT.
OPA     LFR     6,COUNT

        CAD     AVRUC
        DIV     M9.

        STR     AVGR
        MPY     F0
        STR     F3
        CAD     RMRUC
        DIV     M9.
        CALL    SQR1

        STR     RMSR
        MPY     F0
        SUB     F3
        CALL    SQR1
        STR     SIGMAR
        CAD     AVG
        DIV     M9.
        STR     AVGG

        MPY     F0
        STR     F3
        CAD     RMG

        DIV     M9.
        CALL    SQR1
        STR     RMSG
        MPY     F0
        SUB     F3
        CALL    SQR1
        STR     SIGMAG
        CAM     1,SMOUT1
        CALL    PRINT
        ADM     0,8             INCREMENT PAGE COUNTER.
        CAD     15,3,
        STU     AVRUC
```

```
         STU     RMRUC
         STU     AVG

         STU     RMG
         CAM     8,M7-M6

         JNM     8,OPB
         TRA     STXCAL
OPB      CAD     DELRAD
         MPY     DELPHI
         TU      OPH
         CAD     DELRAD
         ASC     AMJOR
OPH      CAD     DELPHI
         ASC     PHIIN
         LFR     5,SETUP
         ADM     7,1
         SFR     5,SETUP
         LFR     6,COUNT
         CAM     11
         SFR     6,COUNT
         CAM     1,SKIP

         CALL    PRINT

         ADM     0,3             INCREMENT PAGE COUNTER.
         TRA     EFPRA
OPC      CAD     X
         STR     XIN
         STR     XINS
         CAD     XD
         STR     XDIN
         STR     XDINS
         TRA     OPX
OPBSS    BSS     1
*
*
ELLIPA   SFR     4,ELLBSS        SAVE RETURN.
         SFR     5,ELLBSS+1
         CJZ     8,ELLIPG
         CJZ     LOOPS,ELLIPC
ELLIPG   CAD     XIN
         MPY     XDIN
         STR     F0
         CAV     15,3,
         VID     F0
         TOR     ELLIPE
```

```
        TRA     ELLIPF
ELLIPE  CSB     1.

ELLIPF  STR     MCTION
        CAD     XIN

        MPY     F1
        MPY     F1
        MPY     F1
        STR     F7
ELLIPB  CAD     XDIN
        MPY     F1
        MPY     2.
        DIV     PSZ
        STR     DELONE
        DIV     F7
        STR     DELTWO

        SUB     RERROR
        TP      ELLIPQ

        CAD     DELTWO          APPROXS. FOR WHEN XZERO IS NEAR
        DIV     4.

        ADD     1.
        MPY     XIN

        STR     XZERO
        CALL    SIGNEA

        CAD     DELTWO
        NDV     4.
        ADD     1.
        STR     TSTCNU
        CAD     DELTWO
        DIV     2.
        CALL    SQR1

        STR     U
        TRA     ELLIPR
ELLIPQ  CAD     DELONE
        ADD     F7
        CALL    SQR1

        CALL    SQR1
        STR     XZERO           X AT ABCISSA
*
        CALL    SIGNEA
```

```
        CAD     XZERO
        VID     XIN
        STR     TSTCNU
*
        CALL    NVERS1
*
*
ELLIPR  CAD     15,3,
        STU     XDZERO
        CAD     RPSZ

        MPY     XZERO
        VID     U

        CAV     15,3,
        STR     TZERO           TIME TO ABCISSA
*
        MPY     MCTION
        SUB     TBY4
        STN     T               NEW TIME
*
*
ELLIPC  CAD     T
        MPY     XZERO
        STR     F7
        CAD     RPSZ

        MPY     F7
        STR     TESTU
*
        CALL    LCOKUP
        CAD     CNU
*
        MPY     XZERO
        STR     X               NEW X
*
        CALL    SIGNEB
*
*
*
*
        CAD     RPSZ
        MPY     XZERO
        MPY     F1
        MPY     SNU
        MPY     DNU

        STN     XD              NEW XD
```

```
        CALL    SIGNEC

        CAD     EQCT
        SAM     MCTION
        JZM     8,ELLIPH
        JUM     LCOPS,ELLIPD
ELLIPH  CAD     XINS
        MPY     XDINS
        TP      ELLIPD
        CAD     PSI
*
        STR     T
*
*
ELLIPD  LFR     4,ELLBSS        DELETE ELLIPD LABEL FOR PH (PRIN
        LFR     5,ELLBSS+1
        JLH     3,,             EXIT
ELLBSS  BSS     2
*
        ASSIGN  DELONE,DELTWO

RERROR  DEC     1.0E-07
HYP1A   SFR     4,HY1BSS        SAVE RETURN.
        SFR     5,HY1BSS+1
        CJZ     LOOPS,HYP1C
        CAD     XIN
        MPY     XDIN
        STR     F0
        CAV     15,3,
        VID     F0
        STR     MOTION
        CAD     XIN

        MPY     F1
        MPY     F1
        MPY     F1
        STR     F7
HYP1B   CAD     XDIN
        MPY     F1
        MPY     2.
        NDV     PSZ
        STR     DELONE
        NDV     F7
        STR     DELTWO

        SUB     RERROR
        TP      HYP1Q
```

```
         CAD     DELTWO          APPROXS. FOR WHEN XZERO IS NEAR
         NDV     4.

         ADD     1.
         STR     TSTCNU

         MPY     XIN
         STR     XZERO

         CALL    SIGN1A
         CAD     DELTWO
         DIV     2.

         CALL    SQR1
         STR     U
         TRA     HYP1R
HYP1Q    CAD     DELONE
         ADD     F7
         CAV     15,3,
         CALL    SQR1
         CALL    SQR1
         STR     XZERO           X AT ABCISSA
*
         CALL    SIGN1A
         CAD     XZERO
         DIV     XIN
         STR     TSTCNU
*
         CALL    NVERS1
*
*
HYP1R    CAD     15,3,
         STU     XDZERO
         CAD     RPSZ

         MPY     XZERO
         VID     U

         CAV     15,3,
         STR     TZERO           TIME TO ABCISSA
*
         MPY     MCTION
         ADD     TBY4
         STR     T
HYP1C    CAD     T
*
         MPY     XZERO
         STR     F7
         CAD     RPSZ
```

```
        MPY     F7
        STR     TESTU
*
        CALL    LOOKUP
*
*
        CAD     XZERO
        DIV     CNU
        STR     X                       NEW X
*
        CALL    SIGN1B
*
*
*
*
        CAD     XZERO
        MPY     F1
        MPY     SNU

        MPY     DNU
        STR     F7
        CAD     RPSZ
        MPY     F7

        DIV     CNU

        DIV     F1
        STR     XD                      NEW XD
*
        CALL    SIGN1C
        CAD     H10CT
        SAM     MOTION
*
*
        LFR     4,HY1BSS                RESTORE RETURN.
        LFR     5,HY1BSS+1
        JLH     3,,                     EXIT
HY1BSS  BSS     2
*
HYP2A   SFR     4,HY2BSS                SAVE RETURN.
        SFR     5,HY2BSS+1
        CJZ     LOOPS,HYP2C
        CAD     XIN
        MPY     XDIN
        STR     F0
        CAV     15,3,
        VID     F0
        STR     MCTION
        CAD     XIN
```

```
        MPY     F1
        MPY     F1
        MPY     F1
        MPY     4.
        STN     F7
        CAD     XDIN

        MPY     F1
        MPY     8.
        DIV     PSZ
        ADD     F7
        CAV     15,3,
        CALL    SQR1
        CALL    SQR1
        STR     F6              F6 = A
        CAD     F7
        MPY     PSZ
        DIV     8.
        STR     F7
HYP2B   CAD     XDIN

        MPY     F1
        ADD     F7
        CAV     15,3,
        CALL    SQR1
        STR     XDZERO          XD AT ORDINATE
*
        CALL    SIGN2A
        CAD     2.
        CALL    SQR1
        MPY     XIN
        DIV     F6
        STR     TSTSBC
        CAV     15,3,
        CALL    NVERS2
*
*
        CAD     15,3,
        STU     XZERO
        CAD     RPSZ

        VID     U
        DIV     F6
        STR     TZERO           TIME TO ORDINATE
*
        MPY     MOTION
        ADD     TBY4
        STR     T
```

```
*
HYP2C   CAD     RPSZ
        MPY     T
        MPY     F6
        STR     TESTU
*
        CALL    LOOKUP

        CAD     CNU
*
        ADD     1.
        STR     F7
        CAD     2.
        CALL    SQR1

        MPY     F7
        STR     F7
        CAD     SNU
        MPY     F6
        DIV     F7
        STR     X               NEW X
*
        CALL    SIGN2B
*
*
*
*
        CAD     PSZ
        DIV     2.
        CALL    SQR1
        MPY     DNU
        MPY     F6
        MPY     F6
        STR     F7
        CAD     CNU
        ADD     1.

        VID     F7
        STR     XC              NEW XD
*
        CALL    SIGN2C
        CAD     H2OCT
        SAM     MCTION
        LFR     4,HY2BSS        RESTORE RETURN.
        LFR     5,HY2BSS+1
        JLH     3,,             EXIT
HY2BSS  BSS     2
```

```
*
NVERS1  SFR     4,NV1BSS        SAVE RETURN.
        STR     F2              F2 = TEST CNU
        CAM     0
        CAM     1,CNARRY.       M1 = CNARRY
        LDM     4,COVAL
        CSM     4,M4
N1A     CAD     F2
        CAV     1,1,
        TP      N1B
        ADM     0,1
        TRA     N1A
N1B     SBM     0,183           ACCURACY CROSSOVER OCCURS AT ENT
        JPM     0,N1C
        CAD     1.              BEGIN APPROX. FOR SMALL TABLE VA
        SUB     F2
        STR     F3
        CAD     1.
        ADD     F2
        VID     F3
        STR     F3
        MPY     F3
        MPY     F3
        NDV     5.
        ADD     F3
        ADE     1
        CALL    SQR1
        TRA     N1D
N1C     ADM     0,183.          2ND ORDER ITERATION FOR REST OF
        SBM     0,900
        JUM     0,N1E
        ADM     0,900
        CAD     F2
        STR     F3
        CAD     2.
        CALL    SQR1
        MPY     F3
        SUB     K
        STN     F0
        CAD     FC
        TRA     N1D
N1E     ADM     0,900

        CAD     M0-1.
        DIV     900.
        MPY     K
        STR     U0
        CAD     CNARRY+M0-1
        MPY     F1
        MPY     F1
```

```
        STR     F3
        CAC     SNARRY+MO-1

        MPY     DNARRY+MO-1
        STR     F2                      F2 = SN(I) * DN(I)

        CAC     TSTCNU
        SUB     CNARRY+MO-1
        NDV     F2
        STR     F0
        MPY     F0
        MPY     F3
        NDV     F2
        MPY     1C,3,2048
        ADD     F0
        ADD     U0
N1D     STR     U
        STR     TESTU
        CALL    LOOKUP
        CAC     CNU
        SUB     TSTCNU
        STR     DELCNU
        CAV     15,3,
        SUB     ERROR

        TZN     N1X
        CJZ     4,EFPR3

        CAC     DELCNU
        DIV     SNU

        DIV     DNU
        ADD     U

        TRA     N1D
N1X     LFR     4,NV1BSS

        JLH     3,,                     EXIT
NV1BSS  BSS     1
*
        ASSIGN  DELCNU,DELSBC

ERROR   DEC     1.0E-12
NVERS2  SFR     4,NV2BSS                SAVE RETURN.
        SFR     5,NV2BSS+1              SAVE F5
        SFR     6,NV2BSS+2              SAVE F6
        SFR     7,NV2BSS+3              SAVE F7
        STR     F5                      F5 = TEST  SN/1+CN
        CAV     SBYC+901
        TP      N2B                     IF SBYC IS IN SECOND QUADRANT.
```

```
        CAM     0
        CAM     1,SBYC          SBYC IS PRIME VALUED.
N2C     CAD     1,1,
        CAV     F5
        TP      N2G
        ADM     0,1
        TRA     N2C
N2G     CAM     2,M0
        SBM     0,183
        JPM     0,N2E
        CAD     F5              BEGIN APPROX. FOR SMALL TABLE VA
        STR     F2
        MPY     F2
        MPY     F2
        MPY     F2

        MPY     F2
        NDV     10.
        ADD     F2
        MPY     2.

        TRA     N2X
N2E     ADM     0,183           2ND ORDER ITERATION FOR REST OF

        ANM     0,8190
        CRM     0,1

        EOM     0,450
        JUM     0,N2F

        CAM     0,M2
        CAD     F5
        MPY     2.
        SUB     1.
        CALL    SQR1
        SUB     1.
        STR     F3
        CAD     2.

        CALL    SQR1
        MPY     F3
        ADD     K
        TRA.    N2X

N2F     CAM     0,M2
        CAD     M1-2

        STR     F2
        CAV     F5
```

```
        STN     F3
        CAD     MC-1.
        DIV     900.

        MPY     K
        STR     UC

        CAD     1.
        ADD     CNARRY+MO-1

        STR     F0
        CAD     1.
        SUB     CNARRY+MO-1
        DIV     F0
        STR     F6
        CAD     CNARRY+MO-1
        ADD     1.
        VID     DNARRY+MO-1
        TRA     N2A
N2B     CAM     1,SBYC+901
        CAM     0
N2D     ADM     0,1

        CAC     1,1,
        CAV     F5
        TN      N2D
        CAC     M1-2
        STR     F2
        CAV     F5
        STN     F3
        CAC     MC-1.

        DIV     900.
        MPY     K

        ADD     K
        STR     UC

        CAD     1.
        SUB     CNARRY-MO+901

        STR     F0
        CAD     1.

        ADD     CNARRY-MO+901
        DIV     F0
        STR     F6
        CSB     CNARRY-MO+901
```

```
         ADD     1.
         VID     DNARRY-MO+901

N2A      STR     F7
         VID     F3
         STR     F3
         MPY     F3
         MPY     F6
         MPY     F2
         DIV     F7
         NDV     4.
         ADD     F3
         ADD     UO
N2X      STR     U
         STR     TESTU
         CALL    LOOKUP
         CAD     CNU
         ADD     1.
         VID     SNU
         CAV     15,3,
         SUB     F5
         STN     DELSBC
         CAV     15,3,
         SUB     ERROR

         TZN     N2XT
         CAD     CNU

         ADD     1.
         MPY     DELSBC

         DIV     DNU
         ADD     U

         TRA     N2X
N2XT     LFR     4,NV2BSS
         LFR     5,NV2BSS+1      RESTORE F5
         LFR     6,NV2BSS+2      RESTORE F6

         LFR     7,NV2BSS+3      RESTORE F7
         JLH     3,,             EXIT
*NV2BSS  BSS     4
 LOOKUP  SFR     4,LKPBSS        SAVE RETURN.
         CAM     0               MO = 0
         IZP     LKP6            TRANSFER IF TESTU .GE. 0

LKP1     ADD     K4              TESTU .L. 0
         TN      LKP1
```

```
LKP2    SUB     K
        IN      LKP3

        ADM     0,1
        TRA     LKP2

LKP3    ADD     K
LKP4    CRM     0,1

        JNM     0,LKP5          JUMP IF MO IS ODD.
        DIV     SCALE

        STR     F2              MO IS EVEN.
        TRA     LKAUX           TRANSFER TO LKAUX.
LKP5    SUB     K               MO IS ODD.
        DIV     SCALE
        STN     F2
        TRA     LKAUX           TRANSFER TO LKAUX.
LKP6    SUB     K4              TESTU .GE. 0

        TP      LKP6
LKP7    ADD     K

        ADM     0,1
        TZN     LKP7

        EOM     0,7             MASK MO FOR U .G. 0 ...
        SBM     0,3             AND SET MO.

        TRA     LKP4
LKPBSS  BSS     1
*
LKAUX   SFR     5,LKXBSS        SAVE F5.
        SIA     4               M4 = TABLE VALUE.
        SBM     4,2             OK IF M4 .GE. 2

        JNM     4,LKX4          JUMP IF M4 .L. 2
        SBM     4,897           OK IF M4 .L. 898

        JNM     4,LKX3          JUMP IF M4 IS IN RANGE.
        CAM     4,SNARRY+894    M4 .GE. 898, END OF TABLE.

        CAM     5,CNARRY+894
        CAM     6,DNARRY+894

        CSM     7,6
LKX1    CAD     4,1,            SET END OF TABLES VALUES.
```

```
        STR     SNARRY+900-M7
        CAD     5,1,
        STN     CNARRY+900-M7
        CAD     6,1,
        STR     DNARRY+900-M7
        CJU     7,LKX1

        CAD     F2
        SUB     894.
        CAM     1,ELKAUX
LKX2    CALL    LAC6
        TRA     ALXLK
LKX3    CAD     F2
        CAM     1,CWLAG6

        TRA     LKX2            TO LAG6.
LKX4    CAM     4,SNARRY+1      M4 .L. 2, BEGINNING OF TABLE.

        CAM     5,CNARRY+1
        CAM     6,DNARRY+1

        CSM     7,6
LKX5    CAD     4,1,            SET BEGINNING OF TABLE VALUES.
        STN     SNARRY-7-M7
        CAD     5,1,
        STR     CNARRY-7-M7
        CAD     6,1,
        STR     DNARRY-7-M7
        CJU     7,LKX5

        CAD     F2
        ADD     6.
        CAM     1,BLKAUX
        TRA     LKX2            TO LAG6.
*LKXBSS BSS     1
AUXLK   JPM     0,AXLK3         JUMP IF M0 IS EVEN.
        CRM     0,1             M0 IS ODD.
        JNM     0,AXLK2         JUMP IF M0 = 3 = 7 =...
        CAD     CNU             M0 = 1 = 5 = ...
        STN     CNU
AXLK1   LFR     4,LKPBSS        RESTORE RETURN.
        LFR     5,LKXBSS        RESTORE F5
        JLH     3,,             EXIT.
AXLK2   CAD     SNU             M0 = 3 = 7 =...

        STN     SNU
        TRA     AXLK1           TRANSFER TO EXIT.
```

```
AXLK3   CRM     0,1             MQ IS EVEN.
        JPM     0,AXLK1         JUMP TO EXIT IF MQ = 0 = 4 =.

        CAD     SNU             MQ = 2 = 6 = ...
        STN     SNU

        CAD     CNU
        STN     CNU

        TRA     AXLK1           TRANSFER TO EXIT.
SIGNEA  MPY     XINS
        TP      SIGNEA+2
        CAD     XZERO

        STN     XZERO
        JLH     3,,
SIGNEB  CAD     XINS
        MPY     XDINS
        TN      SEBA
        CAD     X
        MPY     XINS
        TP      SEBBX
        CAD     X
        STN     X
SEBBX   JLH     3,,             EXIT.
SEBA    CAD     K
        DIV     XZERO

        DIV     RPSZ
        DAV     15,3,
        SUB     TZERO
        STR     PSI
        JZM     LOOPS,SEBC
        DAV     TBY4            FIRST LOOP.
SEBF    TP      SEBD
        CAD     XINS
        MPY     X
        TN      SEBBX
SEBE    CAD     X
        STN     X
        TRA     SEBBX
SEBD    CAD     XINS
        MPY     X
        TP      SEBBX
        TRA     SEBE
SEBC    DAV     3.              SECOND LOOP.
        TRA     SEBF
```

```
SIGNEC  CAD     XINS
        MPY     XDINS
        TN      AUXE

        CAD     TZERO
        JZM     LOOPS,SECA

        CAV     TBY4
SECE    TN      SECB
AUXE    CAD     XD
        MPY     XDINS

        TP      SECCX
SECD    CAD     XD
        STN     XD
SECCX   JLH     3,,             EXIT.
SECB    CAD     XD

        MPY     XDINS
        TZN     SECCX

        TRA     SECD
SECA    CAV     3.

        TRA     SECE
SIGN1A  EQUL    SIGNEA
SIGN1B  MPY     XINS
        TP      SIGN1B+2
        CAD     X

        STN     X
        JLH     3,,             EXIT.
SIGN1C  CAD     XINS
        MPY     XDINS
        TP      AUX1

        CAD     TZERO
        JZM     LOOPS,S1A

        CAV     TBY4
S1E     TN      S1B
AUX1    CAD     XD
        MPY     XDINS

        TP      S1CX
S1D     CAD     XD
        STN     XD
S1CX    JLH     3,,
S1B     CAD     XD
        MPY     XDINS

        TZN     S1CX
        TRA     S1D
```

```
S1A     CAV     3.
        TRA     S1E

SIGN2A  MPY     XDINS
        TP      SIGN2A+2

        CAD     XDZERO
        STN     XDZERO

        JLH     3,,
SIGN2C  MPY     XDINS
        TP      SIGN2C+2
        CAD     XD
        STN     XD
        JLH     3,,
SIGN2B  CAD     XINS

        MPY     XDINS
        TP      AUX2

        CAD     TZERO
        JZM     LCOPS,S2A

        CAV     TBY4
S2E     TN      S2B

AUX2    CAD     X
        MPY     XINS

        TP      S2CX
S2D     CAD     X

        STN     X
S2CX    JLH     3,,             EXIT.
S2B     CAD     X

        MPY     XINS
        TZN     S2CX
        TRA     S2D

S2A     CAV     3.
        TRA     S2E
STXCAL  CAD     DELRAD
        MPY     DELPHI
        TZ      EFPR3
        CAD     AMJOR

        SUB     RADFIN
        TZP     EFPR3
        CAD     DELRAD
        ASC     AMJOR
```

```
        LFR     5,SETUP
        CAM     7,1
        SFR     5,SETUP
        LFR     6,COUNT
        CAM     11
        SFR     6,COUNT
        CAC     15,3,
        TRA     EFPRB
*       CALL    RDUM
*       DECQL   ADUM,ECDUM,PHIDUM,RDUM
RDUM    SFR     2,RDMBSS        SAVE F2.
        SFR     3,RDMBSS+1      AND F3.
        SFR     4,RDMBSS+2      SAVE RETURN.
        SFR     5,RDMBSS+3      AND F5.
        LFR     5,M3            M4 = ADUM,M5 = ECDUM,M6 = PHID
        CAD     M6
        DIV     180.
        CALL    COS1

        MPY     M5
        STR     F2
        MPY     F2
        STR     F2
        CAD     1.
        SUB     F2
        CALL    SQR1

        STR     F3
        CAD     M5
        MPY     F1
        STR     F2
        CAD     1.
        SUB     F2
        CALL    SQR1

        DIV     F3
        MPY     M4
        STR     M7
        LFR     2,RDMBSS

        LFR     3,RDMBSS+1
        LFR     4,RDMBSS+2

        LFR     5,RDMBSS+3
        JLH     M3+1            EXIT.

RDMBSS  BSS     4
```

```
ASSIGN SCALE,RPSZ,Q2,Q4,Q6,Q9,Q12,XINP,XDINP,XINS,XDINS,PSI

ASSIGN AVRUC,RMRUC,AVG,RMG,PHIIN,RADIN,ROUT,RIN

ASSIGN XIN,XDIN,TZERO,XZERO,XDZERO,MOTION,T,X,XD,DELX,DELXD

ASSIGN AQ,CQ,BNQCQ,TESTU,TSTSBC,TSTCNU,U,UD,SNU,CNU,DNU,RADNEW

ASSIGN COUNT,RUCRIN,LARGEG,F,SMALLG,RAD,PHI,XF,XDF,RADOLD,PHIOLD

ASSIGN DELRAD,RADFIN,PHINP,DELPHI,ECCEN,XMAX,SETUP

ASSIGN XPERM,XDPERM,AMJOUT,AMJIN,ECOUT,ECIN,AMJOR

ASSIGN AVGR,RMSR,SIGMAR,AVGG,RMSG,SIGMAG

READIN DECQL   ,XPERM,16,INREAD
INREAD CHR     30,4F15.0,2F10.0/6F10.0,F5.0,3D5*

PRINTN DECQL   ,XPERM,16,NPRINT
NPRINT CHR     48,8H1XPERM =1PE24.15//9H XDPERM =1PE24.15//9H AMJO

         CHR   48,UT =1PE24.15//8H AMJIN =1PE24.15//8H ECOUT =1PE1

         CHR   48,9.10//7H ECIN =1PE19.10//8H AMJOR =1PE19.10//9H

         CHR   48,DELRAD =1PE19.10//9H RADFIN =1PE19.10//8H PHINP
```

```
        CHR     48,=2PE19.10//9H DELPHI =2PE19.10//8H ECCEN =1PE19

        CHR     48,.10//7H XMAX =F10.2//19H FIXED POINT NUMBERD5//2
        CHR     48,OH NUMBER OF ORBITS ISD5//21H NUMBER OF SECTORS

        CHR     5,ISD5*
        ASSIGN  COVAL
CTOFF   DECQL   ,COVAL,1,OFFCT
OFFCT   CHR     3,D5*
CTOFFP  DECQL   ,COVAL,1,OFFPCT
OFFPCT  CHR     24,//16H CUTOFF VALUE ISD5*

SMOUT1  DECQL   ,AVGR,6,OUTSM1
OUTSM1  CHR     48,//17H AVERAGE RUCRIN =1PE14.6,15H   RMS RUCRIN =

        CHR     48,1PE14.6,21H   RUCRIN DEVIATION =1PE14.6//14H   A

        CHR     48,VERAGE G =1PE14.6,10H   RMS G =1PE14.6,16H   G D

        CHR     18,EVIATION =1PE14.6*

HEAD    DECQL   ,,,DAEH
DAEH    CHR     48,1H1,X,3HM11,11X,6HRUCRIN,11X,6HLARGEG,10X,1HF,11
```

```
          CHR     48,X,6HSMALLG,14X,3HRAD,8X,3HPHI,15X,2HXF,14X,3HXDF


          CHR     10,,2X,1HQ//*

OUT       DECQL   4096+3,COUNT,9,TUO
          DECQL   3,SETUP,1,
TUO       CHR     46,D5,1P2E17.9,F11.5,1P2E17.9,F11.5,1P2E17.9,D3/*

SKIP      DECQL   ,,,PIKS
PIKS      CHR     5,3(/)*
*BUFF1    BSS     6
*SNARRY   BSS     901
*BUFF2    BSS     6
*CNARRY   BSS     901
*BUFF3    BSS     6
*DNARRY   BSS     901
*BUFF4    BSS     6
*SBYC     BSS     1702
CWLAG6    DECQL   SNARRY,1,SNU,1
          DECQ    CNARRY,1,CNU,1
          DECQ    DNARRY,1,DNU,
ELKAUX    DECQL   SNARRY+894,1,SNU,1
          DECQ    CNARRY+894,1,CNU,1
          DECQ    DNARRY+894,1,DNU,
BLKAUX    DECQL   SNARRY-6,1,SNU,1
          DECQ    CNARRY-6,1,CNU,1
          DECQ    DNARRY-6,1,DNU,
IGNORE    EQUS    4096
LOOPS     EQUM    2
RFAST     EQUF    3
QFAST     EQUF    2
TBY4      DEC     1.5
K         DEC     1.854074677301372
K4        DEC     7.416298709205488
RINCR     DEC     .55555556555555E-03
Q         DEC     .43213918263772E-01
PSZ       DEC     .037
PI        DEC     3.141592653589793
EOCT      OCTQL   ,65,4343,7147
H1OCT     OCTQL   ,,7030,4701
H2OCT     OCTQL   ,,7030,4702
```

```
PHIST   CAD     DELX                    SUBROUTIN TO CORRECT 'PHI'.
        TP      PHISTA
        TZ      PHISTB
        CAD     180.
        ASC     PHI
        TRA     PHISTX
PHISTA  CAD     DELXD
        TP      PHISTX
        CAD     360.
        ASC     PHI
        TRA     PHISTX
PHISTB  CAD     DELXD
        TP      PHISTC
        CAD     270.
        STR     PHI
        TRA     PHISTX
PHISTC  CAD     90.
        STR     PHI
PHISTX  JLH     3,,                     EXIT.
CXMAX   SFR     4,CBSS                  SAVE RETURN.
        CAM     1,PXMAX

        CALL    PRINT
        LFR     4,CBSS
        TRA     STXCAL
PXMAX   DECQL   ,X,2,XMAXP
XMAXP   CHR     48,1H1///24H **** XMAX EXCEEDED ****//3H X=1PE24.

        CHR     17,//4H XD=1PE24.15*

*CBSS   BSS     1
*
*
*
*
        GO
```

C. Fortran program for the IBM-7094

Input parameters

NSTART: An integer (1,2,3, or 4) representing the quarter-period of p(t) which initiates the motion.

MLTPLS: The number of integer multiples m of the basic mapping period.

PERS: The basic mapping period n.

VINC: The numerical value of the period τ of p(t).

PZERO: The numerical value of the magnitude p_o of p(t).

XMAX: The maximum value of X which a final coordinate is allowed to attain.

XPERM: The X-coordinate of the point to be used as the origin of the polar coordinates.

XDPERM: The $\dot{X}$-coordinate of the point to be used as the origin of the polar coordinates.

ECCEN: The fixed eccentricity e_o corresponding to the initial point in phase-space being mapped.

AMJOR: The semi-major axis a_o corresponding to the initial point in phase-space being mapped.

PHIIN: The original angle θ_o corresponding to the initial point in phase-space being mapped.

PHIINC: An increment in θ_o if a regular series of θ_o values is desired.

PHIFIN: The final θ_o in the desired series of θ_o values (may equal PHIIN).

Output parameters

NCYCLE: The running counter for the number of multiples m of the basic period n.

V(1): The running value of time t_1.

V(2): The mapped X-coordinate $X_1(t_1)$.

V(3): The mapped $\dot{X}$-coordinate $\dot{X}_1(t_1)$.

RAD: The mapped radius r_1 about (XPERM, XDPERM).

PHI: The mapped angle θ_1 about (XPERM, XDPERM).

RUERIN: The ratio of the mapped radius r_1 at the angle θ_1 to the radius r_e of a standard ellipse (specified by AMJOR and ECCEN) at the same angle θ_1. [This is called RUCRIN in the NICAP program.]

FMOSER: Moser's $\Delta\theta$ function = $(\theta_1-\theta_o)$.

GMOSER: Moser's Δr function = (r_1-r_o).

```
      DIMENSION D(4),E(4),F(4),VIP(3),VD(3),V(3)
      COMMON V,VD,VINC,VIP,D,E,F,PZERO,S
    1 READ INPUT TAPE 7,2,NSTART,MLTPLS,PERS,VINC,PZERO,XMAX,
     1XPERM,XDPERM
    2 FORMAT ( I2,I6,2F6.0,2F10.0,2F15.0 )
      D(1) = 0.5
      D(2) = 0.29289322
      D(3) = 1.7071068
      D(4) = 0.16666667
      E(1) = 2.0
      E(2) = 1.0
      E(3) = 1.0
      E(4) = 2.0
      F(1) = -0.5
      F(2) = -0.29289322
      F(3) = -1.7071068
      F(4) = -0.5
      CONV = 0.0174532925
      NTOTAL = 6.0*PERS/VINC
    3 READ INPUT TAPE 7,5,ECCEN,AMJOR,PHIIN,PHIINC,PHIFIN
    5 FORMAT (5F15.0)
12    WRITE OUTPUT TAPE 6,15
   15 FORMAT (18H1 FIXED INPUT DATA ////)
   18 WRITE OUTPUT TAPE 6,20,ECCEN,AMJOR,PHIIN,PHIINC,PHIFIN
   20 FORMAT (10H    ECCEN=1PE16.9, 8H  AMJOR=1PE16.9,8H  PHIIN=1PE16.9,
     1 9H  PHIINC=1PE16.9, 9H  PHIFIN=1PE16.9 //)
   23 WRITE OUTPUT TAPE 6,25,NSTART,MLTPLS,PERS,VINC
   25 FORMAT(11H    NSTART= I2, 11H    MLTPLS= I6, 9H    PERS= F6.2,
     1 9H    VINC= 1PE13.6 //)
   26 WRITE OUTPUT TAPE 6,27,PZERO,XMAX,XPERM,XDPERM
   27 FORMAT(10H    PZERO= 1PE13.6, 9H    XMAX= 1PE13.6,
     1 10H    XPERM= 1PE20.12, 11H    XDPERM= 1PE20.12 ////)
28    WRITE OUTPUT TAPE 6,30
   30 FORMAT (7HONCYCLE,6X,2H T,13X,2H X,12X,5H XDOT,10X,4H RAD,11X,
     1 4H PHI,10X,7H RUERIN,8X,7H FMOSER,8X,7H GMOSER ////)
   50 TOP = (1.0-ECCEN**2)*AMJOR*AMJOR
   51 BOT = 1.0-(ECCEN*COS(PHIIN*CONV))**2
```

```
    52 RADIN = SQRT(TOP/BOT)
    53 RUERIN = 1.0
    55 FMOSER = 0.0
    56 GMOSER = 0.0
    60 V(1) = 0.0
    61 V(2) = XPERM+RADIN*COS(PHIIN*CONV)
    62 V(3) = XDPERM+RADIN*SIN(PHIIN*CONV)
    65 NCYCLE = 0
    70 WRITE OUTPUT TAPE 6, 75,NCYCLE,V,RADIN,PHIIN,RUERIN,FMOSER,GMOSER
    75 FORMAT (1H I4,2X, 8(1H 1PE14.7 ) //)
100    GO TO (105,115,110,120), NSTART
105    S = 1.0
106    T = 1.5
107    GO TO 150
110    S = -1.0
111    T = 1.5
112    GO TO 150
115    S = -1.0
116    T = 3.0
117    GO TO 150
120    S = 1.0
121    T = 3.0
  150 NTRACE = 0
207    NCOUNT = 0
210    VIP(1) = 0.0
211    VIP(2) = 0.0
2111   VIP(3) = 0.0
212    IF (ABSF(V(2)) - XMAX) 216, 213, 213
213    WRITE OUTPUT TAPE 6,214,V
214    FORMAT (5H XMAX 1PE20.12,2(5H     1PE20.12))
215    GO TO 3
216    CALL INTEGR
2161   NCOUNT = NCOUNT + 1
2162   NTRACE = NTRACE + 1
225    IF (NTRACE - NTOTAL) 226, 300, 3
226    NSTEPS = T/VINC
```

```
227    IF (NCOUNT - NSTEPS) 210, 230, 3
  230 IF (T - 2.0) 231, 3, 240
231    T = 3.0
240    S = -S
  241 GO TO 207
  300 DELX = V(2)-XPERM
  301 DELXDT = V(3)-XDPERM
  302 RAD = DELX**2+DELXDT**2
  303 RAD = SQRT(RAD)
  304 PHI = ATAN(DELXDT/DELX)/CONV
 3041 IF (DELX) 3045, 3042, 3042
 3042 IF (DELXDT) 3043, 305, 305
 3043 PHI = PHI + 360.0
 3044 GO TO 305
 3045 PHI = PHI + 180.0
  305 BOTPHI = 1.0-(ECCEN*COS(PHI*CONV))**2
  306 RADPHI = SQRT(TOP/BOTPHI)
  307 RUERIN = RAD/RADPHI
 3071 FMOSER = PHI - PHIIN
 3072 GMOSER = RAD - RADIN
  308 NCYCLE = NCYCLE+1
  310 WRITE OUTPUT TAPE 6, 75,NCYCLE,V,RAD,PHI,RUERIN,FMOSER,GMOSER
  316 IF (NCYCLE - MLTPLS) 100, 317, 350
  317 IF (PHIIN - PHIFIN) 318, 3, 3
  318 PHIIN = PHIIN + PHIINC
  319 GO TO 28
350    CALL SYSTEM
351    END
```

SYSTEM
ATAN
INTEGR
ABSF
SIN
SQRT
COS
PRINT
READ

```
1000  SUBROUTINE INTEGR
      DIMENSION D(4),E(4),F(4),VIP(3),VD(3),V(3)
      COMMON V,VD,VINC,VIP,D,E,F,PZERO,S
1010  DO 1018 J = 1, 4
1011  VD(1) = 1.0
1012  VD(2) = V(3)
1013  VD(3) = -PZERO * S * V(2)**3
1014  DO 1018  K = 1, 3
1015  VD(K) = VINC * VD(K)
1016  R = D(J) * (VD(K) - E(J) * VIP(K))
1017  VIP(K) = VIP(K) + 3.0 * R + F(J) * VD(K)
1018  V(K) = V(K) + R
1019  RETURN
1020  END
```

SYSTEM

LIST OF REFERENCES

1. G. Sansone and R. Conti, Non-Linear Differential Equations, Macmillan Company, New York, (1964).

2. R. Bellman, Stability Theory of Differential Equations, McGraw-Hill Book Company, New York, (1953).

3. E. T. Whittaker, A Treatise on the Analytical Dynamics of Particles and Rigid Bodies, Cambridge University Press, London, (1964).

4. N. Minorsky, Nonlinear Oscillations, D. Van Nostrand Company, Princeton, New Jersey, (1962).

5. J. H. Bartlett, "The Restricted Problem of Three Bodies," Mat. Fys. Skr. Dan. Vid. Selsk. 2, No. 7, (1964).

6. G. Shearing, "Computation of Periodic Orbits in the Restricted Three-Body Problem, Using the Mercury Computer," (Ph.D. Thesis) University of Manchester, England, (1960).

7. M. Hénon, "Exploration Numérique du Problème Restreint," Annales D'Astrophysique 28, No. 6, (1965).

8. A. M. Liapunov, Stability of Motion, Academic Press, New York, (1966).

9. H. Poincaré, Les Méthodes Nouvelles de la Mécanique Céleste (III), Gauthier-Villars, Paris, (1892).

10. H. Poincaré, "Sur un Théorème de Géométrie," Rendiconti del Circolo Matematico di Palermo 33, (1912).

11. G. D. Birkhoff, "An Extension of Poincaré's Last Geometric Theorem," Acta Mathematica 47, (1926).

12. G. D. Birkhoff, "On the Periodic Motions of Dynamical Systems," Acta Mathematica 50, (1927). Also in George David Birkhoff - Collected Mathematical Papers II, American Mathematical Society, (1950).

13. J. H. Bartlett, "Motion Under a Periodic Cubic Force," Mat. Fys. Medd. Dan. Vid. Selsk. 36, No. 11, (1968).

14. V. I. Arnol'd, "Small Denominators and Problems of Stability of Motion in Classical and Celestial Mechanics," Uspekhi Matematicheskikh Nauk 18, Nr. 6 (114), (1963).

15. J. Moser, "On Invariant Curves of Area-Preserving Mappings of an Annulus," Nachr. Akad. Wiss. Göttingen, Math.-Phys. Kl., Nr. 1, (1962).

16. E. D. Courant and H. S. Snyder, "Theory of the Alternating-Gradient Synchrotron," Annals of Physics 3, (1958).

17. J. L. Powell and R. S. Wright, MURA Report RW/JLP, No. 4, (1955).

18. G. Bozis, "On the Existence of a New Integral in the Restricted Three-Body Problem," Astronomical Journal 71, No. 6, (1966).

19. M. Hénon and C. Heiles, "The Applicability of the Third Integral of Motion: Some Numerical Experiments," Astronomical Journal 69, No. 1, (1964).

20. G. W. and R. M. Spenceley, Smithsonian Elliptic Function Tables, Smithsonian Institute, Washington, D. C., (1947).

21. Tables of Lagrangian Interpolation Coefficients, Columbia University Press, New York, (1944).

22. F. Bowman, Introduction to Elliptic Functions, John Wiley and Sons, New York, (1953).

23. J. H. Bartlett and C. A. Wagner, "The Restricted Problem of Three Bodies (II)," Mat. Fys. Skr. Dan. Vid. Selsk. 3, No. 1, (1965).

VITA

Curtis Arthur Wagner was born on [redacted] [redacted] in [redacted] [redacted], where he attended public schools. He entered the University of Wisconsin in 1956, and received the degree of Bachelor of Arts in Physics, with High Honors in the Major, in June, 1960. The same year he enrolled in the Graduate College of the University of Illinois, majoring in physics and minoring in mathematics and astronomy. He was a Woodrow Wilson Honorary Fellow, and held National Science Foundation National and Cooperative Fellowships for four years. During this time he spent a year at the University of Copenhagen studying celestial mechanics. In the succeeding years he has held both teaching and research assistantships in the Physics Department while working with Professor J. H. Bartlett in the field of nonlinear mechanics. He has published one paper, on the restricted problem of three bodies. He married the former Margret Anne Schoenbohm on November 11, 1967.